공학박사학위논문

Design and Optimization of Carbon Dioxide Capture and Storage Process for Low-carbon Power Generation

저탄소 발전을 위한 이산화탄소 포집 및 저장 공정의 설계 및 최적화 연구

2017 년 8 월

서울대학교 대학원

화학생물공학부

안 진 주

Design and Optimization of Carbon Dioxide Capture and Storage Process for Low-carbon Power Generation

저탄소 발전을 위한 이산화탄소 포집 및 저장 공정의 설계 및 최적화 연구

지도교수 한 종 훈

이 논문을 공학박사학위논문으로 제출함

2017 년 5 월

서울대학교 대학원

화학생물공학부

안 진 주

안진주의 공학박사학위논문을 인준함

2017 년 7 월

위 원 장 _____ (인)

부 위 원 장 _____ (인)

위 원 _____ (인)

위 원 _____ (인)

위 원 _____ (인)

Abstract

Design and Optimization of Carbon Dioxide Capture and Storage Process for Low-carbon Power Generation

Jinjoo An
School of Chemical & Biological Engineering
The Graduate School
Seoul National University

Carbon capture and storage (CCS) technologies have been considered a realistic option for mitigating the climate change. Post-combustion CO_2 capture utilizes existing coal-fired power plants, and aqueous monoethanolamine (MEA) scrubbing is the most well proven capture technology. However, the heat and energy requirements of solvent regeneration and CO_2 liquefaction cause a 30% decrease in net power output. This power de-rate is a major obstacle for implementing CCS. Herein, the energy efficient and economical carbon capture, compression, dehydration, liquefaction and injection process is proposed. Firstly, simulation-based parametric optimization is performed to

minimize the power de-rate. Post-combustion CO_2 capture with aqueous MEA scrubbing (85 %, 90 %, and 95 % removals) and CO_2 liquefaction integrated with a 550 MWe supercritical coal-fired power plant is simulated. The liquid to gas ratio and stripper operating pressure of the CO_2 capture process are the selected manipulated variables with steam extracted from the IP-LP crossover pipe and the first LP turbine as possible heat sources. The power de-rate was reduced to 17.7 % when operating at optimum conditions. In addition, the author propose a comprehensive optimal design of CO_2 dehydration process using a superstructure-based optimization. The superstructure model development includes binary interaction parameter regression for NRTL-RK thermodynamic model, unit operation modeling, and identification of all connectivity of the unit operations in the superstructure. The superstructure imbeds 30,720 possible process alternatives, and the optimum process configuration with the least cost and its operating condition are simultaneously identified using Aspen Plus-MATLAB interface. The optimum process includes three-stage contactor, ten-stage still column, lean/rich solvent heat exchanger, and cold rich solvent split flow fed to the sixth-stage of still column. The total annualized cost of the optimum process is 5.67 M$/yr, and it corresponds to the specific annualized cost of 1.80 $/ton$CO_2$. Sensitivity analysis using Monte Carlo simulation is also presented for the optimum process, and the refrigerant and steam are the most influential utility costs. Lastly, the small-scale topside CO_2 injection process for offshore platform is designed from conceptual design

to piping & instrument diagram level with the hazard and operability study is presented.

Keywords: CCS; Post-combustion CO_2 capture; Superstructure optimization; CO_2 dehydration; Offshore topside injection process; Hazard and operability

Student Number: 2015-30215

Contents

List of Figures

List of Tables

CHAPTER 1. Introduction

1.1. Research motivation

The recent climate change Conference of Parties 21 (COP21) in Paris, 2015 achieved a strong universal agreement on the importance of stabilizing atmospheric concentration of greenhouse gases. Among many possible options to limit the global temperature rise, carbon capture and storage (CCS) is clearly one of the dominant technologies to tackle the emission of greenhouse gases. Among many greenhouse gas (GHG) sources, the energy supply sector is known to be the single largest contributor and occupies 35% of the total anthropogenic GHG emissions by 2010 (IPCC, 2011). A shocking fact is that more than 2,400 new coal-fired power plants are expected to be approved and constructed in the next decade in the Asia region alone. Until renewable energy and energy efficiency enhancements are commercially introduced, it is highly possible that fossil fuel related power generation will take in charge of energy supply due to its abundance in the near future. In the current situation of high dependency on fossil fuel, carbon capture and storage technologies should be implemented to mitigate the climate change in order to keep using fossil fuel while minimizing the emission of CO_2 to the atmosphere at the same time.

CCS chain mainly consists of energy generation, capturing from the flue gas, liquefying to facilitate transportation, transporting from capture to

storage sites, and finally injecting CO_2 to safely store for a long period. Different possible options from capture to storage is shown in Figure 1-1. Various CO_2 capture types are suggested such as post-combustion, pre-combustion, and oxy-fuel combustion CO_2 capture systems. Capturing CO_2 from the flue gas produced by the combustion of fossil fuel in air is commonly involved in post-combustion capture. In terms of post-combustion capture, acid gas scrubbing process using monoethanolamine (MEA) is one of the most well-proven and commercially available technologies for reducing CO_2 emission, and can be most economical because it can be installed to existing power plants with retrofit and treat large amount of flue gas. However, energy requirement for regenerating MEA solvent is often considered as a bottleneck to introduce this capture process to power plants. Even more CO_2 may be generated to compensate the energy penalty by combusting more fossil fuel to meet the energy demand. Liquefaction is also energy intensive process, intensifying the energy penalty up to 30% in total. Many researchers have studied process alternatives for standalone capture and liquefaction process. Unfortunately, the suggested new configurations consider the processes separately. This may cause improper evaluation by not taking into accounts non-linearity of integrated process of power generation, capture, and liquefaction in terms of energy efficiency.

Furthermore, numbers of studies focused only on CO_2 capture and liquefaction process owing to their high cost and energy consumption. However, dehydration process, which is small yet important part of liquefaction to injection process, is underestimated in its cost by treated as a simple linear model despite the importance of the process in CCS chain. Dehydrating high purity CO_2 stream after the capture process is essential because CO_2 product stream is usually saturated with water, which may cause operational problems such as CO_2 hydrate formation and corrosion in downstream transportation and injection systems. As a result, dehydration process in CCS has insufficient information compared to capture and liquefaction process.

1.2. Research objectives

The objective of this thesis is to design energy efficient and economical carbon capture, dehydration, and liquefaction process, and to suggest small-scale carbon dioxide injection process design for offshore platform in order to implement CCS technologies into commercial power plants.

Firstly, individual steam cycle, conventional post-combustion CO_2 capture process using MEA solvent, and CO_2 self-refrigerant liquefaction processes are mathematically developed. Most dominant process operating conditions and parameters of the processes in terms of energy penalty are evaluated. The unit process for the process integration is proposed and optimally located. The best-

found operating conditions and parameters to reduce the energy penalty of integrated process is proposed. The author is then explain the economically optimal dehydration process, which is part of liquefaction process, in detail solved by superstructure optimization. The sensitivity analysis of utility costs for the dehydration process alternatives including the optimal process is also presented. Finally, the author suggests the basic design of small-scale CO_2 injection system on the topside of offshore platform with the hazard and operability study of the system in detail.

1.3. Outline of the thesis

Chapter 1 provides the research motivation and the objective of the thesis. In Chapter 2, optimal operating condition to reduce the energy penalty of 550 MWe commercial scale coal-fired power plant integrated with carbon dioxide capture and liquefaction process is described including the mathematical modeling and simulation of the individual process. Chapter 3 gives the techno-economic assessment of carbon dioxide compression and dehydration process using superstructure-based optimization and the sensitivity analysis of the optimal process. In Chapter 4, conceptual and basic design of small-scale offshore carbon dioxide injection system is carried out and the hazard and operability study of the system is explained in detail. Chapter 5 presents the conclusion and the suggestion for the future works.

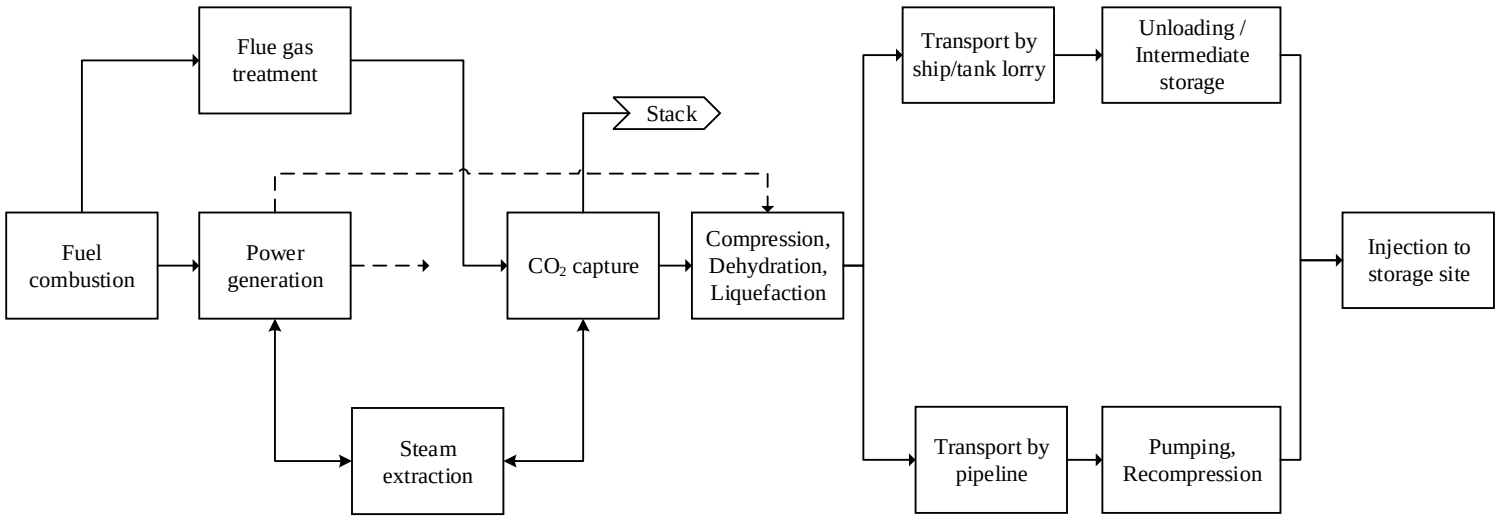

Figure 1-1. Carbon capture and storage (CCS) chain (solid line: mass flow, dashed line: energy flow).

CHAPTER 2. Energy Penalty Reduction in Coal-fired Power Plant with Post-combustion CO_2 Capture and Liquefaction Process*

2.1. Overview

The CCS chain mainly consists of three processes: steam cycle, CO_2 capture, and liquefaction. During the steam cycle, pulverized coal is combusted in a boiler, and heat energy is absorbed by the boiler feedwater. Superheated steam is expanded through high, intermediate, and low pressure turbines connected to an electrical generator. At the same time, a small amount of steam is extracted from the inlet stream of each turbine in order to regenerate the feedwater. By doing so, the irreversibility of steam generation is reduced, and the thermodynamic efficiency of the steam cycle is improved (Elliott et al., 1998). The types of CO_2 capture systems are post-combustion, oxy-fuel combustion, and pre-combustion. Capturing CO_2 from the flue gas produced by the combustion of fossil fuels in air is commonly involved in post-combustion capture (Metz et al., 2005). In the post-combustion capture process, CO_2 is captured through a chemical reaction with a chemical solvent, such as

* This chapter cites the author's published journal article: An, J., Lee, U., Jung, J., & Han, C. (2015). Parametric Optimization for Power De-Rate Reduction in the Integrated Coal-Fired Power Plant with Carbon Capture and Storage. Industrial & Engineering Chemistry Research, 54(18), 5062-5076.

monoethanolamine (MEA), in an absorber column and released in a stripper column by adding heat energy to break the CO_2-solvent bond. Between the two columns, hot CO_2-lean solvent leaving the stripper enters a heat exchanger to preheat cold CO_2-rich solvent, and is then fed back into the absorber column. CO_2 released from the solvent in the stripper is fed into the liquefaction process for facilitating the transport of CO_2. There are many alternative processes for liquefaction using various refrigerants, such as ammonia and CO_2 itself. Among these processes, liquefaction by CO_2 itself is considered eco-friendly because no additional refrigerants are necessary. The inlet stream is compressed to about 54 bar and then expanded. Gaseous CO_2 produced by this expansion has a temperature that is low enough to cool the CO_2 streams before they enter the compressors.

Unfortunately, the power de-rate is a significant issue when introducing the CCS process into an existing steam power plant. The heat requirement for breaking the bond between the solvent and CO_2 is often met using steam extracted from a power plant. Steam extraction for solvent regeneration causes a decrease in net power output, and increases the amount of coal and power plants necessary to compensate this shortage. Consequentially, this process may actually increase CO_2 emission. Furthermore, the compression energy during the liquefaction process also increases the power de-rate. Therefore, reducing the power de-rate is key to CCS implementation and commercialization.

As the steam extraction causes a sudden reduction in the steam flowrate in the turbines, the existing steam cycle is not operable. Moreover, the flue gas, which is originally sent to a stack, becomes the inlet gas of the CO_2 capture process. Some modifications of processes and equipment are therefore unavoidable. Some researchers have focused on retrofit options for using the steam cycle for steam extraction in order to minimize the power de-rate. Lucquiaud et al. presented detailed options using the additional steam turbine and associated steam cycle designs and evaluated the plant efficiency for each option (Lucquiaud et al., 2009). Lucquiaud et al. compared the retrofit costs of subcritical and supercritical power cycle plants and showed that the CO_2 abatement costs are the same for both(Lucquiaud and Gibbins, 2011) . In addition, they showed that the plant efficiency has no intrinsic impact on the performance of the capture process if it is properly retrofitted and effectively integrated. Dave et al. compared the use of LP turbine and throttling valve for the steam extraction (Dave et al., 2011). Zachary showed the impacts of retrofit configuration to extract steam by using throttling valve, floating pressure LP arrangement, clutched LP turbine, and backpressure turbine (Zachary, 2008).

The reduction of the power de-rate by process and heat integration has been examined by some researchers. Harkin et al. used pinch analysis and linear programming optimization to determine possible power de-rate targets in individual power plants and to reduce the overall power de-rate (Harkin et al., 2010). Hanak et al. investigated several heat exchanger network (HEN) designs

for a high ash coal-fired power plant with CCS and proposed the use of flue gas for heating the boiler feedwater (Hanak et al., 2014). Khalilpour et al. reduced the power de-rate from 19.4% to 15.9% by heat integration of the flue gas with the reboiler and of the compressor output with the feedwater regeneration (Khalilpour and Abbas, 2011). Liew et al. analyzed capture module design options for heat and process integration, cooling, and the use of waste heat by HEN design and process modification (Liew et al., 2014).

Many researchers have also evaluated the power de-rate based on different operating scenarios and parametric optimization. Sanpasertparnich et al. studied the impact of coal rank, steam extraction location, and flue gas load on CO_2 capture efficiency (Sanpasertparnich et al., 2010). Dave et al. performed case studies on the plant efficiencies of existing coal-fired power plants (subcritical and supercritical) and new coal-fired power plants (subcritical, supercritical, and ultra-supercritical) by evaluating the CO_2 capture demand and cooling options (Dave et al., 2011). Liang et al. conducted an optimization of some important process parameters, including the operating stripper pressure, CO_2 capture efficiency, and steam extraction location (Liang et al., 2011). Cifre et al. reported the influence of important parameters, such as the stripper pressure, solvent flowrate, and the packing heights of the absorber and the stripper, on the power de-rate and analyzed the power de-rate with different solvents (Cifre et al., 2009). Eslick et al. performed a multi-objective single-variable optimization of a coal-fired power plant with CCS to minimize water

consumption, the levelized cost of electricity, and to maximize the power by using the surrogate model to simplify the optimization problem (Eslick and Miller, 2011). Considered variables included the stripper pressure, lean loading, solvent temperature and column heights.

In addition, modified configurations and methods for power de-rate prediction and reduction have been proposed. Van Peteghem et al. developed an analytical framework that can provide insight on the influence of solvent storage systems and the electricity market by using electricity price (peak and off-peak) to regenerate stored solvent (Van Peteghem and Delarue, 2014). Patiño-Echeverri et al. analyzed the profitability of amine storage systems using historical regional electricity price differentials in the US (Patiño-Echeverri and Hoppock, 2012). Liebenthal et al. proposed correlations to predict the impact of heat duty on solvent regeneration and cooling, and the electricity duty on CO_2 capture and compression (Liebenthal et al., 2011). Zhang et al. proposed two improved capture systems: the flash evaporator (FE) with thermal vapor compressor (TVC) and the heated flash evaporator (HFE) with TVC (Zhang et al., 2014). These systems used high-temperature condensate from the stripper reboiler in the capture process and reduced the power de-rate up to 1%. House et al. suggested a temperature swing separation system to reduce the amount of additional fuel that is necessary to compensate for the energy shortage caused by the power de-rate (House et al., 2009). Liang et al. proposed a bi-pressure

stripper to minimize the power de-rate for CO_2 capture and compression (Liang et al., 2011).

Unfortunately, the suggested new methods and configurations still need to be proven effective, and the existing process systems need to be removed to introduce the new configurations, which will take both capital expenditure and time. As previous studies on power de-rate minimization only considered a few variables, it is difficult to show the overall influence of all the variables on the power de-rate. In this chapter, the power de-rate of an integrated retrofitted coal-fired power plant with CCS is minimized by parametric optimization. To validate the simulation model, a 550 MWe steam cycle integrated with CO_2 capture and liquefaction processes simulation model is developed based on the data for a 0.1 MW CO_2 capture pilot plant. Variables in the existing process that may not require any modification are also evaluated. In addition, the nonlinearity between the selected influential variables and the power de-rate are discussed to achieve insight on the overall process.

2.1.1. Methodology

The main purpose of this chapter is to minimize the power de-rate by manipulating the variables of an integrated process. The integrated process consisted of three processes: a 550 MWe conventional coal-fired steam cycle, CO_2 capture process using aqueous MEA solvent, and self-refrigerant

liquefaction process. Each process is developed based on literature and industrial experience. In each process, there were many variables that could influence the power de-rate. Their effect on the power de-rate is evaluated, and the manipulated variables that applied to the minimization of the integrated process were selected: stripper operating pressure and liquid to gas ratio (L/G). To extract the steam from the steam cycle, two steam extraction unit alternatives were proposed: reducing valve and backup turbine. To investigate the effect of the quality of steam extracted, two possible steam extraction locations were considered: Intermediate pressure-low pressure (IP-LP) crossover pipe and the first LP turbine streams. Also, various CO_2 capture rates (85 %, 90 %, and 95 %) are considered in order to show the influence of the CO_2 removal levels on the power de-rate. The simulation-based optimization is conducted by combining Aspen Plus™ v7.3 with MATLAB to find the optimal values. Finally, the relationship between the power de-rate and the variables is discussed.

2.2. Process Description

The general description of steam cycle, CO_2 capture using MEA scrubbing, and self-refrigerant liquefaction process are provided. A base case is first set and discussed to make a comparison to a case with optimum conditions. The process model is built using Aspen Plus™ v7.3.

2.2.1. Steam Cycle

A 550 MWe supercritical steam cycle is used for this study. The specification of the process is set based on DOE/NETL report (Ciferno, 2008). The steam cycle flow diagram is shown in Figure 2-1. The property method is STEAMNBS, which that uses the NBS/NRC steam tables to calculate any thermodynamic properties of water. The model consists of two high pressure (HP), two intermediate pressure (IP), and five low pressure (LP) turbines, as well as seven feedwater heaters (FWHs), condensers, and condensate pumps. Feedwater is first evaporated into high pressure and temperature steam by passing through an economizer (ECO-L) and superheater (SH-L). The generated steam flows through two stages of HP turbines. Following the HP turbines, the steam enters a re-heater (RH-L) to recover more heat energy from a boiler, and then flows to the IP and LP turbines in sequence and is finally condensed (Condenser). Part of the turbine energy is converted into mechanical energy by rotating electrical generator. Condensed feedwater is pumped back

to the economizer by a condensate pump. During delivery, the feedwater is passed along feedwater heaters, which are heat exchangers that increase the temperature of the feedwater using the latent and sensible heat of a small amount of extracted steam. Steam is extracted from every stage of the turbines (multistage extraction). The amount of steam to be extracted is decided based on the terminal temperature difference (*TTD*), defined as Eqn. (2-1).

$$TTD = T_{sat} - T_{fw} \tag{2-1}$$

T_{sat} is the condensing temperature of the steam extracted and T_{fw} is the temperature of the feedwater leaving the feedwater heater. By regenerating the feedwater, the irreversibility of the system involving steam generation is reduced, thus the thermodynamic efficiency is improved. In this model, a closed feedwater heater is assumed (Elliott et al., 1998). The *TTD* values are determined for each turbine using the values of the model in the DOE/NETL report (Ciferno, 2008). The LP steam from the last stage turbine is in vacuum condition (0.069 bar and 38.7 °C). The flue gas generated from the pulverized coal boiler is sent directly to the CO_2 capture process. Any pressure drops in heat exchangers and pipelines are ignored. The detailed design specifications and simulation results are listed in Table 2-1.

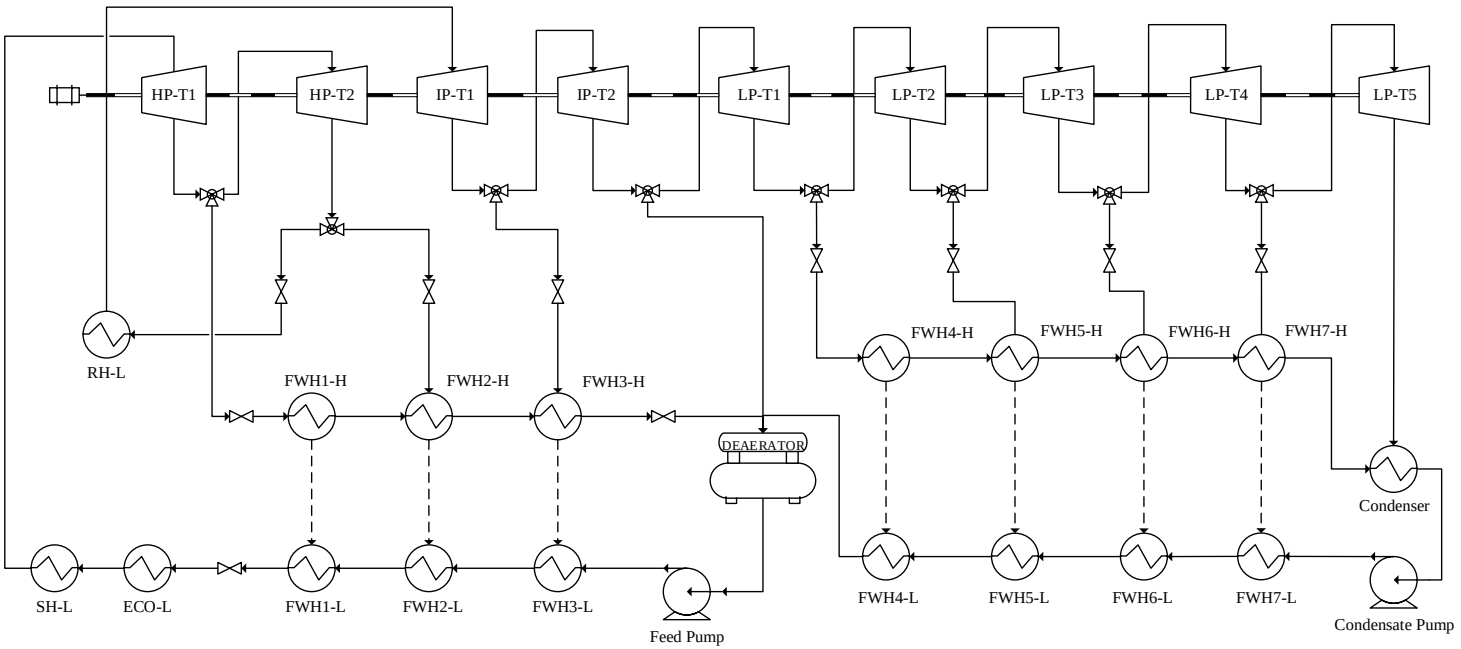

Figure 2-1. Process flow diagram of a 550 MWe steam cycle with a simple boiler model.

Table 2-1. Design specifications and simulation results for the steam cycle.

Net plant power	550 MWe
Net plant efficiency (LHV)	39.4%
Turbine discharge pressure, bar	
High Pressure	76.91 / 49.01
Intermediate Pressure	21.38 / 9.49
Low Pressure	5.012 / 1.324 / 0.579 / 0.241 / 0.069
SH steam	242.35 bar, 598.89 °C
RH steam	49.01 bar, 621.1 °C
TTD, °C	
FWH1	-1.084
FWH2	-0.023
FWH3	-1.113
FWH4	2.803
FWH5	2.747
FWH6	2.7637
FWH7	2.7542
Turbine power output, MWe	
High Pressure	146.3 / 39.7
Intermediate Pressure	93.1 / 72.6
Low Pressure	42.9 / 69.0 / 35.2 / 31.1 / 36.7
Auxiliary load [1], MWe	16.7

[1] $W_{aux} = W_{p,cond} + W_{p,fw}$

2.2.2. CO_2 Capture Process

2.2.2.1. Conventional MEA Scrubbing for CO_2 Capture

A typical CO_2 capture process with an absorber and a stripper with a lean-rich solvent heat exchanger is used for this study, as indicated in Figure 2-2. As flue gas from coal-fired power plants has a low concentration and partial pressure of CO_2, chemical absorption is more suitable than physical absorption. Aqueous MEA is selected for the chemical solvent. Acid gas removal using MEA has been studied over the last decades; thus, much of the MEA data needed for the simulation are easily obtained from the literature. Furthermore, one main focus of this study is to optimize the process operating condition without modifying the process itself, and MEA fits well with this goal.

The flue gas generated from the boiler is cooled to 40 °C before entering the bottom of the absorber. In the absorber, cold lean MEA is fed to the top of the column and selectively absorbs CO_2 by an exothermic chemical reaction. Cold CO_2-rich MEA solvent is drained out from the bottom of the column. The remaining flue gas is sent back to the stack and purged to the atmosphere. Cold rich MEA solvent is preheated in the lean-rich MEA heat exchanger and is fed to the top of the stripper column. The hot rich MEA solvent desorbs CO_2 by an endothermic reaction at high temperature and is then drained out from the bottom of the stripper. The vapor is cooled by the stripper condenser and

gaseous captured CO_2 is ready for the liquefaction process. The hot lean MEA drained from the stripper is sent to the lean-rich MEA heat exchanger to be cooled and then sent back to the absorber column as the cold lean MEA solvent.

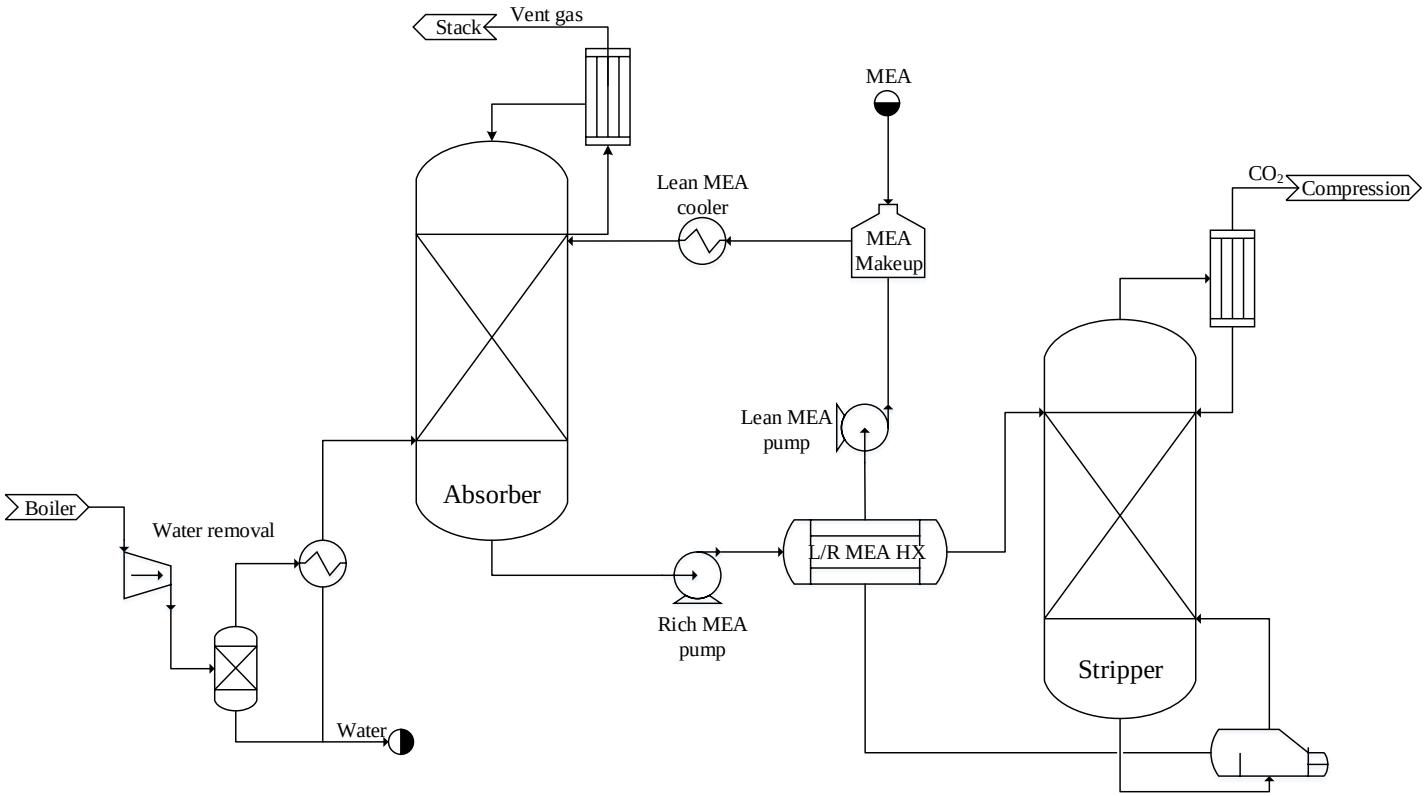

Figure 2-2. Process flow diagram of conventional post-combustion CO_2 capture.

2.2.2.2. Model Specification

The specifications of the simulation were based on the data from a 0.1 MW CO_2 capture pilot plant in Boryeong, Republic of Korea, which was built by the Korea Electric Power Corporation (KEPCO E&C) and the Korea Midland Power Corporation (Figure 2-3). Detailed information on the plant specifications are listed in Table 2-2 and the major process operation indicators are presented in Table 2-3. The capture efficiency of the plant is 90% CO_2 removal when 30 wt% aqueous MEA is used as the amine solvent, and the heights of the absorber and the stripper are 16.8 m and 11.25 m. Many researchers mentioned difficulties in up-scaling the system from a small pilot plant to a large commercial plant due to size and construction issues (Lawal et al., 2009; Onda et al., 1968; Reddy et al., 2003; Singh et al., 2003; Steeneveldt et al., 2006). Owing to the large volumetric flowrate of flue gas entering the both columns, the diameters of the columns become so large that more than one column may be required due to poor liquid and vapor distributions and site-specific fabrication limitation. However, keeping the number of columns to be minimum lowers capital cost and satisfies the space restriction. Hence the number of the columns should be determined by considering lots of factors such as a plant site, utility availability, efficiency, turndown ratio.

Based on the experience from the pilot plant, a base case of 550 MW CO_2 capture model was developed assuming 90% CO_2 removal with 30 wt% MEA

the solvent. To calculate the diameter of the columns, 4 ft/s of superficial velocity is used. A rate-based Radfrac model with film theory is used for the absorber and the stripper, and Intalox Metal Tower Packing (IMTP) is selected as a packing material. To appropriately establish the model, mass transfer coefficient and interfacial area methods were used. The interfacial area factors for the absorber and the stripper were 0.7 and 0.5, respectively, and Onda et al. model is used to predict the column temperature profile (Onda et al., 1968). The Electrolyte-NRTL model is employed to estimate the thermodynamic properties of the MEA–H_2O–CO_2 system. To calculate the reaction kinetics of MEA–H_2O–CO_2, a kinetic model suggested by Hikita et al. (Hikita et al., 1977) is used. A summary of the process specifications are shown in Table 2-4. MEA degradation at temperatures lower than 120 °C is assumed to be negligible. This process is assumed to handle 100% of the flue gas from the 550 MWe power plant; detailed information for the flue gas (Ciferno, 2008) is listed in Table 2-5.

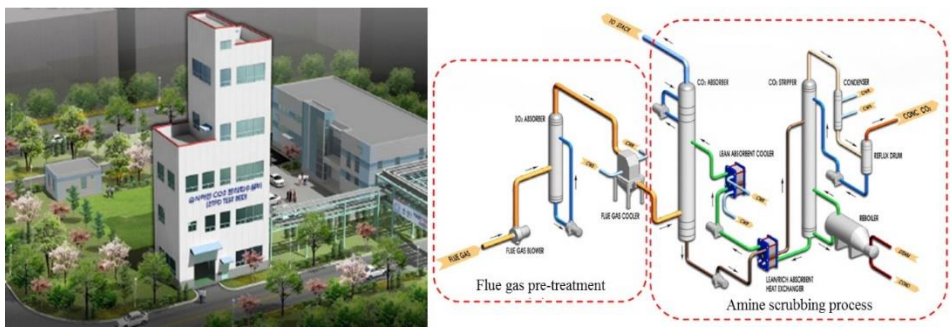

Figure 2-3. 0.1 MW CO_2 capture pilot plant in Boryeong, Republic of Korea (Jung et al., 2015).

Table 2-2. Specifications of a 0.1 MW CO_2 capture pilot plant.

Feed conditions	
Temperature	43.0 °C
Pressure	0 barg
Flowrate	331.8 Sm^3/hr
Composition	dry-vol %
N_2	80.81
CO_2	14.90
O_2	4.29
SO_2	4.4 ppmdv
Lean amine temperature	40.0 °C
Lean amine flowrate	1,235 L/hr
Lean amine concentration	30.0 wt.%
Absorber	
Temperature (top)	40.0 °C
Pressure (top)	0.018 barg
The height of column	16.8 m
Stripper	
Temperature (top)	83.4 °C
Pressure (top)	0.5 barg
The height of column	11.25 m

Table 2-3. Operation results for a 0.1 MW CO_2 capture pilot plant.

Process Indicators	
Capture efficiency	89.74 %
Capture capacity	1.91 ton/day
L/G ratio	3.7 L/Sm^3
Regeneration energy	3.99 GJ/tonCO_2
Cooling water	63 m3/tonCO_2
MEA solvent circulation flowrate	15.5 m3/tonCO_2
Utility	
Steam flowrate	150 kg/hr
Cooling water	9.7 m^3/hr
Auxiliary power consumption	40.0 kW

Table 2-4. Design specifications of a 550 MW CO_2 capture process (base case).

Capture efficiency	90 %
MEA Solvent	
Concentration	30 wt.%
Lean solvent loading	0.228 mol CO_2/mol MEA
Rich solvent loading	0.567 mol CO_2/mol MEA
Absorber	
Temperature (top)	40.0 °C
Pressure (top)	1.01 bar
The height of column	37 m
Stripper	
Temperature (top)	82.0 °C
Pressure (top)	1.01 bar
The height of column	8 m
Lean-rich solvent heat exchanger	
Minimum temperature approach (MTA)	9 ºC

Table 2-5. Properties of the flue gas flowing into the capture process.

Molar flowrate	162,877 lbmol/hr
Temperature	57 ºC
Pressure	0.1 MPa
Composition	mole fraction
H_2O	0.1517
CO_2	0.1353
N_2	0.6808
O_2	0.024
Ar	0.0082

2.2.3. Self-refrigerant CO_2 Liquefaction

For transporting CO_2 with ship and/or tank lorry, CO_2 liquefaction process is considered. The simulation model for the liquefaction process is built based on the report of Lee et al. The liquefaction model proposed by Lee et al. consumed a minimum compression energy of 98.1 kWh/t CO_2 without using an external refrigerant (Lee et al., 2012). Figure 2-4 shows the process flow diagram for the liquefaction model. Soave-Redlich-Kwong (SRK) is used as the property method with a modified binary interaction parameter (kij) of 0.193 in the van der Waals mixing rule (Heggum et al., 2005). Captured CO_2 is fed to a seawater heat exchanger (Seawater HX-1) to reduce the temperature before entering the multi stream process heat exchanger (Process HX-1). Cold gaseous CO_2 cools down the inlet CO_2 to remove H_2O contained in the inlet stream through condensation. Four-stage compressors and seawater heat exchangers are used to cool and compress CO_2 up to 54.4 bar. The determinant of the number of compressor stages is the outlet pressure of the last compressor. In this liquefaction system, the optimum pressure depends on the amount of volatiles in the feed and the temperature of seawater. If cold seawater is not available, it is necessary to compress the stream to 95 bar to be totally liquefied. Hence, four-stage compressor gives the process flexibility. Aspelund et al. (Aspelund and Jordal, 2007) and Zahid et al. (Zahid et al., 2014) also used four-stage compressor for the same purpose of self-refrigerant liquefaction system. Between each compressor stage, the stream is reduced in temperature by being

fed to a process heat exchanger (Process HX-2). Before entering the compressors, flash separators (FLs) drain out any liquid phase to protect the compressors. The drained liquid (mainly water) is fed back to the first flash separator (FL-1) and water is removed from the system. The compressed CO2 stream is fed to a seawater condenser (Condenser), and then goes through multistage expansion. The cold CO_2 gas generated by expansion is used to decrease the temperature of the streams in the multi stream process heat exchangers (Process HX), and then fed back to the compressors. Finally, cold liquefied CO_2 is obtained at the target conditions (6.5 bar and -52 °C).

The recompression of flash CO_2 gas increases the compression energy roughly 10 % than pipeline transport, which requires a supercritical CO_2 (74 bar at 31 ºC) to avoid two-phase flow (Aspelund and Jordal, 2007). Since the current liquefaction process already compresses CO_2 to 54.4 bar and liquefies it, it requires relatively less compression energy for liquid CO_2 to be increased in the pressure to desired level using CO_2 pump for the pipeline transport. Hence, the power de-rate of ship transport is higher approximately 0.5 %. The major process parameters and input stream composition are listed in Table 2-7. More detailed descriptions of the process are available in the literature.

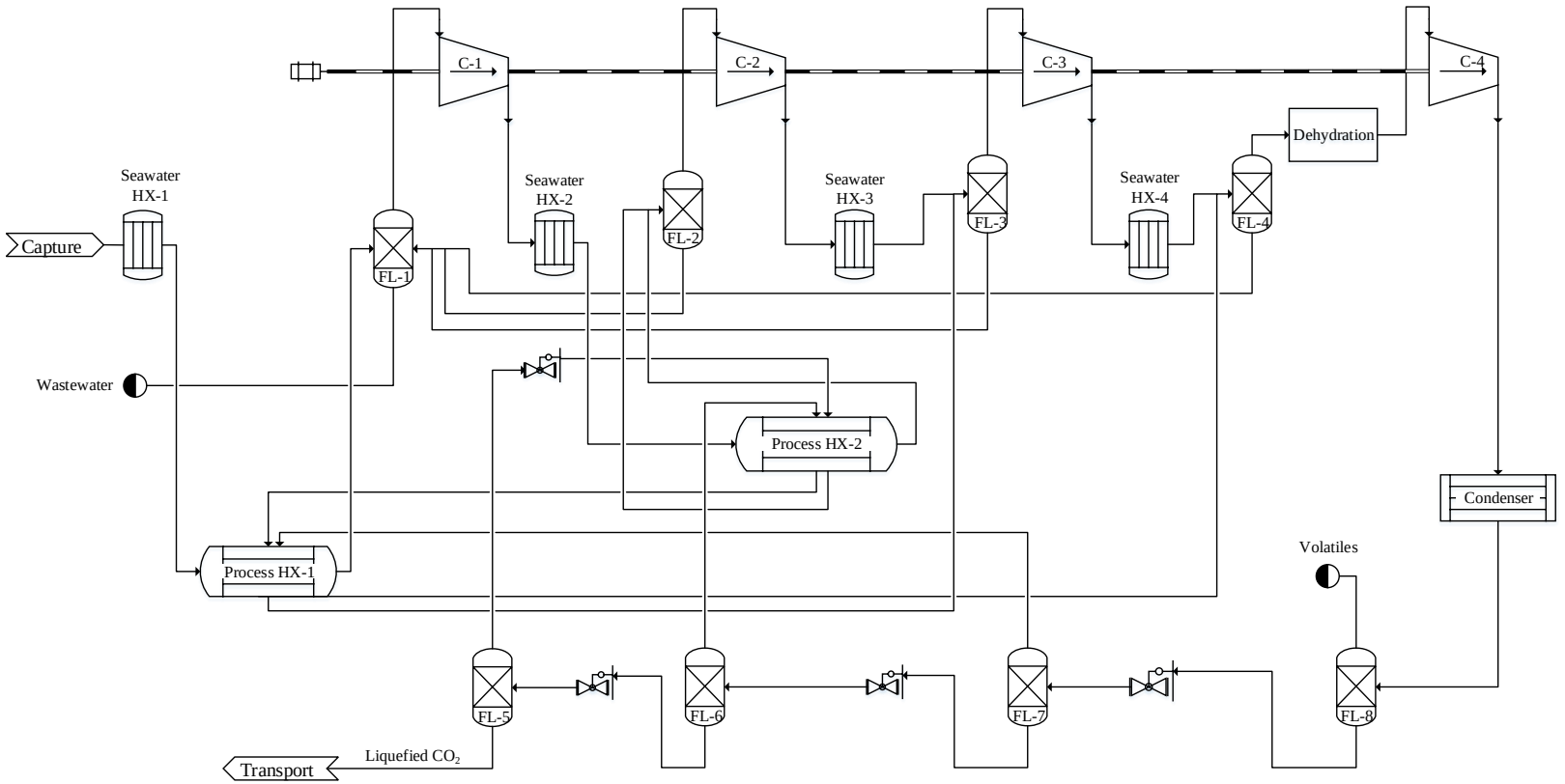

Figure 2-4. Process flow diagram of self-refrigerant CO_2 liquefaction (Lee et al., 2012).

Table 2-6. Design specifications of the CO_2 liquefaction process.

Target CO_2 product	
Temperature	-52 ºC
Pressure	6.5 bar
Compressor efficiency	82 %
Pump efficiency	85 %
Process heat exchanger	
Minimum temperature approach	3 ºC
Seawater heat exchanger	
Minimum temperature approach	5 ºC
Seawater temperature	10 ºC
Input stream composition (base case)	
CO_2	92.46 mol%
H_2O	7.48 mol%
Volatiles	0.06 mol%
Compressor outlet pressures (base case)	2.78 / 7.73 / 21.49 / 54.4

2.3. Integration of Steam Cycle with CO_2 Capture and Liquefaction Process

2.3.1. Definition of Power De-rate

To introduce CCS processes into existing steam cycles, a heat source should be supplied to a reboiler of the stripper for solvent regeneration. Unfortunately, the reboiler of the stripper is known to be an energy intensive unit and one of the main obstacles to CCS implementation. Among the many methods for supplying heat to a reboiler, it is advantageous to use steam extracted from the steam cycle. This is not only because building a CO_2 capture plant near the power plant reduces the cost of flue gas transport, but also because the steam cycle is relatively abundant in low pressure and temperature steam. However, the steam has to be depressurized and reduced in temperature because the stripper reboiler mainly uses the latent heat in exchanging heat. The compression energy in the liquefaction process also decreases the net plant power. The inevitable plant efficiency penalty from extracting steam for the stripper reboiler and compression energy is reported to reach 15–30% (Alabdulkarem et al., 2012; Cousins et al., 2011). This is the so-called "power de-rate" (D) and is calculated using the following Eqn. (2-2).

$$Power\ \ derate(D) = 1 - \frac{Net\ \ plant\ \ power\ \ with\ \ CCS}{Net\ \ plant\ \ power\ \ without\ \ CCS} \quad (2\text{-}2)$$

An increase in the power de-rate means a power plant produces less energy than the original power plant with the same amount of coal. Thus, the power

de-rate can be used as an indicator of operational economics.

2.3.2. Steam Extraction from an Existing Power Plant

Figure 2-5 shows possible locations for steam extraction and the pressures at these locations. Among these locations, there are two suitable locations in the steam turbines to extract steam: the IP-LP crossover pipe (D) and the first low pressure turbine (E). The higher temperatures and pressures before the crossover pipe are too high, whereas after the first LP turbine the temperatures and pressures too low to use as hot stream in a stripper reboiler. Finding an optimum steam extraction point is important to avoid extracting steam with unnecessarily high temperature and pressure and minimize the power de-rate.

A steam extraction unit is necessary to obtain suitable conditions for the reboiler. Figure 2-6 shows alternatives to the steam extraction unit. Steam extraction units consist of three pieces of equipment: depressurizer ((a) pressure reducing valve and (b) turbine), desuperheater, and saturated water pump. The depressurizer and desuperheater vary the pressure and temperature of the extracted steam to be suitable for a reboiler. Only the latent heat of the steam can be used for solvent regeneration in the reboiler. For example, if the temperature at the reboiler is 102.4 °C, the pressure of steam should be 1.56 bar as saturated steam when considering the 10 °C minimum temperature approach (MTA) of a reboiler. However, since the steam pressures from the IP-LP

crossover pipe and first LP turbine are 9.5 and 5.0 bar, respectively, the steam should be reduced in pressure and temperature. Following depressurization to the required pressure, steam is still in superheated. The desuperheater reduces the temperature of the steam to the saturation temperature. Furthermore, MEA thermal degradation and the power de-rate can be decreased by using the minimum temperature of steam for reboiler. As steam pressure increases, the amount of latent heat per unit mass decreases, which means more steam has to be extracted because the steam is a wet fluid. Because the work done by the steam turbines is theoretically proportional to the steam flow rate, as indicated Eqn. (2-3), decreasing steam extraction directly reduces the power de-rate. Lastly, a saturated water pump is used after the steam is saturated in the reboiler to pump the condensate back into the steam cycle.

$$\dot{W} = \dot{m}\eta \frac{kRT_1}{k-1}\left[\left(\frac{P_2}{P_1}\right)^{(k-1)/k} - 1\right] \quad (2\text{-}3)$$

It is obvious that depressurizing using a backup turbine (b) can recover some energy from the extracted steam and reduce the power de-rate. However, a backup turbine (b) costs much more than a reducing valve (a) in both purchase and installation costs for the turbine itself and the electric generator. Therefore, it is necessary to consider both cases ((a) and (b)) for the purpose of future work and economic analysis. Figure 2-7 is a process flow diagram of the integrated CCS process.

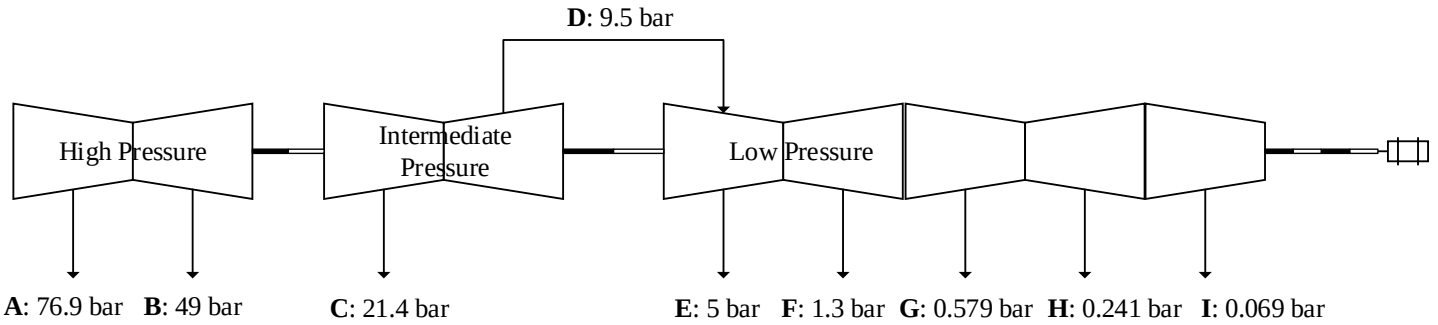

Figure 2-5. Possible steam extraction locations: (A, B) high pressure steam, (C) intermediate pressure steam, (D) IP-LP crossover steam, (E – I) low pressure steam.

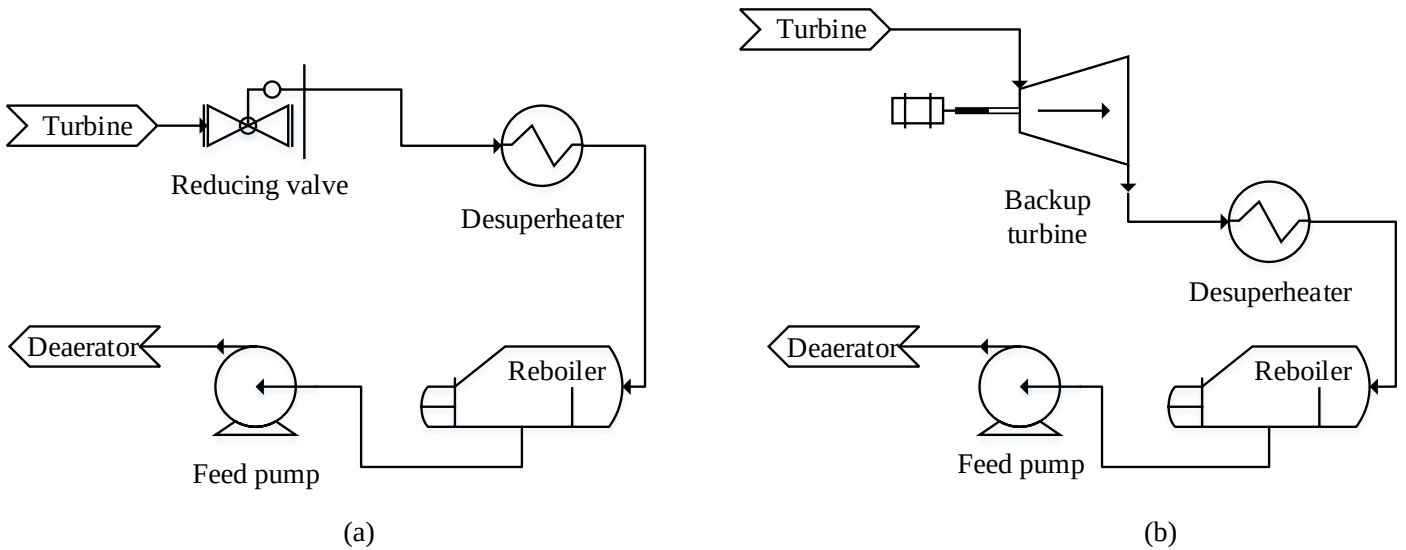

Figure 2-6. Alternatives for the steam extraction unit process: (a) reducing valve, (b) backup turbine.

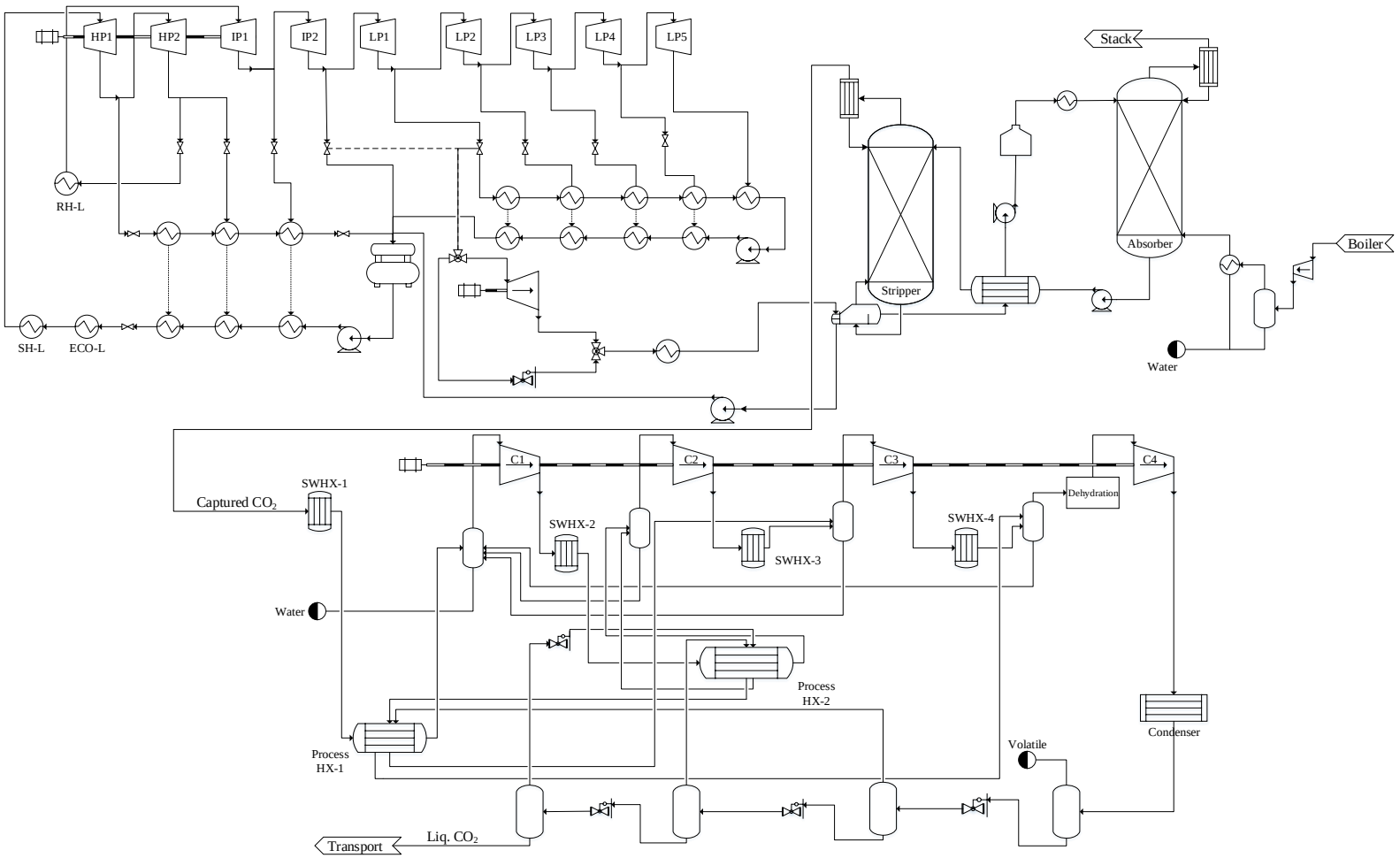

Figure 2-7. Flow diagram of the steam cycle with a steam extraction unit process (dashed line: IP-LP crossover steam, solid line: LP steam).

2.3.3. Variable Selection

The power de-rate (D) of a power plant can be expressed using several parameters and variables of the three processes as Eqn. (4).

$$D = f(x_i) \tag{2-4}$$

The following variables (x_i) possibly influence the power de-rate.

- CO_2 capture process: temperature of flue gas (T_{fg}), liquid to gas ratio (L/G), stripper operating pressure (P_{str}), temperature of lean solvent (T_{lean}), temperatures of condensers of absorber and stripper (T_c), minimum temperature approach (MTA) of lean-rich heat exchanger
- CO_2 liquefaction process: pressure ratio of compressors (C_R)

The MTA of the lean-rich heat exchanger is excluded because there is no constraint on temperature in the hot-rich solvent stream in the model used. If minor solvent evaporation in the rich solvent stream by heat exchange is ignored, it is obvious that a small MTA value is beneficial for the absorption of more heat from the hot-lean solvent. Parameter evaluation is performed to investigate the influence of each parameter and to decide which parameters should be included in the analysis. The above parameters is assigned $x_1 = T_{fg}$, $x_2 = L/G$, $x_3 = P_{str}$, $x_4 = T_{lean}$, $x_5 = T_{c,abs}$, $x_6 = T_{c,str}$, and $x_7 = C_R$, and the degree of influence on the power de-rate is expressed as the following Eqn. (2-5).

$$J = \frac{\partial D}{\partial x_i} \tag{2-5}$$

By evaluating the degree of a change in the power de-rate by manipulating a selected variable, it is possible to determine if the variable has a dominant influence on the objective. If $\partial D / \partial x$ is close to zero, it has little impact on the power de-rate within a chosen range. The results of the variable evaluation showed that x_1, x_4, x_5, and x_6 had no net effect on the power de-rate, whereas x_2, x_3, *and* x_7 are relatively influential. However, because the effect of x_7, compression ratios, on the power de-rate is negligible compared with that of x_2 and x_3, it is not considered further. As a result, P_{str} and L/G are selected as the manipulated variables. The results of the variable evaluation are listed in Table 2-7.

Table 2-7. Results of variable evaluation.

Variables	Range	D_{Max}	D_{Min}	J [a]
CO_2 capture				
Stripper pressure	1–2 bar	21.4	17.7	7.5
L/G	2.9–4.5 L/m^3	22.5	17.7	7.3
Flue gas cooling temperature	5–45 °C	17.9	17.6	0.3
Lean amine cooling temperature	30–50 °C	17.8	17.8	0.0
Absorber condenser temperature	30–55 °C	17.8	17.8	0.0
Stripper condenser temperature	30–55 °C	17.8	17.8	0.0
Liquefaction				
Compression ratio [b]	Optimization			

[a] $J = \left| \frac{D_{Max} - D_{Min}}{\frac{x_{i,max} - x_{i,min}}{\Delta x}} \right|_{x_j}$

[b] J for the compression ratio is calculated using the optimization problem

2.4. Results and Discussion

2.4.1. CO_2 Capture Process

2.4.1.1. Effects of Stripper Operating Pressure

The operating pressure of the stripper not only affects the solvent regeneration energy but also determines the inlet pressure of the liquefaction process, that is, the compression ratios of four compressors and the compression energy. Consequently, the power de-rate is mainly influenced by the operating pressure of the stripper, which is the sole parameter that directly concerns the overall integrated process. A simulation for calculating the power de-rate is performed by manipulating the stripper operating pressure without changing the L/G value. The operating range is from 1 to 2 bar based on the reboiler temperature. Rochelle reported that MEA loss owing to thermal degradation mainly occurs in the reboiler and reboiler sump, and that the higher temperature of the stripper lowers not only the energy requirement of the stripper but the capital cost of the stripper column and compressors (Rochelle, 2012). Therefore, the operating condition range of the stripper is solely determined by thermal degradation of the solvent. Although Davis (Davis and Rochelle, 2009) proposed an operating pressure of 3 bar and 132 °C for 30 wt% MEA, many CO_2 capture systems with aqueous MEA have been designed to operate at a maximum temperature of 120 °C, which is equivalent to 2 bar in the system used in this study. The profiles of temperature and mass fraction of the absorber and the stripper are shown in Figure 2-8 and Figure 2-9. Figure 2-

10 (Abu-Zahra et al., 2007; Ahn et al., 2013; Gao et al., 2014; Oexmann and Kather, 2010) is comparisons of the simulation results with other articles. The regeneration energies according to stripper pressure and L/G ratio have good agreements in the tendencies with those. Figure 2-11 and Figure 2-12 clearly shows the overall effect of changing the operating pressure of the stripper. In the CO_2 capture process, an increased operating pressure tends to decrease the solvent regeneration energy and elevate the temperature at the reboiler of the stripper. The result of the base case CO_2 capture process is 3.4 GJ/tonCO_2 regeneration energy and a reboiler temperature of 114 °C (90 % CO_2 removal, 1.5 bar of stripper pressure, and 3.7 L/Sm^3). The regeneration energy is sharply decreased to 3.59 GJ/tonCO_2 for an operating pressure of 1.25 bar and then stabilizes at about 3.3 GJ/tonCO_2 as the operating pressure of the stripper is further increased in 90% CO_2 removal. With CO_2 removal rate of 95 %, the regeneration energy is higher than the ones of 90 % and 85 % CO_2 removal rates. At higher stripper pressure, the difference in the regeneration energy tends to be smaller. Unlike the regeneration energy, the stripper reboiler temperature shows no variation according to the CO_2 removal rate.

Based on the result of the simulation for the CO_2 capture and liquefaction processes, the power de-rate is calculated for steam extraction at the IP-LP crossover pipe and the first LP turbine, as shown in Figure 2-13. The power de-rate is higher using pressure reducing values compared with using backup turbines. Moreover, steam extraction at the IP-LP crossover pipe resulted in a

higher power de-rate than using steam from the first LP turbine with pressure reducing valves. In base case, the power de-rates for extraction at the IP-LP crossover pipe and LP turbine are 27.0 % and 23.0 %, respectively. Also, with backup turbines the IP-LP crossover pipe steam had a slightly higher power de-rate than the LP steam (18.9 % and 17.9 %, respectively). Therefore, the steam extraction location for lower power de-rate should be the first LP turbine (Figure 2-5, (E)). However, the cost of turbine is significantly higher than pressure reducing valve. Other factors, such as capital cost, easiness of retrofit, or modifiability of the process control to use an additional backup turbine should be taken into account.

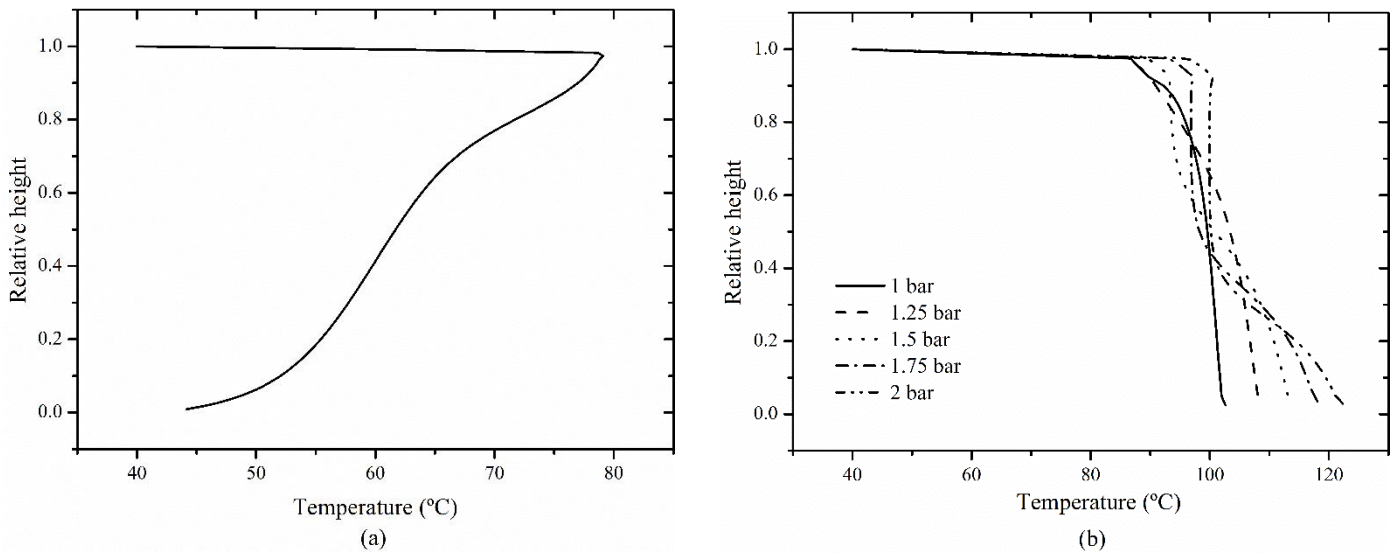

Figure 2-8. Temperature profiles of (a) the absorber and (b) the stripper at different operating pressures.

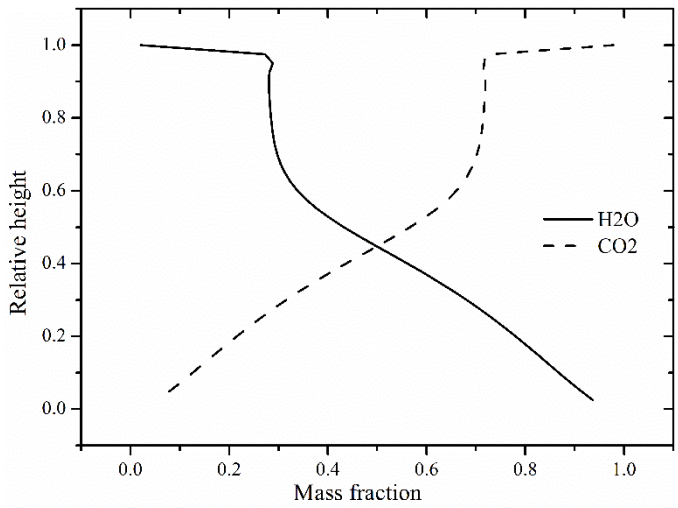

Figure 2-9. H_2O and CO_2 mass fraction according to the relative height of the stripper column.

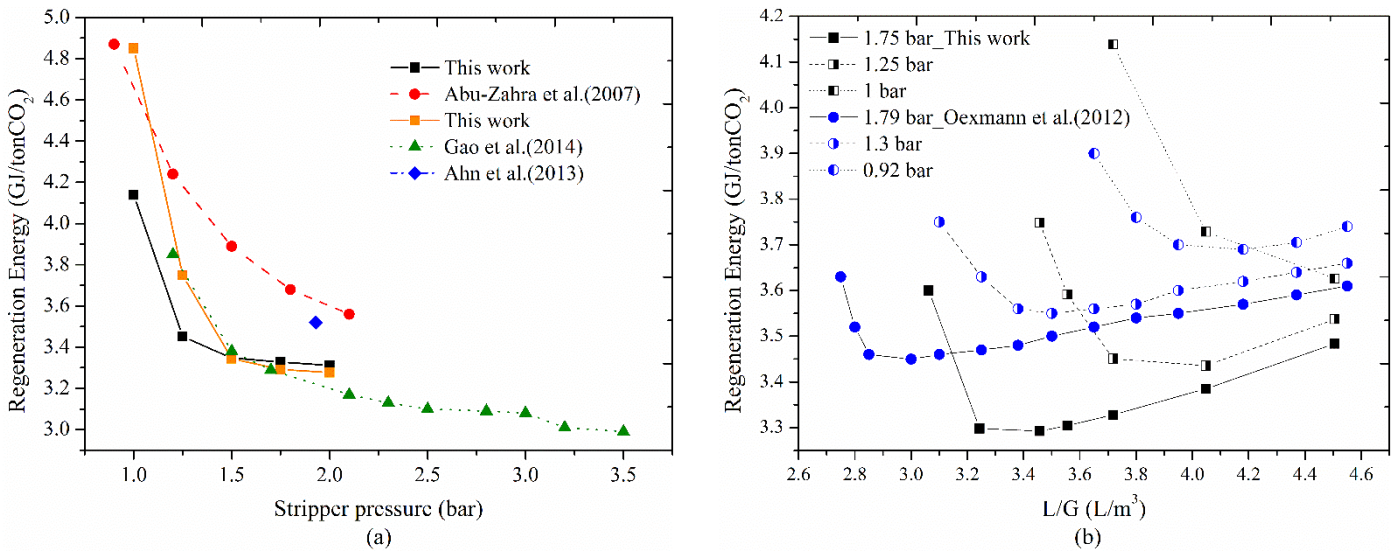

Figure 2-10. Result comparisons of the regeneration energy according to (a) stripper pressure and (b) L/G ratio (Lean loading information of ■ (black) 0.24, ■ (orange) 0.22, ● (red) 0.242, ▲ (green) 0.25, ◆ (blue) 0.231).

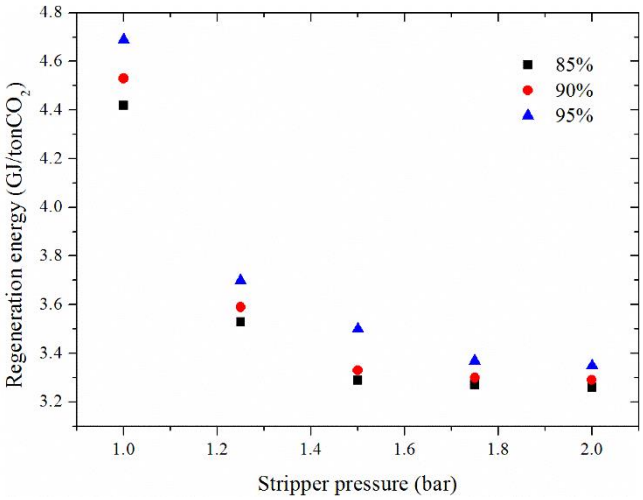

Figure 2-11. Stimulation results for the effect of the stripper operating pressure on the regeneration energy.

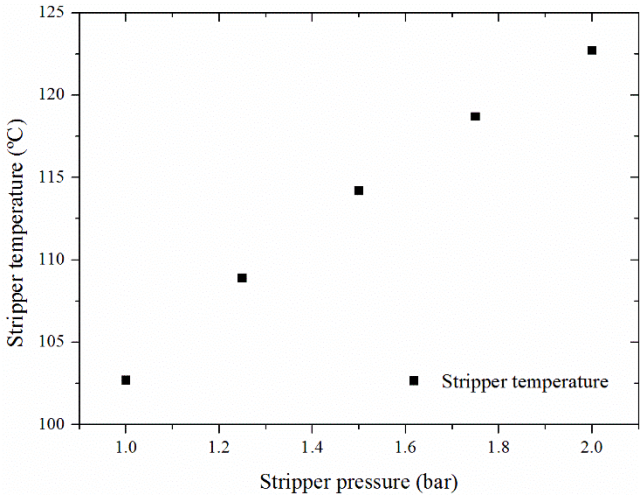

Figure 2-12. Simulation results for the effect of the stripper operating pressure on the stripper temperature.

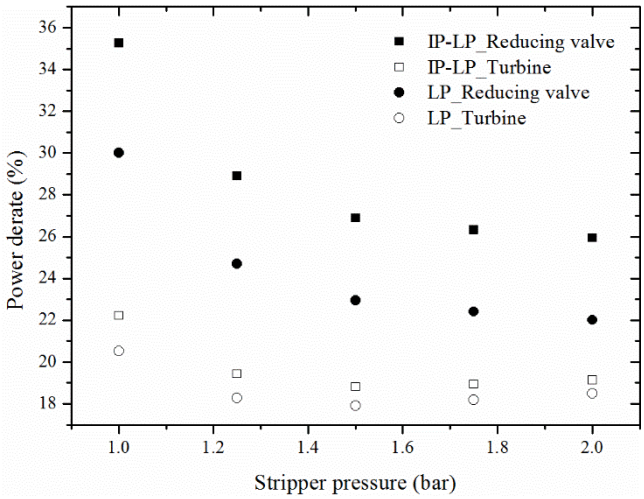

Figure 2-13. Simulation results for the effect of the stripper operating pressure on the power de-rate of the steam cycle (90% capture rate).

2.4.1.2. Effect of Liquid to Gas Ratio

The liquid to gas ratio in the capture process is the amount of lean amine solvent supplied compared with the amount of incoming flue gas to the absorber; this variable is solely influential in the capture process. As the amount of incoming flue gas is constant in the used model, L/G can be explained solely with the lean amine solvent flow rate (liquid, L) and the amount CO_2 held in the lean amine solvent (lean loading). Explanations of L/G often involve $\Delta\alpha$, which is the difference between rich loading and lean loading; however, rich loading is dependent on the amine flowrate and lean loading to satisfy a targeted amount of CO_2, as shown in the following simplified Eqn. (2-6) and Eqn. (2-7).

$$\dot{m}_{CO_2} = \dot{m}_{MEA}\Delta\alpha \tag{2-6}$$

$$\Delta\alpha = \alpha_{rich} - \alpha_{lean} \tag{2-7}$$

Figure 2-14 shows the simulation result for the regeneration energy when L/G is manipulated at fixed stripper operating pressures. The regeneration energy is first reduced by increasing L/G until an optimum value is reached when the slope of the curve is near zero, and then the regeneration energy slightly increases at higher L/G values. The regeneration energy is more affected by L/G at the lower stripper pressure. At 1 bar, the regeneration energy varies from 9.9 to 3.63 GJ/tonCO_2, whereas it varies from 3.71 to 3.25 GJ/tonCO_2 at 2 bar. This result means that it is critical to operate the capture

process near the optimum L/G for a stripper operating pressure to minimize the regeneration energy and power de-rate, especially at lower stripper pressures.

As the stripper operating pressure increased, the optimum L/G is observed at lower values. For example, in the case of 90 % CO_2 removal, at 1 bar, the minimum regeneration energy is observed at L/G of 4.51 L/m^3, whereas at 2 bar, the minimum value is observed at L/G of 3.24 L/m^3. The lowest regeneration energy is 3.25 GJ/tonCO_2 at L/G of 3.24 L/m^3 and a stripper operating pressure of 2 bar. Also, with the case of 95 % CO_2 removal, the minimum regeneration energy is at higher L/G ratio than the cases of lower removal rates.

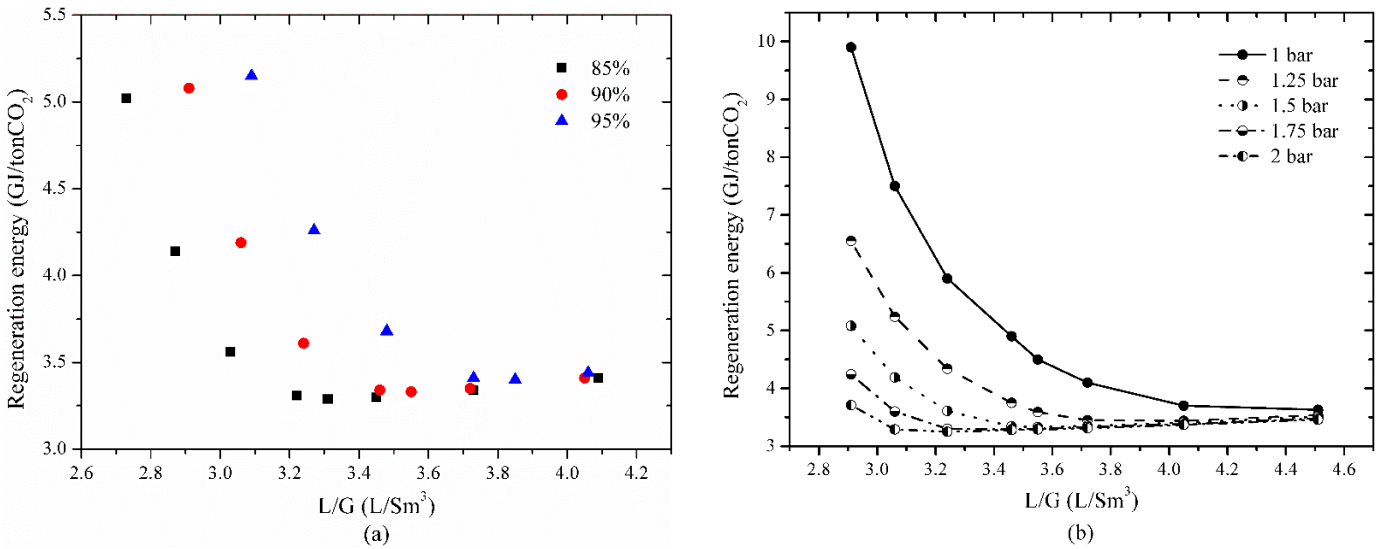

Figure 2-14. Simulation results for the effect of liquid to gas ratio on the regeneration energy (a) at stripper pressure of 1.5 bar and (b) of 90% CO_2 removal.

2.4.2. Liquefaction Process for Shipping

A major energy consumer in the liquefaction process is the compression. The compression energy is mainly determined by the compression ratio (P_2/P_1) and flowrate ($\dot{m}$), as indicated in equation (3). The inflow rate to the first compressor is determined by the pressure and temperature of the inflow gas. The amount of CO_2, which is the majority of the inflow species, is a constant value set by the design specifications of the CO_2 capture process and is independent of the stripper pressure. However, the composition of the inflow is determined by the mixture vapor-liquid-equilibrium (VLE) at a certain pressure and temperature (partial condenser, 40 °C), and the total inflow rate varies, mainly owing to the amount of H_2O. Furthermore, the composition of the inflow gas is not significantly changed by manipulating L/G. Therefore, the compression energy is mainly effected by the stripper pressure. As stripper pressure increases from 1 to 2 bar, the compression energy for the liquefaction process linearly decreases in all cases of removal rates, as shown in Figure 2-15.

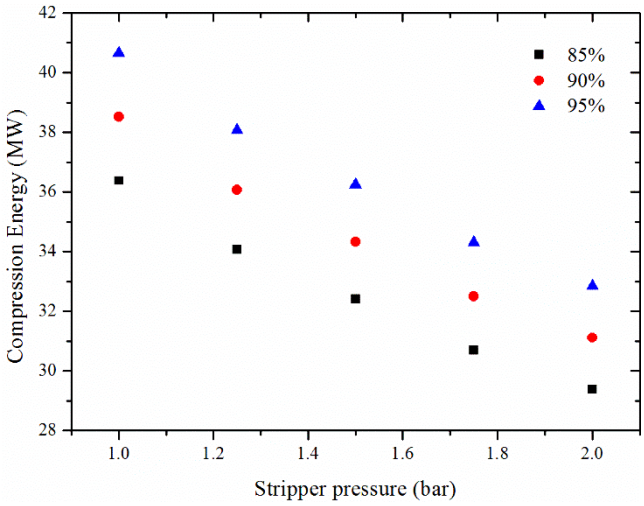

Figure 2-15. Effect of stripper pressure on compression energy requirement.

2.4.3. Power De-rate Reduction

The power de-rate is derived from the simulation result for the integrated process using Aspen Plus-MATLAB interface to reduce cumbersome procedures. Figure 2-16 show a 3-dimensional power de-rate graphs for the backup turbine case obtained by manipulating the stripper operating pressure and L/G ratio. Higher power de-rates are observed at lower operating pressure with lower L/G, whereas high operating pressures generally generate lower power de-rates regardless of L/G over a selected range. However, the minimum power de-rate using a backup turbine and steam extraction at the LP crossover pipe occurs at a lower pressure (Figure 2-16), for example, with an intermediate L/G of 1.25 bar and 4.05 L/m^3 in the case of 90 % removal. As the power de-rate in this integrated system is minimized by manipulating the most influential variables, it is predicated that the minimum achievable power de-rate that could be obtained by including all the possible variables would be similar. The details of the optimizations are listed in Table 2-8.

Lowering the regeneration energy has been at the core of research on the capture process and many researchers improved the regeneration energy through process modifications and alternatives. Figure 2-17 shows the relationship between the power de-rate and regeneration energy of the capture process. In general, an integrated process with a lower regeneration energy tends to have a lower power de-rate; however, the minimum power de-rate does not occur at the condition that generates the lowest regeneration energy. The

minimum power de-rate is 17.7%, which is 0.7% lower than that at the lowest regeneration energy with a stripper pressure of 2 bar and a L/G of 3.24 L/m^3. This result is significantly different from previous research that proposed higher stripper pressures for optimum operating conditions. This indicates that the optimum operating conditions for the unit processes (capture and liquefaction processes) are different from those for the integrated process owing to the steam extraction process.

In the stripper reboiler, the heat duty for solvent regeneration decreased with increasing stripper pressure, whereas its temperature increased. Higher temperatures in the reboiler require steam with a higher temperature and thus with a higher pressure. Therefore, the turbine train in the steam cycle is able to reduce the power output loss more than when the lower stripper pressure is used by extracting less steam, as shown in Figure 2-18. However, the expansion ratio of the backup turbine in the steam extraction unit is decreased. Furthermore, the compression energy in the liquefaction process decreased with increased stripper pressure. This is why the optimum condition for the power de-rate occurred at a lower stripper pressure even though more extracted steam and compression energy are required. The operating conditions for the lowest steam extraction are not equivalent to those for the minimum power de-rate. Table 2-9 shows the optimized power de-rate value according to each design option.

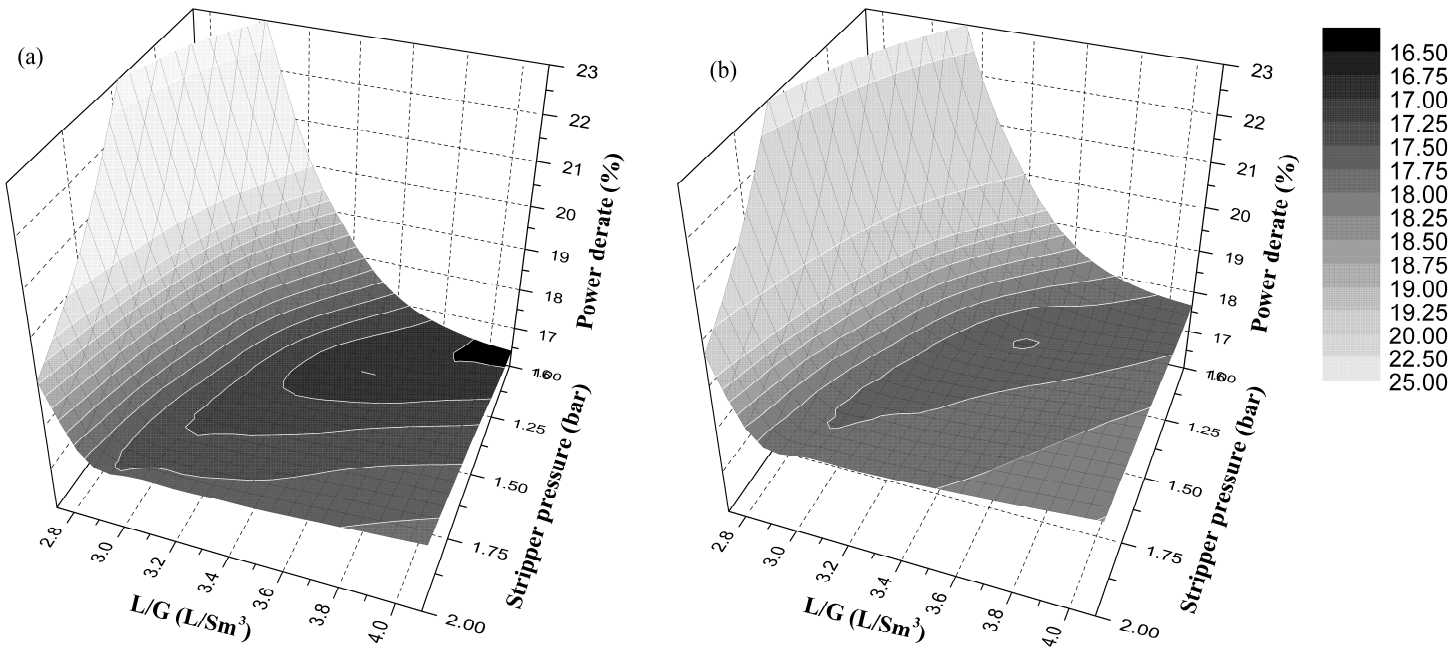
(a)
(b)
Power derate (%)
23
22
21
20
19
18
17
L/G (L/Sm3)
2.8
3.0
3.2
3.4
3.6
3.8
4.0
Stripper pressure (bar)
2.00
1.75
1.50
1.25
16.50
16.75
17.00
17.25
17.50
17.75
18.00
18.25
18.50
18.75
19.00
19.25
20.00
22.50
25.00

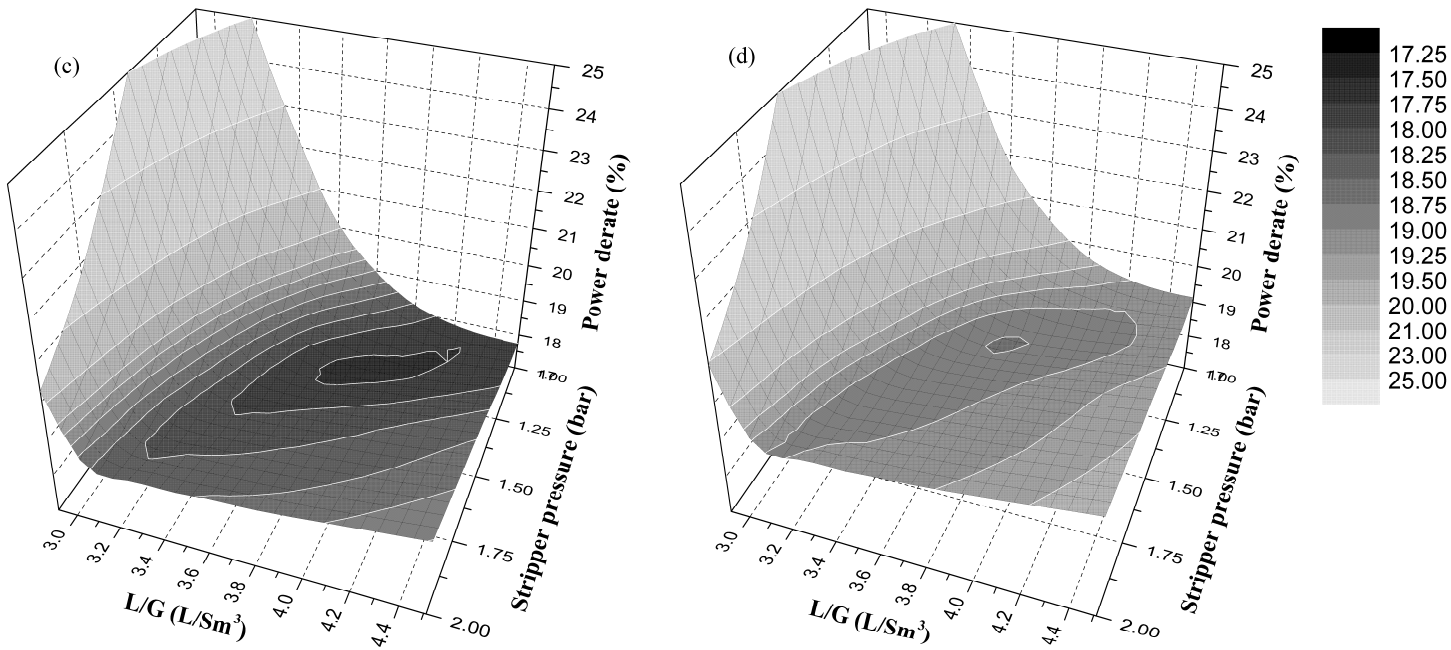
(c)
(d)
Power derate (%)
Stripper pressure (bar)
L/G (L/Sm3)
25
24
23
22
21
20
19
18
1.00
1.25
1.50
1.75
2.00
3.0
3.2
3.4
3.6
3.8
4.0
4.2
4.4
17.25
17.50
17.75
18.00
18.25
18.50
18.75
19.00
19.25
19.50
20.00
21.00
23.00
25.00

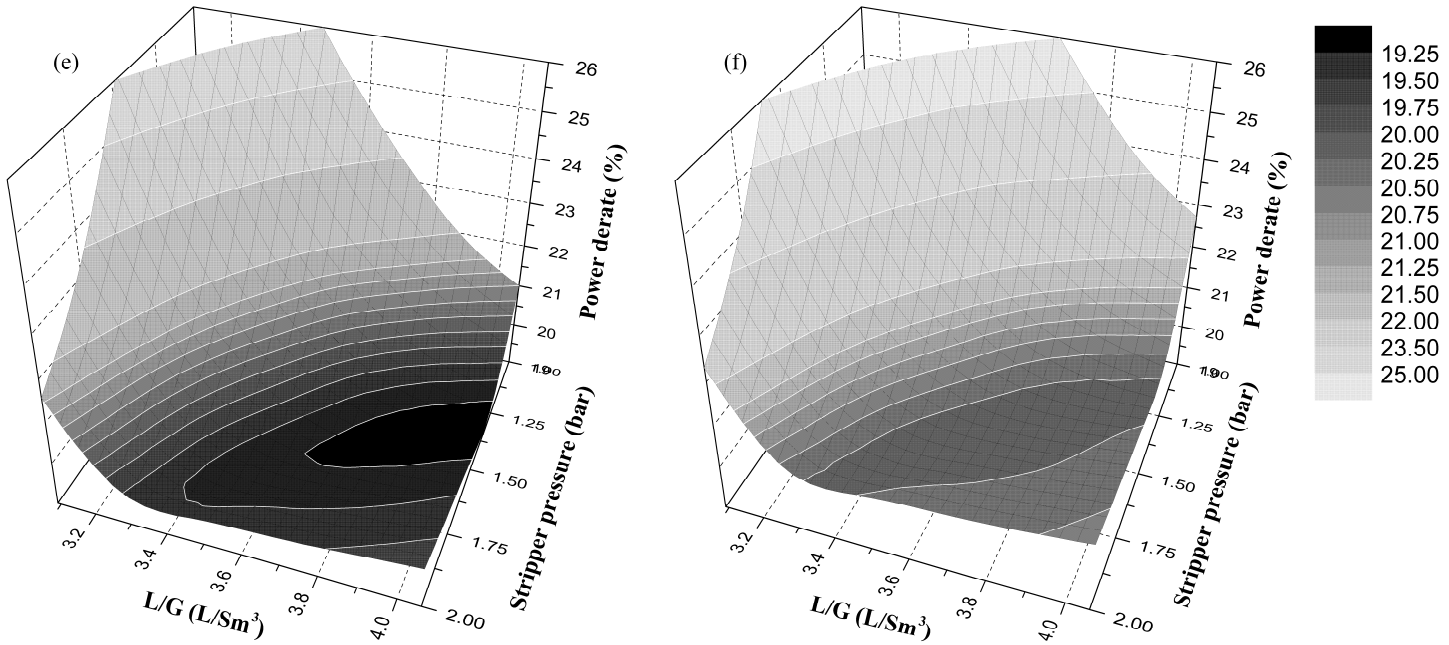

Figure 2-16. Effect of stripper pressure and L/G on the power de-rate (steam extraction unit process with backup turbine): (a) 85% capture, LP steam; (b) 85% capture, IP-LP crossover steam; (c) 90% capture; (d) 90% IP-LP crossover steam; (e) 95% capture, LP steam; (f) 95% capture, IP-LP crossover steam.

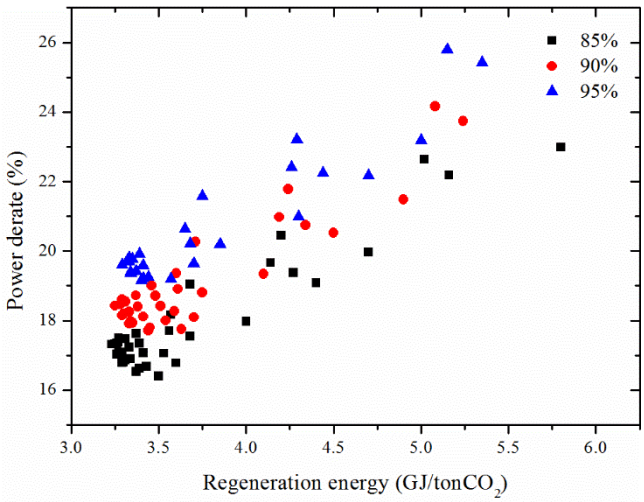

Figure 2-17. Power de-rate at different regeneration energies.

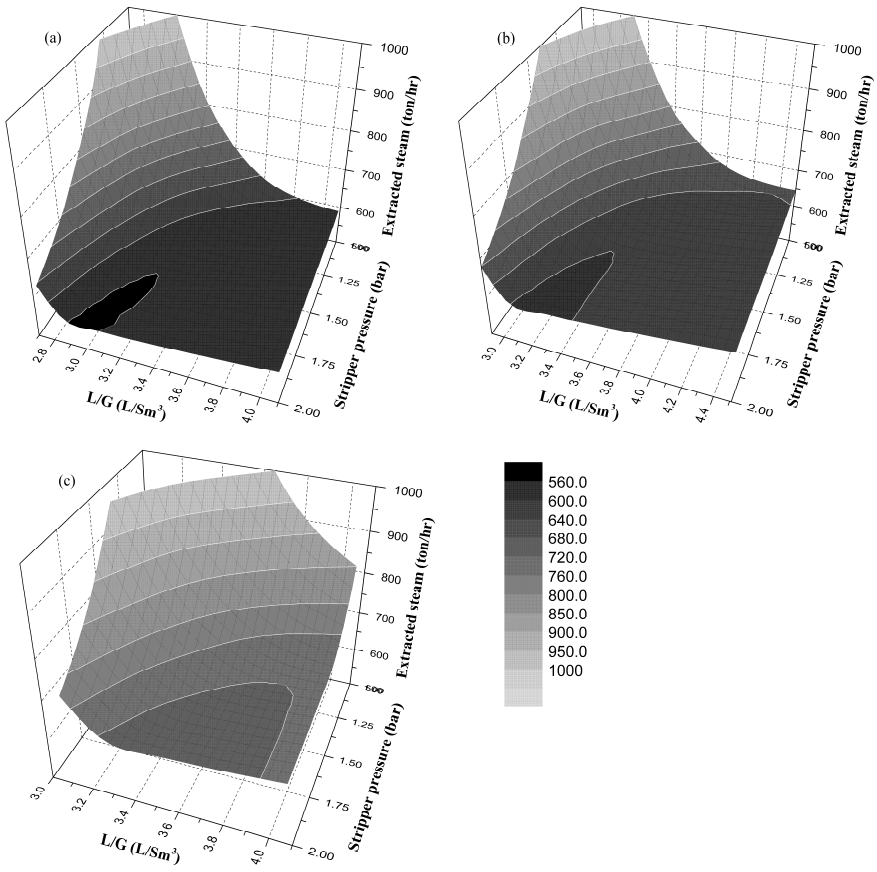

Figure 2-18. Effect of stripper pressure and L/G on extracted steam flow rate: (a) 85% capture, (b) 90% capture, and (c) 95% capture.

Table 2-8. Optimization results (90 % removal).

P_{str}	RB duty	Regen. E	RB T	Opt. L/G	$\dot{m}_{ex}$	$P_{bt,ratio}$	E_{comp}	Power output [a]	BT power	D [b]
bar	GJ/hr	GJ/tonCO_2	°C	L/m^3	ton/hr		MW	MW	MW	%
1	1,436	3.63	102.2	4.51	645.7	6.2	38.5	448.6	42.3	17.8
1.25	1,360	3.44	108.6	4.05	616.6	5.0	36.1	454.6	34.0	17.7
1.5	1,319	3.33	114.0	3.55	602.2	4.2	34.3	458.1	27.7	17.9
1.75	1,303	3.29	118.7	3.46	598.7	3.7	32.5	459.6	23.1	18.2
2	1,289	3.25	122.8	3.24	595.3	3.2	31.1	461.1	18.7	18.4

[a] Plant power output with CO_2 capture process

[b] Net plant power with CCS = Power output + Backup turbine power − Compression energy

Table 2-9. The optimized power de-rate according to each design option.

CO_2 capture rate	Type of depressurizer	Steam extraction location			
		IP-LP crossover steam		LP steam	
85 %	Pressure reducing valve	24.2 %	2 bar, 3.0 L/Sm^3	20.5 %	2 bar, 3.0 L/Sm^3
	Backup turbine	16.4 %	1 bar, 4.1 L/Sm^3	17.6 %	1.25 bar, 3.7 L/Sm^3
90 %	Pressure reducing valve	25.7 %	2 bar, 3.2 L/Sm^3	21.8 %	2 bar, 3.2 L/Sm^3
	Backup turbine	18.8 %	1 bar, 4.5 L/Sm^3	17.6 %	1.25 bar, 4.1 L/Sm^3
95 %	Pressure reducing valve	27.4 %	2 bar, 3.5 L/Sm^3	23.2 %	2 bar, 3.5 L/Sm^3
	Backup turbine	20.2 %	1.75 bar, 3.7 L/Sm^3	19.6 %	1.25 bar, 4.1 L/Sm^3

CHAPTER 3. Design of Carbon Dioxide Dehydration Process using Derivative-free Superstructure Optimization

3.1. Overview

Numbers of studies focused on CO_2 capture and liquefaction process owing to their high cost and energy consumption (Aspelund and Jordal, 2007; Figueroa et al., 2008; Lee et al., 2012; Lin and Chen, 2011; Padurean et al., 2011; Rubin et al., 2007; Scheffknecht et al., 2011; Versteeg and Rubin, 2011; Wall et al., 2011). Dehydration processes, on the other hand, is approximated using simple models thus they are often economically underestimated in spite of the potential importance of the process in CCS chain (Kemper et al., 2014). Dehydrating high purity CO_2 stream after the capture process is essential because the CO_2 product stream is usually saturated with water, which may cause operational problems such as hydrate formation and corrosion in downstream transportation and injection systems. Low water content is, therefore, critical for the process operation and safety.

Dehydration processes lowering the water content of captured CO_2 include compressor inter stage cooling, Joule-Thomson cooling, refrigeration, supersonic separation, solid desiccants, and liquid desiccants (Kemper et al., 2014; Machado et al., 2012; Netusil and Ditl, 2011; Scholes et al., 2012). Some of these processes such as compressor inter stage cooling and J-T cooling

cannot achieve low water content, thus additional dehydration is often required to meet specifications for CO_2 transportation. Triethylene glycol (TEG) based absorption and molecular sieve adsorption are known to be the most suitable to meet the severe water content specification for CCS purpose (Kemper et al., 2014). Glycol system is widely and successfully used for natural gas dehydration due to its advantages such as simplicity in operation (GSAP, 2004). Especially, TEG has low vapor pressure, evaporation loss, and thermal degradation compare to other glycol solvents.

The high energy requirement for the dehydration process has encouraged many researchers and companies to develop enhanced glycol processes. Most of these processes regenerate the water-rich TEG to the water-lean TEG to minimize solvent usage, and can achieve the low water concentration. Advanced process configurations can also achieve the reasonably low water concentration with the lower energy consumption. Stripping gas injection is one of the process alternatives often implemented. Patented process Drizo™ by Proser-NAT is an alternative design to traditional stripping gas units by using internally generated stripping gas. COLDFINGER® by Gas Conditioners International condenses and extracts water from the vapor phase using a cold coil or tube bundle (Netusil and Ditl, 2012). Also, a mixture of TEG with other solvents were proposed by Rincón et al. (2016), a mixture of TEG with lean oil (LO), by Paymooni et al. (2011), a mixture of TEG with toluene or isooctane

(Paymooni et al., 2011; Rincon et al., 2016). However, most of these processes are applicable only to the natural gas dehydration, so it is difficult to apply directly to CO_2 dehydration system. Alternatives for absorption process include column intercooling, interheating, split flow or staged feed, and vapor compression (VRC). These alternatives lower the solvent regeneration energy by reducing the latent or sensible heat requirement of the regeneration column reboiler. Column intercooling and feed gas split flow increase the solvent's absorption capacity and rich solvent loading by cooling the mid-bottom of the absorber (Biliyok et al., 2012; Chang and Shih, 2005; Jung et al., 2013b; Le Moullec and Kanniche, 2011; Moser et al., 2011; NETL, 2011; Plaza et al., 2010). Column inter heating and staged feed of cold rich solvent decrease the temperature of inlet stream or top stage (Aroonwilas and Veawab, 2007; Karimi et al., 2012b; Soave and Feliu, 2002; Van Wagener and Rochelle, 2011). Lean, rich, and mechanical vapor compression (LVR, RVR, and MVR) decrease the temperature of inlet stream by vaporizing the solvent under the lower pressure, recompressing, and sending to the column bottom (Fernandez et al., 2012; Jassim and Rochelle, 2006; Jeong et al., 2015; Jung et al., 2015; Karimi et al., 2011, 2012a; Le Moullec and Kanniche, 2011; Lee et al., 2016). Some of these alternatives show the improvement in terms of energy efficiency, but they may increase the process capital cost due to additional equipment or utilities.

Solid desiccants including gels, alumina, and molecular sieves are also possible options for dehydrating captured CO_2. Dehydration units using these desiccants are able to achieve very low dew point temperature in product or outlet streams. For example, −150°F of dew point can be achieved with molecular sieves (GSAP, 2004; IEAGHG, 2014b). However, they are generally more expensive than glycol units in operation and maintenance. Therefore, their use is limited in cases that very low dew point temperature or water content is essential.

The optimal design of CO_2 dehydration process can be carried out using the superstructure optimization. Almost all process alternatives are included in a superstructure, thus the optimal process design can be obtained through mathematical formulation and optimization. Recently, superstructure optimization using rigorous process model is applied in the optimum CO_2 capture and conditioning process design (Lee et al., 2016) and micro channel reactor (Na et al., 2017a). Trespalacios and Grossmann (Trespalacios and Grossmann, 2014) presented a comprehensive review of superstructure optimization method in process design. To find the optimal process configuration in a given superstructure, mixed integer non-linear programming (MINLP) has been widely used (Grossmann, 1985; Grossmann, 1989; Grossmann, 1990).

In this chapter, the superstructure-based techno-economic evaluation of CO_2 dehydration process with four-stage compression is performed. In the chapter 3.2, detail description of CO_2 dehydration process using TEG is given with thermodynamics modeling. Experiment data set is used for validating the selected model with estimated parameters. Superstructure design is described in the chapter 3.3, which gives detail information of unit operations and the reason why each unit operations should be considered. In the optimization formulation section, chapter 3.4, derivative-free process simulator based mixed integer nonlinear programming (MINLP) formulation is introduced. Finally, the optimal CO_2 dehydration process is suggested, and sensitivity analysis and Monte Carlo simulation is performed with several sub-optimal alternatives.

3.2. Modeling Basis

3.2.1. Design Specification

Flue gas from power plants combusting hydrocarbon fuels contains some impurities such as air components, SO_2, NO_2, CO, and H_2O. Many researchers discussed how these impurities affect CO_2 sequestration and what the allowable concentrations in the stream are (Skaugen et al., 2016; Wetenhall et al., 2014). Among these impurities, the presence of free water in gas and liquid CO_2 stream may cause problems on the operation and safety of the CO_2 sequestration such as corrosion and hydrate formation. Transporting CO_2 with pipelines from the source to the injection location without strict limitations on contaminants (e.g., free water, acidic compounds, and oxygen) causes a significant corrosion problem by generating aqueous phase forms with an strong acidity in the presence of water (Choi et al., 2010; Cole et al., 2011). CO_2 hydrate also causes operational problems by blocking the pipelines and/or damaging rotating equipment such as a pump. Therefore, the precise control of water content is a top priority to keep the process safe and economical. Burgass et al. (2014) performed an experimental study in equilibrium between CO_2 and hydrate. CO_2 and hydrate are in equilibrium at 70 ppm mole of water at 20 bar and 253.15 K (Chapoy et al., 2014). Also CO_2 storage projects such as OCAP, Snøhvit LNG, Kingsnorth, Lacq, and Weyburn used 50 ppmv of water content in CO_2 stream (Maldal and Tappel, 2004; Noothout et al., 2014). We set the design specification of CO_2 water content to 50 ppmv for this study.

3.2.2. Thermodynamic Model

In order to predict thermophysical property of TEG, CO_2 and water, an activity model and equation of state are used for describing the liquid and the vapor phase, respectively. Eqn. (3-1) indicates iso-fugacity relation between liquid and vapor phase.

$$\phi_i^v y_i P = \gamma_i x_i f_i^l \tag{3-1}$$

Activity coefficient $\boldsymbol{\gamma_i}$ are calculated by Non-random two-liquid (NRTL) model (Renon and Prausnitz, 1968). The equation for the NRTL model for species i in a mixture of n component can be described as Eqn. (3-2) – (3-7).

$$\ln(\gamma_i) = \frac{\sum_{j=1}^{n} x_j \tau_{ji} G_{ji}}{\sum_{k=1}^{n} x_k G_{ki}} + \sum_{j=1}^{n} \frac{x_j G_{ij}}{\sum_{k=1}^{n} x_k G_{ki}} \left(\tau_{ij} - \frac{\sum_{m=1}^{n} x_m \tau_{mj} G_{mj}}{\sum_{k=1}^{n} x_k G_{kj}} \right) \tag{3-2}$$

$$G_{ij} = \exp(-\alpha_{ij} \tau_{ij}) \tag{3-3}$$

$$\tau_{ij} = a_{ij} + \frac{b_{ij}}{T} \tag{3-4}$$

$$\alpha_{ij} = c_{ij} \tag{3-5}$$

$$\tau_{ii} = 0 \tag{3-6}$$

$$G_{ii} = 1 \tag{3-7}$$

Where a_{ij} and b_{ij} are unsymmetrical interaction parameters.

For calculating gas pressure, Redlich-Kwong (RK) EOS (Redlich and Kwong, 1949) is used and the equation of RK for gas pressure for species i in a mixture of n component is given in Eqn. (3-8) – (3-12).

$$P = \frac{RT}{V_m - b} - \frac{a}{\sqrt{T}V_m(V_m + b)} \quad (3\text{-}8)$$

$$\sqrt{a} = \sum_{i=1}^{n} x_i \sqrt{a_i} \quad (3\text{-}9)$$

$$b = \sum_{i=1}^{n} x_i b_i \quad (3\text{-}10)$$

$$a_i = \frac{1}{9(\sqrt[3]{2} - 1)} \frac{R^2 T_c^{2.5}}{P_c} \quad (3\text{-}11)$$

$$b_i = \frac{\sqrt[3]{2} - 1}{3} \frac{RT_c}{P_c} \quad (3\text{-}12)$$

3.2.3. Data Regression and Validation

For the dehydration process modeling, NRTL-RK thermodynamic model is used in Aspen Plus. Note that Aspen Plus databank (APV88 ENRTL) does not completely provide interaction parameters of the dehydration system, thus we regressed interaction parameters using experimental data available in literatures. Vapor-liquid equilibria of TEG and water at 85 kPa experimental data (Mostafazadeh et al., 2009) is used for validating. The objective function of the parameter estimation problem is formulated using maximum likelihood method, Eqn. (3-13). Where NDG is the number of data groups in the regression case, NP is the number of points in data group n, and NC is the number of components present in the data group.

$$\text{obj} = \sum_{n=1}^{NDG} w_n \sum_{i=1}^{NP} \left[\left(\frac{T_i^e - T_i^m}{\sigma_{T,i}} \right)^2 + \left(\frac{P_i^e - P_i^m}{\sigma_{P,i}} \right) + \sum_{j=1}^{NC-1} \left(\frac{x_{i,j}^e - x_{i,j}^m}{\sigma_{x,i,j}} \right)^2 + \sum_{j=1}^{NC-1} \left(\frac{y_{i,j}^e - y_{i,j}^m}{\sigma_{y,i,j}} \right)^2 \right] \quad (3\text{-}13)$$

Decision variables are a_{ij}, a_{ji}, b_{ij}, and b_{ji}. Since c_{ij} usually set to a symmetric and constant parameter, c_{ij} set to 0.3 which is appropriate to small deviations from ideality. The objective function is solved using Britt-Luecke as the algorithm and Deming as the initialization method. The optimized regression parameter result of NRTL-RK model is shown in Figure 3-1. The weighted sum of squares is 78,149.9 and the liquid and vapor fraction are relatively accurately predicted at the required temperature interval. The regressed model is validated with the experimental data at 700 ppm and 800 ppm for the dew point, as shown in Figure 3-2. Thus, the thermodynamics model can be adequate applied to the process simulation and the optimization which will be following in the next sections. Table 3-2 summarizes the values of the binary parameters used throughout the optimization part and thesis.

Table 3-1. Binary Interaction Parameters for the System Water(i) + TEG(j).

Couple of components	Interaction parameters (NRTL)				
	aij	aji	bij	bji	cij (symmetrical)
Water + TEG	3.58898	8.21429	953.847	2,180.55	0.300

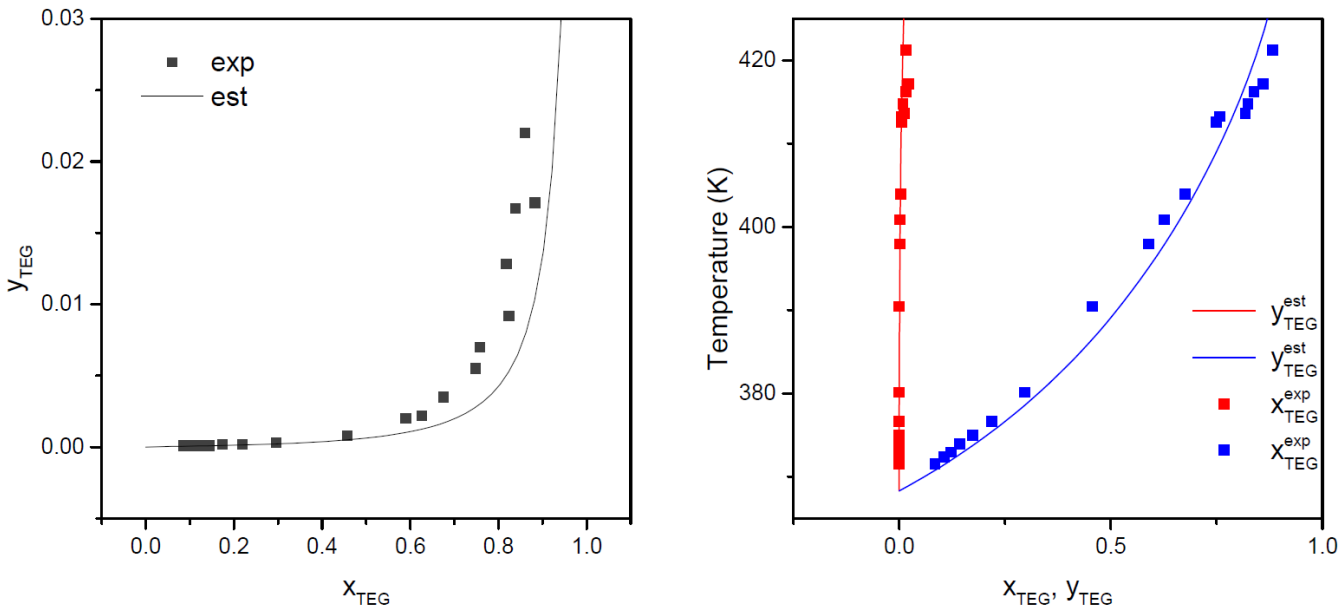

Figure 3-1. Validating result of NRTL-RK parameter regression by (a) T-xy curve and (b) x-y VLE curve.

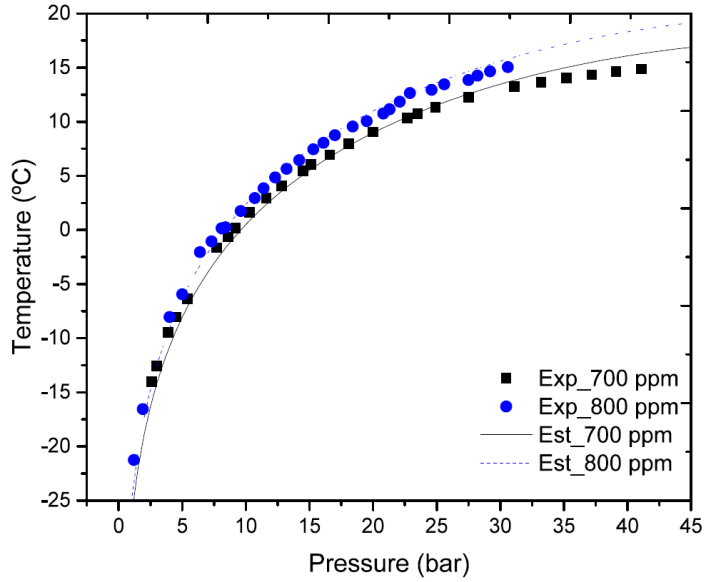

Figure 3-2. Water-CO_2 mixture dew point estimation using parameter regressed NRTL-RK method (Jarne et al., 2004).

3.3. Design of Superstructure

Herein, the design of the CO_2 dehydration process is carried out via superstructure optimization. A superstructure contains most of potential structural options of the process and the optimal design, operating conditions, equipment size, and cost are simultaneously decided though mathematical modeling and optimization. The superstructure modeling and the flowsheet simulation are carried out using Aspen Plus™ v8.8

Figure 3-3 shows the superstructure of the CO_2 dehydration process built for this study. The superstructure mainly consists of two parts; compression and dehydration. The compression receives CO_2 from the post combustion CO_2 capture process and compresses it to the high pressure that liquefies the CO_2 stream using cold seawater (20°C). The compressor has four stages, and intercooling units are placed in between the stages. The cooled CO_2 stream can be either further dried in the dehydration process or introduced to next compression stage. The dehydration process receives water saturated CO_2 stream and selectively absorbs water from the stream using TEG. The water rich TEG stream is, then, thermally regenerated in the still column and recycled back to the contactor to close the loop. The superstructure contains 30,720 possible process configurations. Four integer variables describes place of the dehydration process, the number of contactor stage, the number of still column

stages, and the feed stage of the still column. Five binary variables select process alternatives imbedded in the superstructure.

3.3.1. Compression Process

The CO_2 feed condition adopted in this study is taken from the Boryeong coal power plant operation data, and listed in Table 3-2. Note that we assume no impurities in the CO_2 stream except water based on the operation data. However, impurities such as H_2S, NO_x, and SO_x may appear in the captured CO_2 stream causing physical property change of the CO_2 stream and additional pretreatment processes may require when impurities are presented in the stream.

Table 3-2. The CO_2 feed condition.

Specification	Value
Temperature [C]	40
Pressure [bar]	1.5
Mass Flow [ton/hr]	406
Composition [mole %]	
H_2O	5%
CO_2	95%

The CO_2 feed stream is pressurized to 64 bar through the four-stage compression. The hot outlet stream from each compressor stage is cooled to 40°C using cooling water, and condensed water from the cooling is removed with flash separators. The dehydration process can be placed in between the compression stages. The dehydration process in before the first compressor

stage or after the last compressor stage is not considered because consequent processes either need huge amount of TEG solvent or cannot be regenerated to water lean solvent due to the presence of azeotrope at high pressure. Several tradeoffs are existed according to the location of the dehydration process. As the dehydration is located in the early stages, volumetric flow rates of the gas streams are increases resulting bigger equipment size. In addition, the more solvent may require reaching the same stream dehydration specification, since the saturation moisture level in the dehydration inlet stream is decreased as the pressure increases. However, the process operation with mild pressure is favorable in most time and the operation energy for pumps is also lower than that of the high pressure process. Therefore, the location of the dehydration process should be systematically selected rather than relying on heuristics.

3.3.2. Dehydration Process

The dehydration process mainly consists of an absorber (Contactor), a regeneration column (Still column), and a lean/rich stream heat exchanger. The water saturated CO_2 stream is introduced to the contactor and dried using TEG solvent. The dried CO_2 stream has >50 ppmv water concentration and send to the next stage of the compressor. The water rich TEG stream is then, preheated in lean/rich solvent heat exchanger by using the bottom stream of the still column. The reboiler duty of the still column can be reduced through the heat

integration in lean/rich heat exchanger. The water rich TEG solvent is thermally regenerated in the still column and sent back to the contactor through a cooler. The solubility of the water in TEG is increases as the temperature decreased (Figure 3-1), thus the low temperature is thermodynamically preferred for the TEG solvent introducing the contactor. However, the cold TEG solvent stream requires expensive refrigeration utilities. Therefore, the outlet temperature of the cooler is decided in the systematic method by treating it as a decision variable for the optimization.

The superstructure includes process alternatives such as rich solvent stream flash, rich solvent preheating, stripping gas injection, split flow configurations, and lean vapor recompression, and standalone process alternatives and combination of the alternatives are evaluated using an optimization solver.

The rich solvent stream flash separates fraction of light gases using pressure difference between the contactor and the still column. The still column is operated near ambient pressure while the pressure of the contactor is usually far higher depending on the location of the dehydration process. The rich TEG solvent stream, thus, inevitably lower the pressure, and light gases such as CO_2 and water are evaporated. These light gases can be separated using a simple flash separator and the flow rate of the still column feed stream can be reduced. The amount of vapor is increased through the heat integration between the condenser of the still column and the cold rich TEG solvent stream. With the

heat integration, the feed flow rate of the still column can be further reduced. However, the rich solvent stream flash and preheating may increase the reflux rate of the still column because the distillate tends to have higher concentration of the light key component, water.

The regeneration energy of the TEG solvent can be improved by introducing additional stripping gas. The vapor stream from the rich solvent stream flash can be used as stripping gas because it usually has high CO_2 concentration. The stripping gas can lower the concentration of water in the distillation, thus reflux rate, thus the TEG solvent regeneration energy can be reduced. However, the stripping gas is only available together when the flash separation and the bigger still column may be required due to the vapor flow rate increase in the column. The vapor stream from the flash separator is purged when the stripping gas option is not selected during the optimization.

One of the key factors lowering the still column reboiler duty is reducing the heat duty of the condenser. The solvent stream split flow configuration is one of the most straightforward ways to lower the condenser heat duty. The cold rich TEG solvent from the contactor is separated into two streams and the fraction of the cold stream directly introduce to the top of the still column without heat integration. The cold solvent stream reduces the heat duty of the condenser, and consequently the reboiler duty is decreased. However, the implementation of the split flow configuration should be selected carefully

because it often reduces the heat duty of the lean/rich heat exchanger due to the temperature pinch within the lean/rich solvent exchanger and may increase the TEG solvent regeneration energy. The lean vapor recompression process is another method that reduces the condenser duty of the column. The lean vapor recompression is a popular methodology reducing a solvent regeneration energy in an absorber-regenerator system and widely applied in the post combustion carbon capture process (Lee et al., 2016). The bottom stream of the still column is expanded through a valve making a liquid-vapor two phases. The generated vapor is separated using a flash column than reintroduce to the stripping section of the still column. The pressure difference owing to the expansion is compensated using a compressor. In the lean vapor recompression, a fraction of the heat of the hot stream is recovered through vapor and supplied directly to the stripping section. Consequently, the heat integration in the lean/rich solvent heat exchanger is reduced resulting the lower still column feed temperature while the same amount of heat is recovered from the hot stream. The condenser duty is decreased as the feed temperature decreases, thus the TEG solvent regeneration energy is also decreased (Jung et al., 2015; Lee et al., 2016). However, the LVR process requires additional unit operations such as a compressor, a flash column, and a valve. Thus, the capital investment cost is higher than the conventional dehydration process.

In the proposed superstructure, several nonlinear equality constraints are imbedded using Aspen Plus design spec blocks. The GA solver in MATLAB can be inefficient for solving MINLP with nonlinear equality constraints because of its randomness of the initial population generation. With the design spec block, the nonlinear inequality constraints can be handled within the process simulator and hided from the GA optimization.

$$x_{TEG,Distill}(reflux\ \ rate) = 100\ \ ppm \tag{3-14}$$

$$T_{rebolier}(P_{still\ \ cloumn}) < 200\ \ °C \tag{3-15}$$

$$x_{water,drygas}(\dot{\mathrm{m}}_{TEG}) = 50\ \ ppmv \tag{3-16}$$

The water purge stream from the still column should not contain TEG more than 100 ppm by mass because of the solvent loss and environmental issues (Eqn. 3-13). The high regeneration temperature of the solvent can degrade TEG, thus we limit the highest regeneration temperature to 200°C (Eqn. 3-15). In addition, the water content of the dry gas is limited to 50 ppmv (Eqn. 3-16). Although a permissible amount of water concentration in the CO_2 stream is still controversial, the 50 ppmv is generally accepted and thus used in many other studies concerning CO_2 transportation.

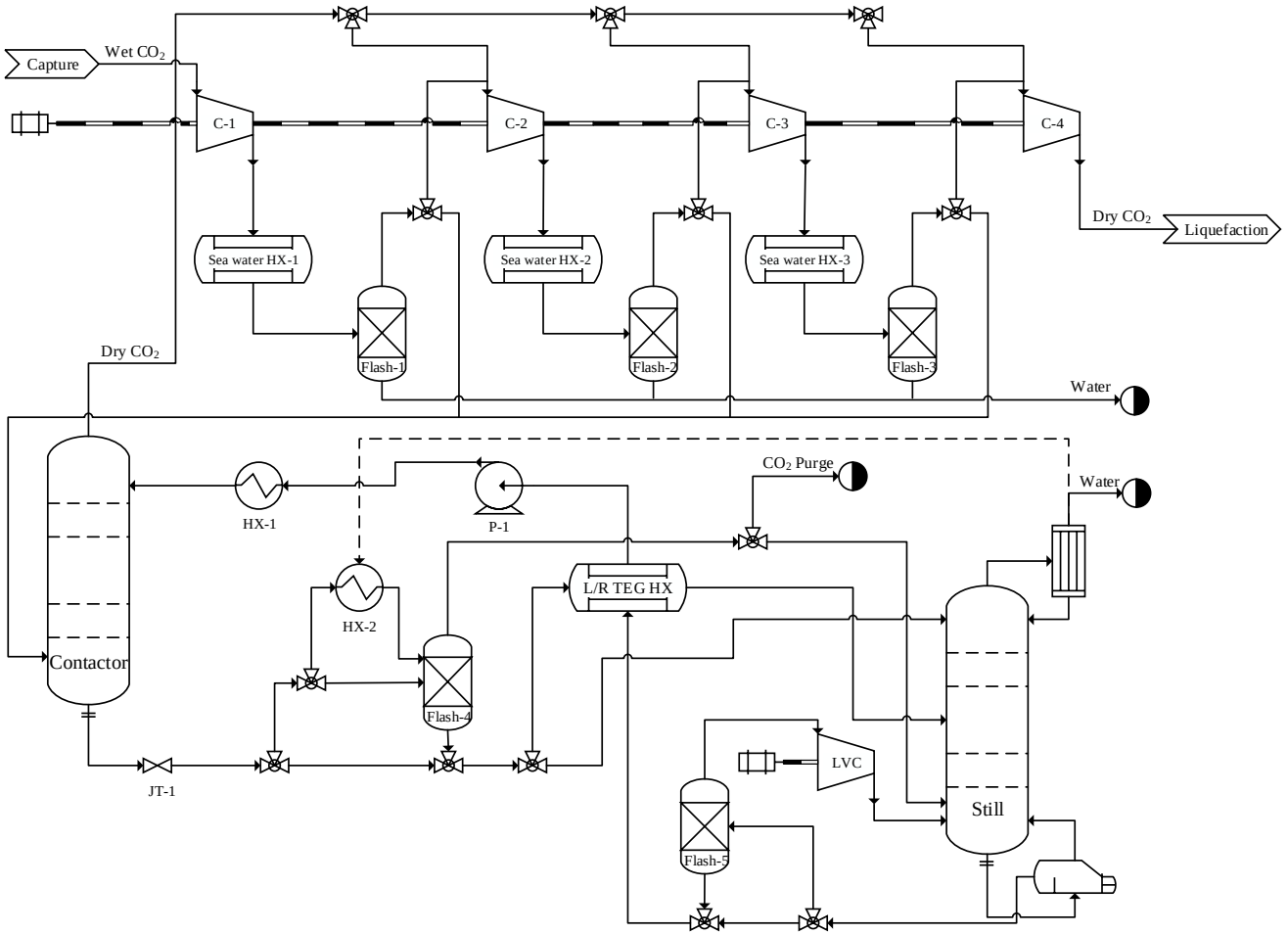

Figure 3-3. The superstructure of the CO_2 compression and dehydration process.

3.4. Process Optimization

Herein, we used the decomposition based superstructure optimization method proposed in Lee et al. (Lee et al., 2016). The proposed process methodology externally calculates the process simulation part using a sequential process simulator (Aspen Plus), thus it is structurally difficult to obtain the derivative value for each design variable. This type of optimization methodology is called derivative-free optimization (Conn et al., 2009). Stochastic solvers often apply to derivative free optimization, and it is able to obtain reasonable solutions for the mixed integer nonlinear programming (MINLP). Note that the convergence of the stochastic solver can become poor when hidden constraints exist because stochastic solvers generate the random population. The feasibility of the constraints can only be identified by the direct evaluation. If there is too much infeasible offspring in the early population, it tends to fail to escape to the feasible area appropriately in the next generation selection. Therefore, we try to overcome this by using enumeration with preprocessing and screening, and then proceed with MINLP superstructure optimization using GA.

3.4.1. Preprocessing & Screening

The three different process configurations of the compression process with dehydration are enumerated rather integrated in the superstructure. Each configuration is, then, optimized in terms of energy consumption.

$$\text{Min}\, E = \quad f(r) \tag{3-17}$$

$subject\ \ to$

$0 \leq r_i \leq 4, \qquad i = 1,2,3$

$h_j(\mathrm{r}) = 0, \qquad j = 1,2,3, \ldots\ldots, q$

where *r* represents pressure ratio of the first, second, and third compressor stage, and $h_j(\mathrm{r}) = 0$ represents equality constraints from process model equations.

The solution of the optimization problem together with unit operation and thermodynamic model in the process simulator provides input condition of the dehydration process. With the enumeration, the initial condition for the dehydration process can be assigned differently for different configurations, thus the convergence of the flowsheet can be greatly improved.

3.4.2. Optimization Problem Formulation

Optimization is performed with seven integer design variables and three continuous operating variables that make up the superstructure. Design variables can be further divided into four binary variables and three integer variables. Existence of flash (x(1)), preheater (x(2)), stripping gas injection (x(3)), and LVR (x(4)) are set as binary variables. In the case of the number of stage of contactor (x(5)), still column (x(6)), and inlet stream feed stage of still column (x(7)), integer variables are assigned for optimization. For operating variables, lean TEG cooling temperature (y(1)), stripping gas preheating temperature (y(2)), cold solvent split fraction (CSSF) (y(3)) are set to

continuous variables (Table 3-3). Base structure of the optimization problem is shown in Eqn. (J1). Constrained MINLP optimization type is included, and it is extremely difficult to solve this type of optimization problem involving both equality and inequality constraints and optimization with 10-dimensional variables. Fortunately, in the case of equality constraint (hs (x, y)), the process is already formulated as a process simulator model, so the optimizer automatically finds whether the area is feasible or infeasible for a particular design variable. If it is determined that it is an infeasible area in the simulator, it is not necessary to directly perform constraint handling on the GA because the aspen simulator itself returns fail in the convergence check and recognizes it as a hidden constraint and deactivates it using the penalty function on the optimization platform.

$$\min TAC(\mathrm{x}) = AIC(x,y) + AOC(x,y) + \gamma p(x,y)^2 \qquad \text{(P)}$$

$$h_o(\mathrm{x}) \leq 0$$

$$\mathrm{x} \subset \mathbb{Z}^{1\times 7}, y \subset \mathbb{R}^{1\times 3} \;\; \& \;\; \mathrm{LB} \leq \mathrm{x} \leq \mathrm{UB}$$

$$\mathrm{p(x,y)} = \begin{cases} 0 & if \;\; \mathrm{h_s(x)} = 0 \\ 1 & if \;\; \mathrm{h_s(x)} \neq 0 \end{cases}$$

Brief description of mathematical format of the optimization problem is given in Eqn. (P). Total annualized cost (TAC) is sum of an annualized investment cost (AIC), an averaged operating cost (AOC) and penalty term as $\gamma p(x,y)^2$ where p(x,y) is convergence of the process simulator. Thus, if

process simulator checks that the set of variable is infeasible for the process systems, it set p(x,y) as 1 for activate the penalty value ($\gamma = \$6.66 \times 10^9$). If flash exists, heater and stripping gas unit should be exist. Thus, the inequality eqn. (J1)-(J2) are set to internal constraints to verify that logics. Moreover, the still column feed stage should be located under the total stripper stages. Thus, the inequality eqn. (J3) is also set to satisfy it.

$$x(1) - x(2) \leq 0 \quad \text{(J1)}$$

$$x(2) - x(3) \leq 0 \quad \text{(J2)}$$

$$x(7) - x(6) + 1 \leq 0 \quad \text{(J3)}$$

Equations of investment cost of each units and consistence of operating cost follow the procedure of several literatures and detailed information is given in (Hasan et al., 2012; Lee et al., 2016).

Table 3-3. Summarizes type, description, and bounds of each variables.

Variables	type	Description	Upper bound	Lower bound
x(1)	Binary	flash (1= no flash)	0	1
x(2)	Binary	preheater (0 = no preheater)	0	1
x(3)	Binary	SG (1 = no stripping gas)	0	1
x(4)	Binary	LVR (1 = no LVR)	0	1
x(5)	Integer	contactor stage	3	10
x(6)	Integer	still column stage	3	10
x(7)	Integer	still column feed stage	2	9
y(1)	Continuous	lean TEG temperature	3	10

y(2)	Continuous	stripping gas preheating temperature	60	100
y(3)	Continuous	CSSF	0.01	0.2

3.4.3. Genetic Algorithm Interface Setting and Execution

GA algorithm is used to calculate the main MINLP. The GA formulation is performed in MATLAB and used a platform integrated through Aspen plus v8.8 and active X to calculate the objective function. 50 Populations are used, and the crossover fraction is set to 0.4, 0.6, and 0.8 for obtaining maximum reproducibility through various crossover fractions. Mersenne Twister is used for random number generation. There are two termination criteria, which are stall generation limitation and maximum generation. We set the consecutive stall generation limit as 5, and the maximum generation is set to 50. The GA optimization is terminated if one of the termination criteria satisfied, otherwise next generation is evaluated.

3.5. Results and Discussion

3.5.1. Optimization Results

The optimization is carried out using Aspen Plus v8.8 and MATLAB R2016a on a desktop computer with Intel® Xeon CPU E3-1230 v3 processor at 3.30 GHz (4 CPUs) and 16 GB RAM running Window 10. The average computation time for a function evaluation in process simulator is about 1.4 seconds. The trajectory of the best-found solution changes according to the number of function evaluations is shown in Figure 3-4. We enumerate the superstructure according to the compressor stage and the initial guesses for each superstructure are separately provided. The superstructures receive their feed stream from the 1 to 3 stage of the compressor and each of them is optimized independently. The crossover fraction of the GA is changed to 0.4, 0.6, and 0.8 for validating the reproducibility of the best-found solution. Since the population size is 50 and the maximum generation is 50, the maximum function evaluation is possible up to 2500 times. Note that five consecutive stall generations can be achieved within the 50 total generations.

The optimum process of the CO_2 compression and dehydration among 30,720 possible process configurations is shown in Figure 3-5. As in

Table 3-4, the optimum process configuration with the crossover fraction of 0.8 includes CSSF option with CO_2 feed stream extracted from the third stage of compression, three-stage contactor, ten-stage still column, and the feed

stream of still column goes into the sixth stage. The temperature of the lean TEG flowing into the top of contactor is 3.02°C and the fraction of the cold rich solvent fed to the top of still is 0.01. Note that x(2), x(3), and y(2), which are the existence of rich solvent preheater, whether the stripping gas is injected, and the temperature of stripping gas, have no physical meaning because the optimal process does not include a flash drum, $x(1) = 1$. These values exist only for improving the convergence of the simulation model in Aspen Plus by having a tiny amount in their streams. The total annualized cost (TAC) of the optimal process configuration is 5.67 M$/year. The rich solvent stream flash, rich solvent preheating, stripping gas injection, and LVR options are not selected. Detailed thermodynamic and economic analyses of the solution are further discussed in following sections.

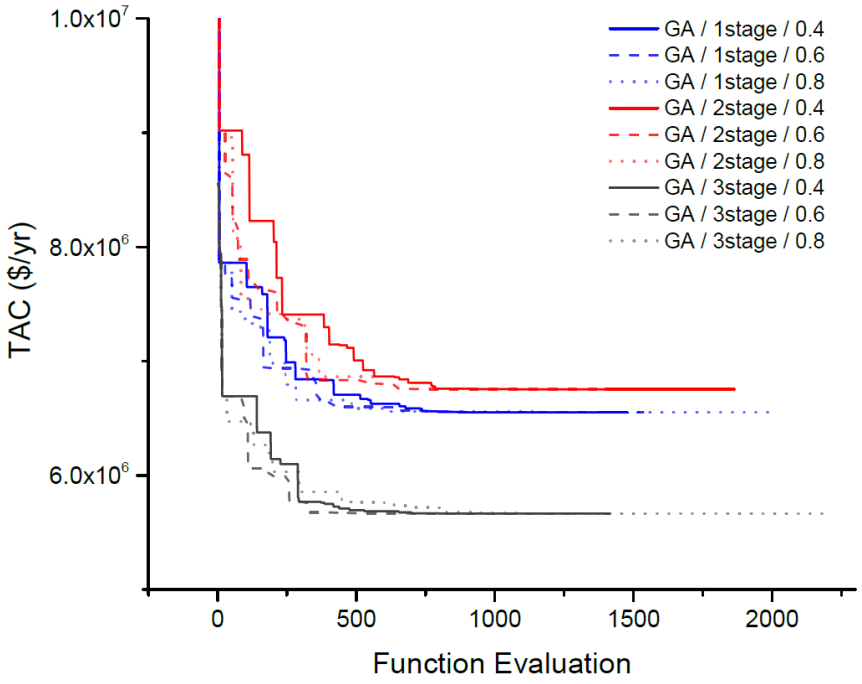

Figure 3-4. Best found solution trajectory of total annualized cost of non-convex MINLP problem with function of carbon dioxide dehydration process simulation model through function evaluation.

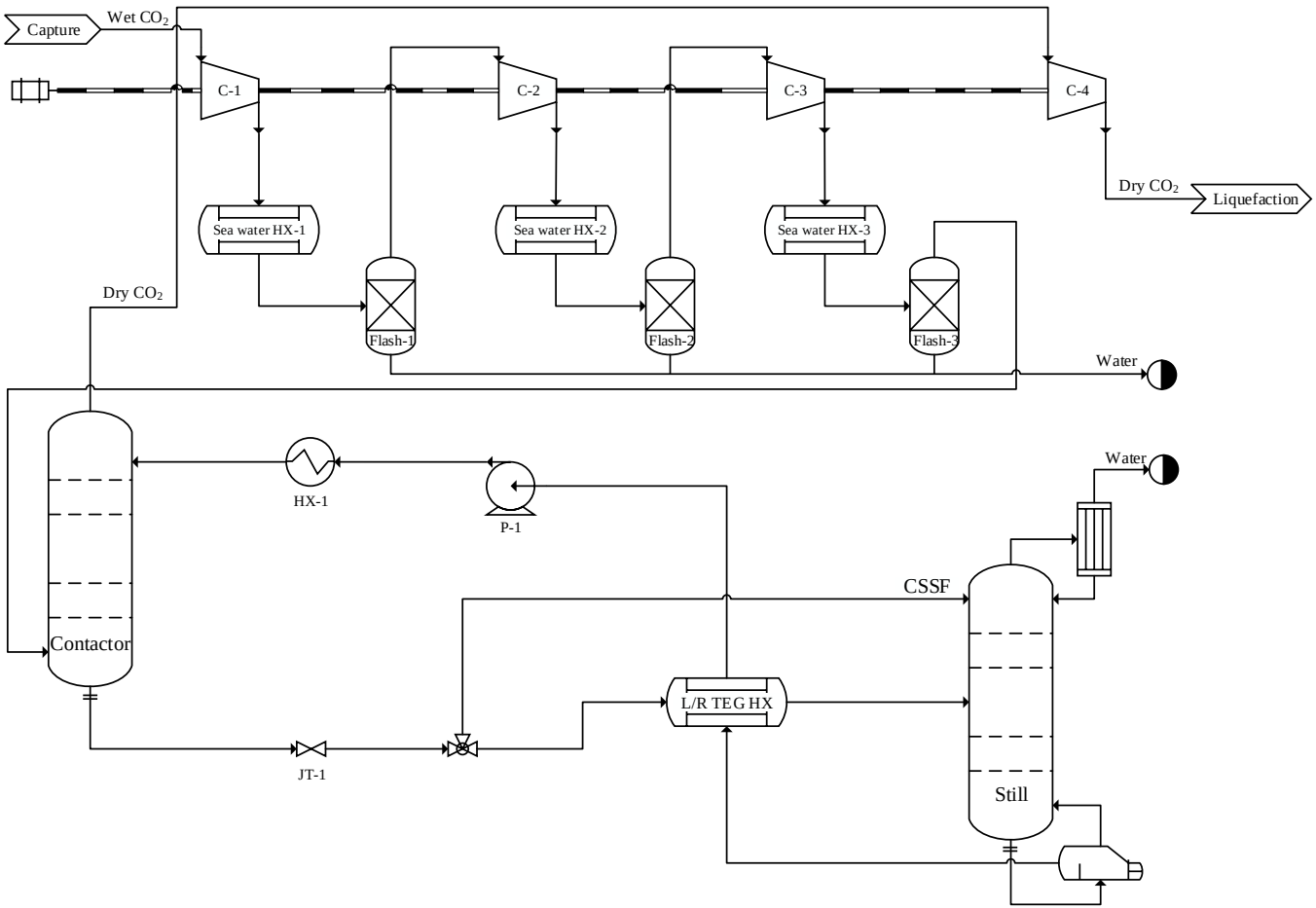

Figure 3-5. The optimal process configuration of the CO_2 compression and dehydration.

Table 3-4. Optimal solution for each compression stage and crossover fraction.

GA condition		Ob fn. value	Variables									
Comp. stage	Crossover fraction	TAC [$/yr]	x(1)	x(2)	x(3)	x(4)	x(5)	x(6)	x(7)	y(1)	y(2)	y(3)
1	0.4	6,551,573	1	1	0	1	3	10	8	3.00	60.02	0.01
1	0.6	6,551,561	1	1	1	1	3	10	4	3.00	60.12	0.01
1	0.8	6,551,599	1	1	1	1	3	10	8	3.00	60.26	0.01
2	0.4	6,754,213	1	1	0	1	3	10	8	3.00	60.00	0.01
2	0.6	6,754,217	1	1	0	1	3	10	7	3.00	60.02	0.01
2	0.8	6,863,350	1	1	0	1	5	8	4	4.28	60.63	0.01
3	0.4	5,665,761	1	1	0	1	3	10	5	3.00	60.01	0.01
3	0.6	5,665,796	1	1	0	1	3	9	4	3.00	60.63	0.01
3	0.8	5,665,640	1	1	1	1	3	10	6	3.02	62.80	0.01

3.5.2. Thermodynamic Evaluation

The optimal solution has two major characteristics in its configuration and operating condition: CSSF and in contactor. The condenser cooling duty is a function of the temperature at the top of the column. The sensible heat requirement is a function of minimum temperature approach (MTA) in lean/rich TEG heat exchanger (L/R TEG HX), the solvent stream flowrate, and heat capacity of the solvent. In the traditional stripper configuration, the temperature at column top and MTA of heat exchanger have a trade-off relationship because the temperature of an inlet stream to stripper rises when MTA is tight. The CSSF solves this problem by directly introducing a cold stream to the top of the column, which consequently reduces the reboiler heat requirement with decreased water vapor fraction, as previously mentioned in section 3.2.

The stream discharged from the third stage of compression has the highest pressure of 26.1 bar among three possible inlet streams to dehydration, which makes the volume flowrate of the stream smaller. Furthermore, the stream contains less saturated water content compared to other two stream cases by cooling a compressed stream and separating condensed water in flash drums, and therefore requires smaller amount of TEG solvent. By expanding rich TEG stream with the higher pressure at JT-1 to the atmospheric pressure, the split cold rich stream has lower temperature. As a result, the reboiler heat requirement for regenerating rich TEG to high purity is reduced.

The rich TEG is regenerated to 98% in purity and cooled down from 199°C to 3°C by cold rich solvent in lean/rich heat exchanger and cooler (HX-1). As the temperature in contactor is lower, the water vapor fraction is lower in CO_2 gas and the dehydration efficiency is higher, so the regenerated lean TEG is cooled to the lowest operating temperature condition.

3.5.3. Economic Evaluation

Economic analysis of CO_2 dehydration process has been rarely presented by other researchers, yet it provides the intuitive comparison among various process configurations. In this section, cost break down of optimal dehydration process is presented. The sizing and cost evaluation of the dehydration is carried out using our own economic model based on the Aspen Plus flowsheet information.

Table 3-5 shows the total annualized cost (TAC) of the optimum dehydration process. TAC is the sum of annualized investment cost (AIC) and annualized operating cost (AOC), which is proportional to the equipment purchase cost (EPC) and the equipment installation cost (EIC), and the AOC is composed of costs of steam, electricity, cooling water, and refrigerant. The dehydration with CSSF shows the minimum TAC which is 5.67 M$/year, which is 1.80 $/ton$CO_2$ of the specific annualized cost. AIC and AOC of the optimum process account

for 77.7 % and 22.3 %, respectively. This result indicates that the proposed process configuration with the additional installation of equipment worsen the process economic efficiency because operating cost occupies much less than capital cost. Therefore, configurations with additional pieces of equipment such as flash drum, stripping gas preheater, LVR options are excluded due to the high AIC.

The refrigerant and steam costs are the first and the second largest parts of the process AOC, which occupy 65.1 % and 34.9 % respectively. By decreasing the pressure of the rich solvent stream, drawn from the bottom of contactor by JT-1, the temperature of the rich solvent becomes slightly low and the small fraction of this stream is directly fed to the top of still column reducing the condenser duty and the reboiler duty.

Table 3-5. Total annualized cost of the optimum dehydration process.

Item	Value [$/yr]
TAC (Total annualized cost)	5,665,640
AIC (Annualized investment cost)	4,402,230
AOC (Annualized operating cost)	1,263,409
Steam	440,474
Electricity	106
Cooling water	646
Refrigerant	822,183

3.5.4. Sensitivity Analysis

Sensitivity analysis based on Monte Carlo simulation of five process alternatives including the optimal configuration is carried out to check the

tendency of TACs to the cost volatility of cooling water, refrigerant, middle pressure steam, and electricity. The selected process alternatives are shown in Figure 3-6 and explained in Table 3-6. The sensitivity analysis is carried out based on the optimal solution. To set base cases to the selected alternatives, integer variables of the each alternative are fixed and continuous variables are decided to the optimal points by solving the nonlinear programming using DIRECT/sub-dividing algorithm (Na et al., 2017b) with 1,000 times iteration. The detailed cost information of the base cases is listed in Table 3-7.

Figure 3-7 shows the results of sensitivity analysis according to the utility cost variation. The slopes of TAC graphs indicate the effect of each utility cost to the alternatives' economics. The steeper the slope is, the stronger the influence is to the process TAC. Cooling water cost does not affect TACs in all alternatives. The refrigerant and the middle pressure steam have strong effects to TACs in overall. Electricity, on the other hand, shows its strong effect only on alternative 3 and 4, ones that include LVR options, due to use of a compressor. In alternative 2 and 4, the slopes according refrigerant cost variation are much steeper than other alternatives, ones with preheating option.

Table 3-8 shows the TAC of the best-found process configurations with the different CO_2 feed specifications according to the stream extraction locations in compression. Case 1, 2, and 3 are the process configurations with the minimum TACs among the solutions with the same feed stream extraction

locations in the compression. Case 3 shows the least TAC among the cases and is discussed as the optimum solution in the previous sections. The pressures of the feed stream of the cases are 3.1 bar, 9.5 bar, and 26.1 bar respectively. TAC of case 1 and 2 are quite similar, but the proportion of AOC in case 2 is higher mainly due to steam and refrigerant used much for the reboiler of still column and the cooler, HX-1. On the other hand, case 3 has much lower AOC, especially due to lower steam cost.

Table 3-6. The selected dehydration process alternatives.

Case	Description	x(5)	x(6)	x(7)	y(1)	y(2)	y(3)
Optimum	CSSF	3	10	6	3.00	60.07	0.01
Alter. 1	SG injection, CSSF	3	5	3	3.00	60.03	0.01
Alter. 2	SG injection, preheating, CSSF	3	7	2	3.00	60.00	0.01
Alter. 3	LVR, CSSF	4	4	2	3.80	60.00	0.02
Alter. 4	LVR, SG injection, preheating, CSSF	4	9	5	3.13	63.05	0.01

Table 3-7. Total annualized cost of the base cases of the selected alternatives.

Case	TAC	AIC	AOC	Steam	Electricity	Cooling Water	Refrigerant
	[M$/yr]			[$/yr]			
Optimum	5.67	4,402,230	1,263,409	440,474	106	646	822,183
Alter. 1	5.98	4,406,980	1,569,698	636,919	132	1,676	930,971
Alter. 2	6.72	4,363,606	2,358,109	609,670	139	1,482	1,746,818
Alter. 3	8.48	6,153,550	2,323,031	1,025,214	600,113	11,171	686,533
Alter. 4	8.89	5,450,033	3,438,015	1,769,987	59,327	13,569	1,595,132

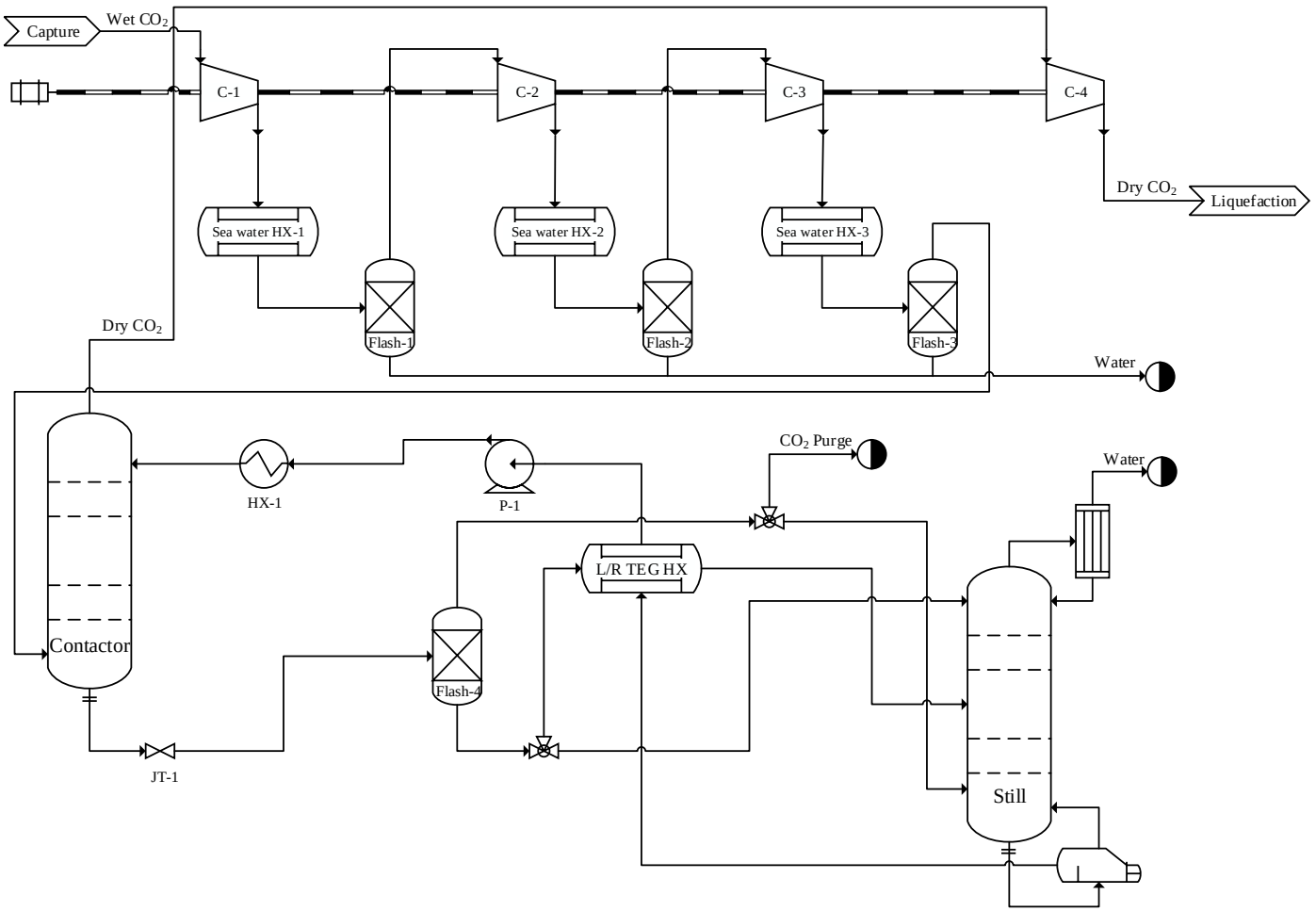

(a) Alternative 1

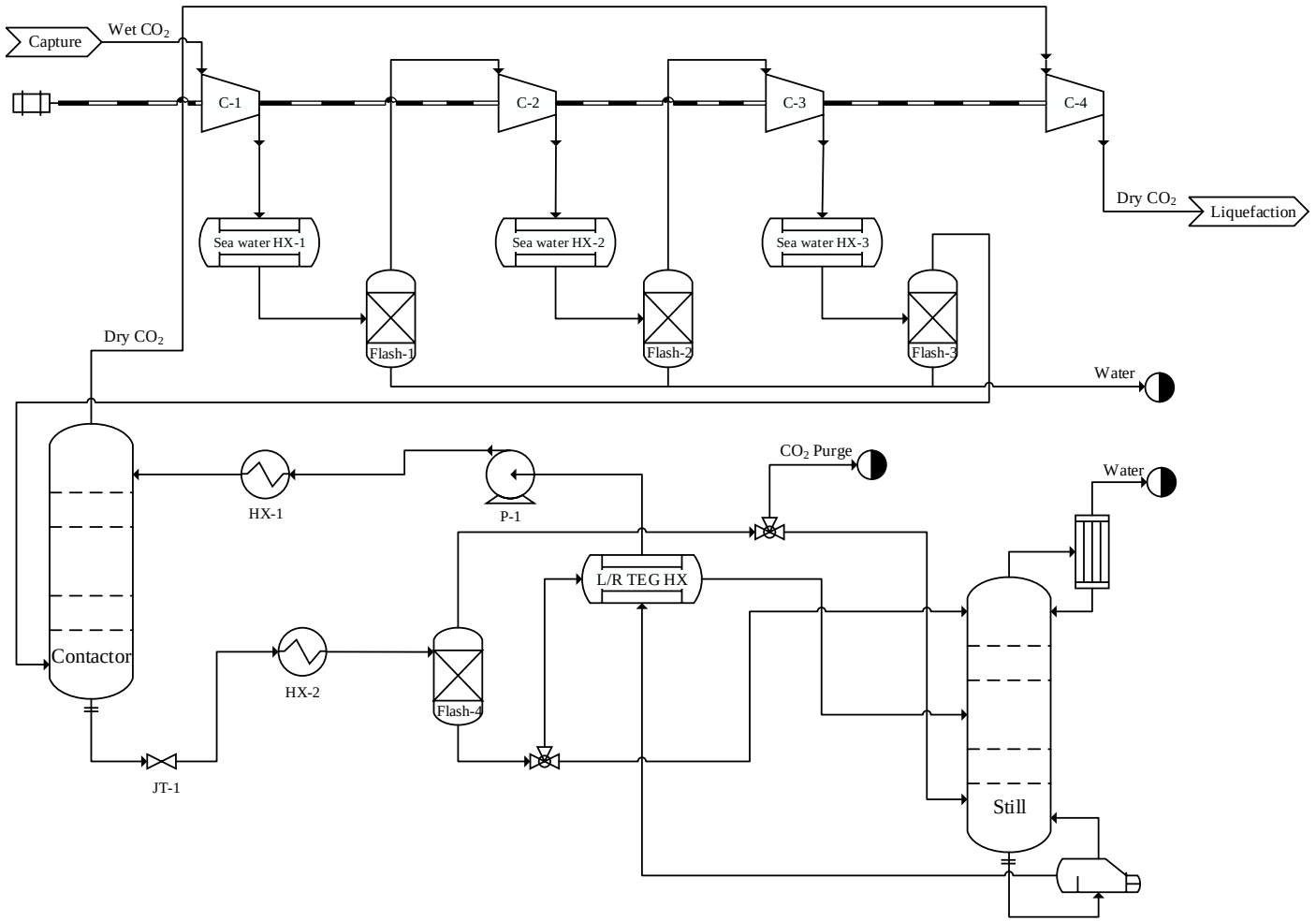

(b) Alternative 2

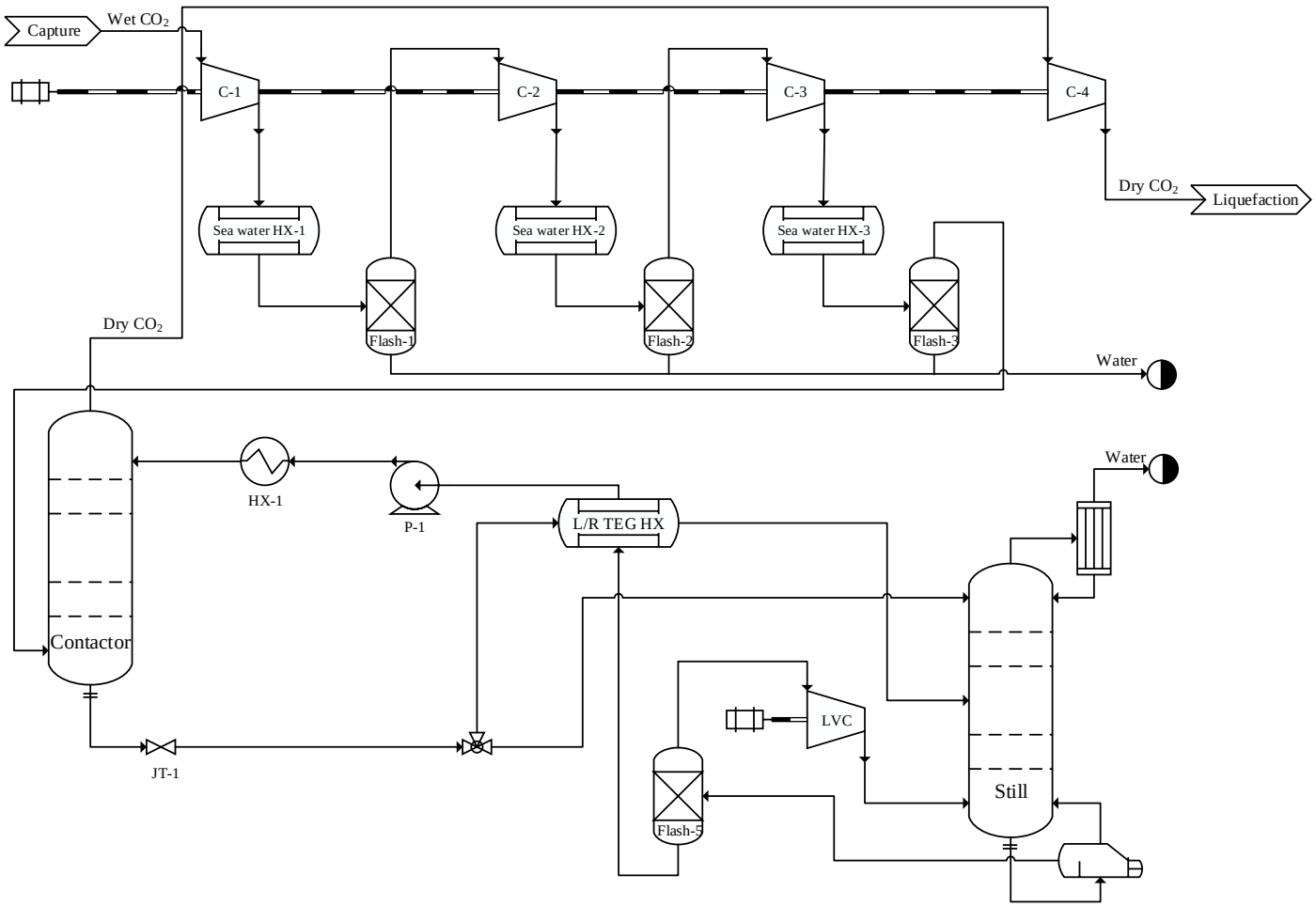

(c) Alternative 3

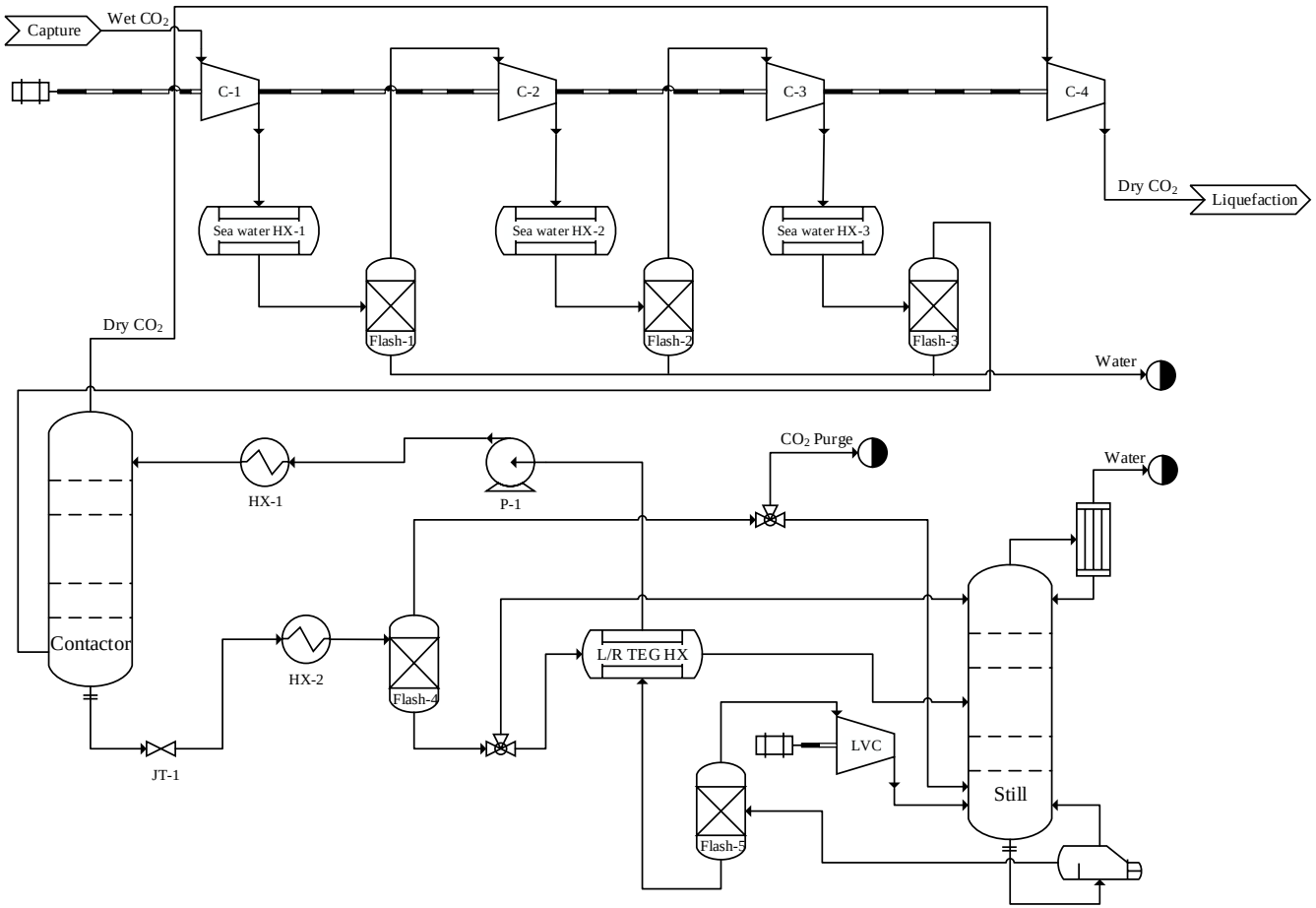

(d) Alternative 4

Figure 3-6. Alternative CO_2 dehydration process design for the sensitivity analysis: (a) alternative 1, (b) alternative 2, (c) alternative 3, and (d) alternative 4.

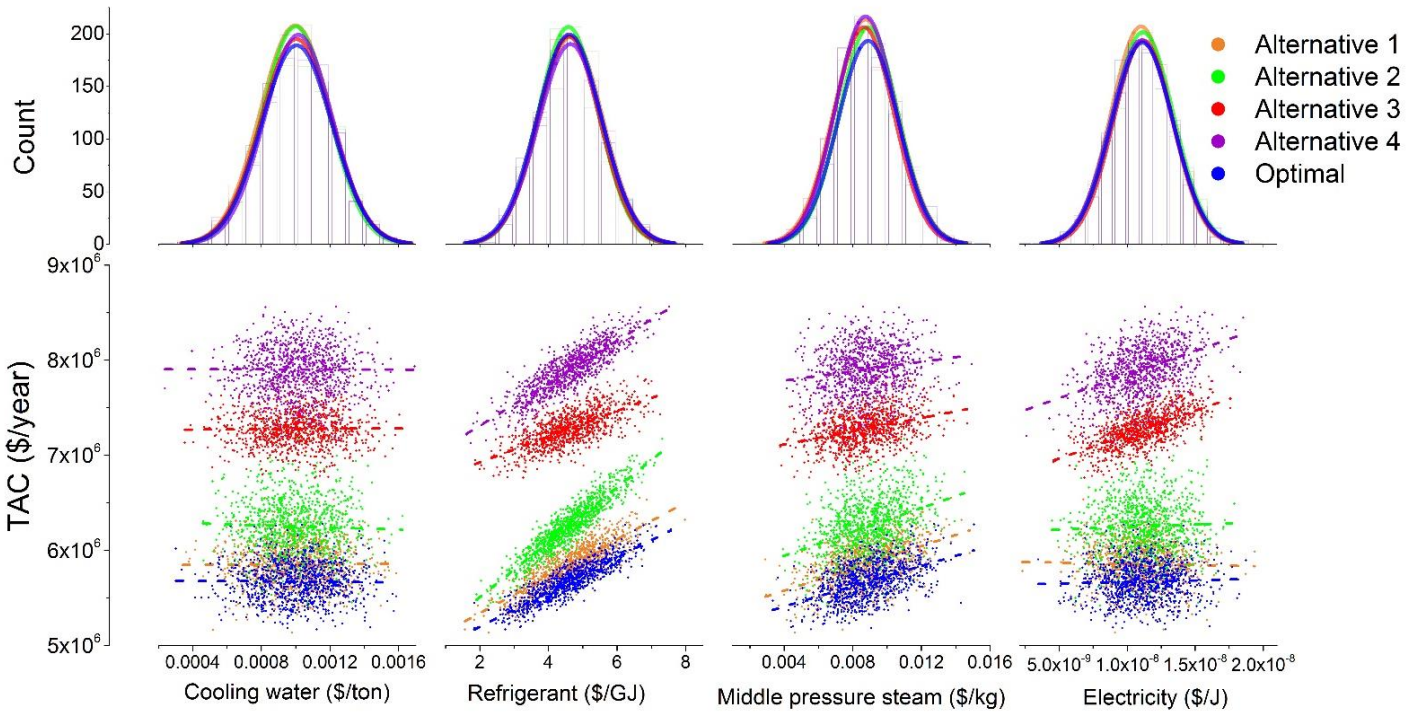

Figure 3-7. Sensitivity analysis for the five different alternative process configurations with the normal distribution random inputs of utility cost.

Table 3-8. Comparison of the best-found solutions with the different compression stages.

Item	Value [$/yr]					
	Case 1		Case 2		Case 3	
Feed stream extraction location in compression	After 1st stage		After 2nd stage		After 3rd stage	
Stream pressure	3.1 bar		9.5 bar		26.1 bar	
TAC	6,551,561		6,754,213		5,665,640	
AIC	4,620,957	70.5%	4,521,580	66.9%	4,402,230	77.7%
AOC	1,930,604	29.5%	2,232,633	33.1%	1,263,409	22.3%
Steam	847,112		1,044,614		440,474	
Electricity	3		168		106	
Cooling water	2,370		4,062		646	
Refrigerant	1,081,119		1,183,790		822,183	

CHAPTER 4. Design of CO_2 Injection Topside Process for Offshore Platform in Pohang, South Korea[†]

4.1. Overview

The geological site for long-term CO_2 storage can be an enhanced oil recovery (EOR) site, depleted oil and gas reservoir, enhanced coal bed storage or a saline aquifer depending on the storage site location. EOR-CO_2 projects exist as early as 1972 and new projects continuously added up over the years (Whittaker and Perkins, 2013). Most of the currently operational CCS projects are transporting the CO_2 from the source site to the sink locations through pipelines. There are more than 6,500 km of CO_2 onshore pipelines around the world with most of their network present in the US and Canada mainly for EOR application (IEAGHG, 2014a). CO_2 is mainly transported in supercritical phase through pipeline which is a mature technology. Many studies reported the transport of CO_2 in supercritical phase to be economical and somehow safe from an operational point of view (Jensen et al., 2014; Llamas et al., 2016; Mcclung, 2013; Witkowski et al.,

[†] This chapter was a part of the R&D project *"Small-scale CO_2 Injection-Demonstration Project in Offshore Pohang Basin"* supported by the Energy Efficiency & Resources Core Technology Program of the Korea Institute of Energy Technology Evaluation and Planning(KETEP) granted financial resource from the Ministry of Trade, Industry & Energy(MOTIE), Republic of Korea (No. 20132010201760).

2014). On the other hand, few studies investigated the liquid CO_2 (L-CO_2) transport to be more economically feasible (Teh et al., 2015; Zahid et al., 2014; Zhang et al., 2012). This may be the case especially when the storage site location is offshore and installment of an offshore pipeline requires a huge capital cost. In such a situation, ship or tank lorry transportation can be an alternative where L-CO_2 is transported from the capture location to the sink site. Ship transportation also offers operational flexibility between sources and sink locations in terms of its route selection. Liquid CO_2 can be produced by liquefying the gaseous CO_2 and many studies have reported various CO_2 liquefaction cycle design (Lee et al., 2015; Yoo et al., 2013; Zahid et al., 2014). There are some technical benefits associated with the L-CO_2 transport. For example, L-CO_2 have high density compared to the supercritical phase that can lead to an increased transport capacities and lower pipeline sizes. In addition, the required pressure at certain temperature to keep CO_2 in a liquid phase is lower that can save pumping costs. On the other hand, a significant amount of insulation is required to keep the heat leaks minimum into the system that can vaporize the L-CO_2. Many studies compared the CO_2 transport in supercritical phase by pipeline and liquid phase by ship (Geske et al., 2015; Knoope et al., 2015; Roussanaly et al., 2013). The results of these studies is mostly site specific and cannot be generalized to other locations.

One of the potential offshore storage locations in South Korea is Ulleung basin that is located 60 km away from the East coast in the East Sea. Two integrated CCS projects (KCCS-1 and KCCS-2) currently at an evaluation stage plan to transport 1.0 Mtpa of CO_2 by ship from a post-combustion capture facility to the Ulleung basin. Some studies investigated the transport scenarios from various capture sites to the Ulleung basin. Jung et al. (Jung et al., 2013a) compared the offshore pipeline transportation with shipping and performed an economic analysis. They concluded the offshore pipeline transport to be less costly compared to that of the shipping. Kang et al. (Kang et al., 2014) estimated the pipeline transport cost in South Korea based on different source site locations and concluded that the transport routes can affect the cost considerably. Similar studies were performed for an offshore CO_2 storage in the Japan (Miyazaki et al., 2013; Nakazawa et al., 2013; Ozaki et al., 2013). Most of these studies explored the design of mechanical equipment that can physically connect the ship and injection well. For example, CHIYODA Corporation published a report (Omata, 2011) that investigated the design of ship vessel, flexible riser pipe and pickup buoy system. Once the ship arrives at the storage location, the unloading of L-CO_2 from the ship and its injection into the geological storage takes place in a sequential manner. Most of the recent studies focusing on ship transportation of CO_2 set their research boundary upstream of an injection system. On the other hand, studies investigating the storage mechanism in the EOR field or

other geological locations assumed the fixed CO_2 conditions from the literature. Though, L-CO_2 unloading from the ship and its injection in the well represents a small section of an overall CCS chain, nevertheless, it is a critical part from an operational point of view that should not be overlooked.

The injection system comprise of pressurizing and heating equipment that can maintain conditions required at the reservoir wellhead. The temperature and pressure conditions required at reservoir wellhead are reservoir specific for each injection site, however, heating and pumping is always required. The injection system can be either equipped on the ship or installed on the offshore platform. Few studies have investigated the design and operation of an injection system. Aspelund et al. (Aspelund et al., 2006) considered the storage site to be in North Sea. They proposed the use of Submerged Turret Loading (STL) system that consists of submersible bouy connecting the flexible riser to the injection platform. They suggested the pressurizing and heating of LCO_2 to 60 bar and -45 ^oC respectively on the ship and an additional pumping and heating on the platform. More recently, You et al. (You et al., 2014) proposed to utilize the cold energy of liquid CO_2 before injection by making use of a Rankine cycle. They also evaluated the exergy efficiency and performed the life-cycle cost for the injection system. A detailed liquid CO_2 injection modelling study was conducted by Krogh et al. (Krogh et al., 2012). They simulated the case studies for Snohvit and Sleipner

projects using OLGA and Aspen HYSYS® software. The study performed the heat transfer modelling in an injection well and considered other start-up and shut down scenarios.

In this section, the design of topside L-CO_2 injection process on offshore platform, which is built and operated in Pohang, South Korea, is introduced. The system injects 60 tonCO_2 in total, which is the small demonstration scale process. Firstly conceptual process design is carried out using Aspen Hysys v8.8 with SRK EOS to predict the thermodynamic properties of the system. Based on the conceptual design, preliminary piping and instrument diagram (P&ID) is presented in simplified version. To develop safer process design, hazard and operability study (HAZOP) is performed. The results of HAZOP analysis and revised P&ID are explained in detail.

4.2. Process Description

Herein, the conceptual design of small-scale carbon dioxide injection process in Ulleng basin, South Korea is presented in this section. Figure 4-1 is an input-output information of the topside injection process. Input stream is CO_2 in liquid phase with 20 barg and 50 ppmv of water content after capture, compression, dehydration, and liquefaction processes as introduced in previous chapters. The liquid CO_2 contained in ISO tank containers is transported by tank lorry. Output stream is in liquid CO_2 with 130 barg in considering the conditions in the injection well. The process flowsheet simulation is carried out using Aspen Hysys v8.8 with Soave-Redlich-Kwong (SRK) EOS (Soave, 1972) to predict thermodynamic property of nearly pure CO_2.

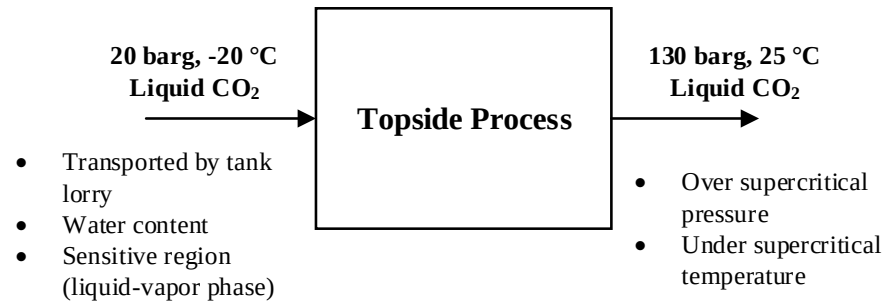

Figure 4-1. Input-output information of the topside process.

Figure 4-2 is a flow diagram of conceptual design of CO_2 injection process. This process consists of three CO_2 ISO tank containers (T-1A~C), pumps (P-1 and P-2), heat exchanger (HX-1), and wellhead. The ISO tank container is selected as a CO_2 container because not only can it be used during transporting

liquid CO_2 but also as a temporary storage tank on the actual offshore platform. ISO containers play an important role as a buffer system between the capture and liquefaction site and storage site until CO_2 is finally injected to the well. The pumps pressurize liquid CO_2 to supercritical pressure (130 barg) to overcome hydrostatic pressure of seawater and the pressure in injection well. P-1 is a centrifugal type for increasing the pressure up to 30 barg before the P-2, metering plunger pump, and facilitating pressure control. The heat exchanger increases the temperature of CO_2 to 25 °C for the injection well to avoid thermal shock by cold CO_2. Based on the conceptual design of the injection process, preliminary piping and instrument diagram (P&ID) is developed, and provided by Korea National Oil Corporation (KNOC). A simplified P&ID of the injection process is shown in Figure 4-3.

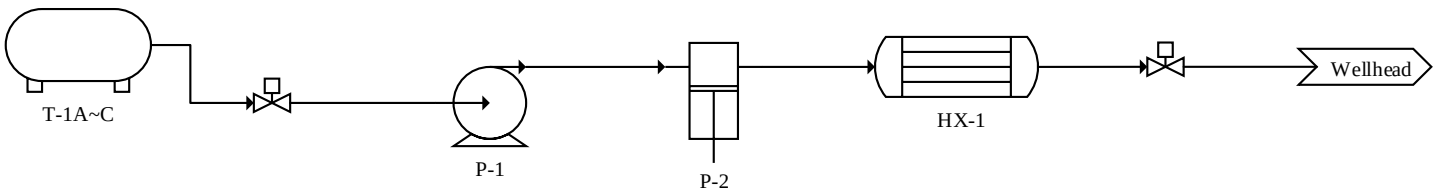

Figure 4-2. Conceptual design of carbon dioxide injection process with dual pump system.

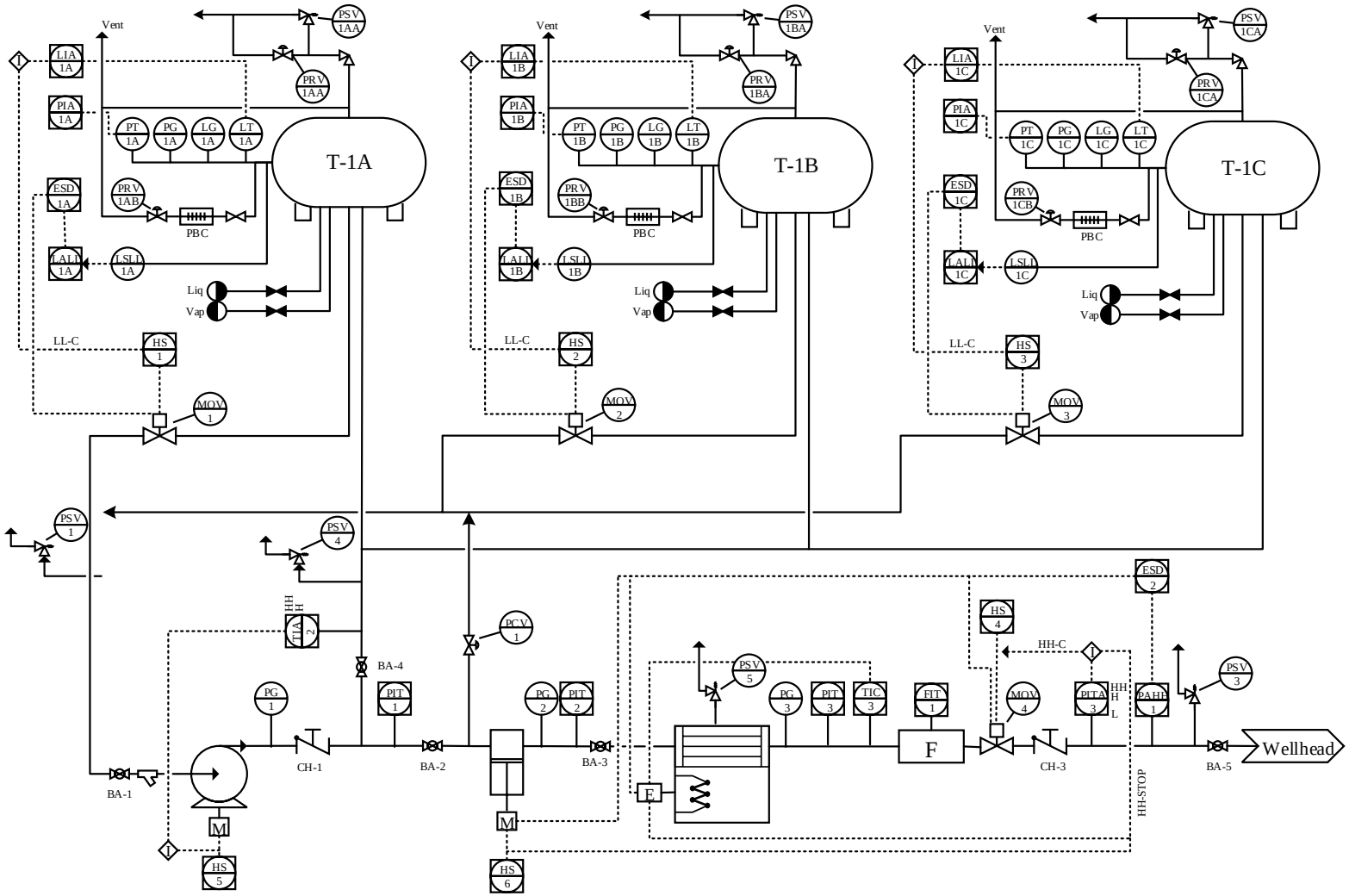

Figure 4-3. Preliminary P&ID of CO_2 injection topside process (simplified).

4.3. Hazard and Operability (HAZOP) Analysis

To identify the potential hazards of the developed preliminary P&ID of the injection process and resolve the hazards, a hazard and operability study is carried out. A hazard and operability study (HAZOP) is a systematic examination method to check the operating intentions of the process, potential mal-function or mal-operation of individual pieces of equipment, and consequential effects on the facility and human based. Table 4-1 explains the important terminology for HAZOP analysis.

Table 4-1. HAZOP terminology (by Dr. Gordon Mckay, Process Safety Management and Risk Hazard Analysis).

Term	Definition
Process Sections (or Study Nodes)	Sections of equipment with definite boundaries (e.g., a line between two vessels) within which process parameters are investigated for deviations. The locations on P&IDs at which the process parameters are investigated for deviations (e.g. reactor)
Operating Steps	Discrete actions in a batch process or a procedure analyzed by a HAZOP analysis team. May be manual, automatic, or software-implemented actions. The deviations applied to each step are somewhat different than the ones used for a continuous process
Intention	Definition of how the plant is expected to operate in the absence of deviation. Takes a number of forms and can be either descriptive or diagrammatic (e.g., process description, flowsheets, line diagrams, P&IDs)
Guide Words	Simple words that are used to qualify the design intention and to guide and stimulate the brainstorming process for identifying process hazards

Process Parameter	Physical or chemical property associated with the process. Includes general items such as reaction, mixing, concentration, pH, and specific items such as temperature, pressure, phase, and flow
Deviations	Departures from the design intention that are discovered by systematically applying the guide words to process parameters (flow, pressure, etc.) resulting in a list for the team to review (no flow, high pressure, etc.) for each process section. Teams often supplement their list of deviations with ad hoc items
Causes	Reasons why deviations might occur. Once a deviation has been shown to have a credible cause, it can be treated as a meaningful deviation. These causes can be hardware failures, human errors, unanticipated process states (e.g. change of composition), external disruptions (e.g. loss of power), etc.
Consequences	Results of deviations (e.g. release of toxic materials). Normally, the team assumes active protection systems fail to work. Minor consequences, unrelated to the study objective, are not considered
Safeguards	Engineered systems or administrative controls designed to prevent the causes or mitigate the consequences of deviations (e.g. process alarms, interlocks, procedures)
Actions (or Recommendations)	Suggestions for design changes, procedural changes, or areas for further study (e.g. adding a redundant pressure alarm or reversing the sequence of two operating steps)

The procedure for HAZOP study is shown in Figure 4-4.Firstly, the process is divided into the sections or nodes to be studied based on the main pieces of equipment, process intention, and thermodynamic specification. Each node is thoroughly examined by ‘deviations’: what the potential ‘causes’ are that make

the ‘deviation’, how the ‘consequences’ of the deviations/causes are, what kind of ‘safeguards’ are equipped, and what ‘recommendations’ are required to reduce risk rank. The important rule is that ‘causes’ are considered within each node and ‘consequences’ are considered regardless of nodes. Table 4-2 is the selected deviations for the injection system.

Table 4-2. Selected deviations for HAZOP analysis.

Parameters	Guide Words			
	More	Less	No	As well as
Flow		O	O	O
Pressure	O	O		
Temperature	O	O		
Level		O	O	
Phase				O

Table 4-3 show the description of risk rank and deviations used for HAZOP of the injection process. Risk rank (RR) is decided by severity and likelihood, and the lower the rank is, the safer the process is. Likelihood is how often the accident (the consequences when deviations occur) happens, and severity is how severe the accident is. The damage level to human, process (equipment), environment, and property decides severity of accidents. If risk rank of a certain consequence exceeds rank IV, which is rank I, II, and III, more safeguards or some recommendations/actions are required to reduce the risk rank to IV or V. A HAZOP procedure is recorded in HAZOP worksheet, which is used as an

educational material for operators, during the process operation, and as an evidential material of safety evaluation of the process.

Table 4-3. Severity, likelihood, and risk rank for the injection process.

A. Severity

Rank	Description
A(5)	• One or more casualties or more than 10 casualties • Property lost more than 500 million won • Environmental pollutant emissions exceeding legal limit of 100% or environmental pollution accidents for 3 days
B(4)	• 5 or more casualties • Property lost from 100 to 500 million won • Environmental pollutant emissions exceeding legal limit of 100% or environmental pollution accidents less than 3 days
C(3)	• 1 or more casualties or more than 10 slightly injured people • Property loss from 10 million to 100 million won • Environmental pollutant emissions exceeding legal limit of 80 - 100% or environmental pollution accident occurred but can be taken immediately
D(2)	• More than one slightly injured person • Property loss less than 10 million won • Environmental pollutant emissions less than 80% of legal limit or no possibility of environmental pollution accident
E(1)	• No loss of life or property • No environmental pollutant emission or accident

B. Likelihood

Rank	Description
5	More than once per year
4	Once per 1 year to 10 years
3	Once per 10 years to 50 years
2	Once per 50 years to 100 years
1	Very unlikely

C. Risk rank

Likelihood / Severity	5	4	3	2	1
A(5)	I	I	II	III	IV
B(4)	I	II	III	IV	V
C(3)	II	III	III	IV	V
D(2)	III	IV	IV	IV	V
E(1)	V	V	V	V	V

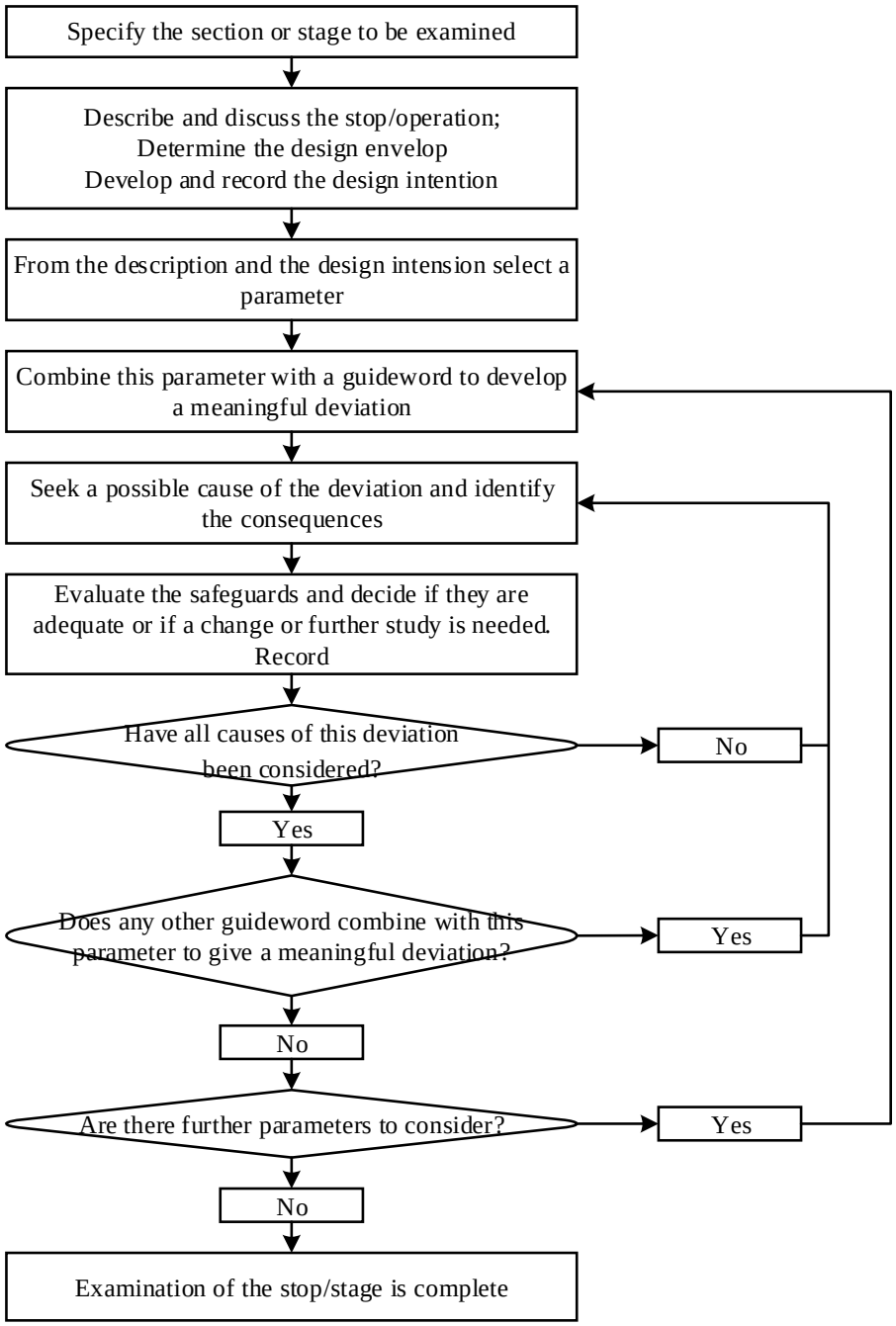

Figure 4-4. Flow diagram for the HAZOP analysis of a section or stage of an operation (the parameter first approach).

4.3.1. Node Selection

The injection process is divided into three nodes as shown in Figure 4-5. The nodes are decided by the pressure and temperature condition of the CO_2 stream flowing in each node and the main piece of equipment, so that hazard and operability of the process can be evaluated in detail and order.

Node 1 is from the three ISO container tanks (T-1) to prior to centrifugal pump (P-1) and marked in red color. CO_2 stream in this node has the same pressure and temperature condition as the transport condition, which is 20 barg and -20 °C, and the three ISO container tanks are the main piece of equipment. Each ISO container tank contains 14.5 tonCO_2 and keeps the pressure and temperature as the original condition. To monitor the condition inside of the tanks, pressure gauge (PG)/transmitter (PT) and level gauge (LG)/transmitter (LT) are installed. In case of the situations such as very low level and too high pressure in the tanks, alarms are set for the operators to recognize the situation in high (H), low (L), high-high (HH), and low-low (LL) conditions. The emergency shutdown (ESD) system is also introduced to close the motor operated valves (MOVs) in severer conditions of low-low level and high-high pressure. The pressure safety valve (PSV) and pressure relief valve (PRV) are installed to manage the pressure of the tanks. If the pressure increases and exceeds the normal condition, PRV releases CO_2 to reduce the pressure. If the pressure increases more than 10% of the normal condition (RP, 2000) and is not

relieved, PSV is ruptured. Pressure buildup coil (PBC) vaporizes the liquid CO_2 in the tank in case that the pressure in the tank decreases and exceeds the normal condition. MOVs, which is the first valve after the tanks, have valve position indicator to check the valve malfunction. PSV is installed in node 1 to avoid any pressure buildup in pipeline.

Node 2 is from centrifugal pump to prior to electric heater and marked in blue color. Liquid CO_2 is pressurized up to 30 barg and 130 barg by two pumps in this node. Y type strainer sieves any solid impurities before the liquid CO2 flows into the centrifugal pump. PG, PT, and pressure indicator (PI) are installed to check if the discharge pressure is enough to reach the suction pressure of the plunger pump (P-2). Between the pumps, two branch of pipeline is connected to prime the pump, which is called recirculation line (RL), and to maintain the normal operation of the centrifugal pump, which is called circulation line (CL). RL is used at startup operation to cool the pipeline and pump down to -20 °C. Once the temperature indicator at RL shows the target temperature, it is safe to assume that the precooling procedure is finished and to close ball valve number 4 (BA-4) to block the flow. To prevent the pump startup and suck the gas before the precooling is finished, temperature indicating alarm (TIA) is installed and interlock control logic is set to keep the pump stationary. CL is used during the normal operation to manage the CO_2 flow to the plunger pump stable. PRV and pressure reducing valve manage the

pressure condition in CL. The plunger pump pressurizes up to 130 barg. The same measurements and safety system is prepared as the centrifugal pumps such as PG, PT, and PI. PSV is especially important in discharge pipeline due to the high pressure. Speed indicating controller manages the pump stroke to manipulate the flowrate of CO_2 manually.

Node 3 is from electric heater (HX-1) to prior to wellhead and marked in yellow color. Pressurized CO_2 is heated to 25 °C by warm water. For pressure safety in pipeline, PSV is installed in tube side in case of rapid evaporization. PG and TG, temperature transmitter (TT) and temperature indicate controller (TIC) shows the condition of the CO_2 after heating. Feedback control logic is set to satisfy the temperature design condition in discharge line. Flow transmitter (FT) and flow indicating totalizer (FIQ) record the mass flowrate to keep the record regardless of the phase of CO_2. Interlock system for pumps and heater and ESD stop the operation in case that the pressure of discharge line flowing to wellhead is HH to avoid the well damage. Check valves (CV) block the inverse flow in the discharge line. Finally, CO_2 is sent to wellhead.

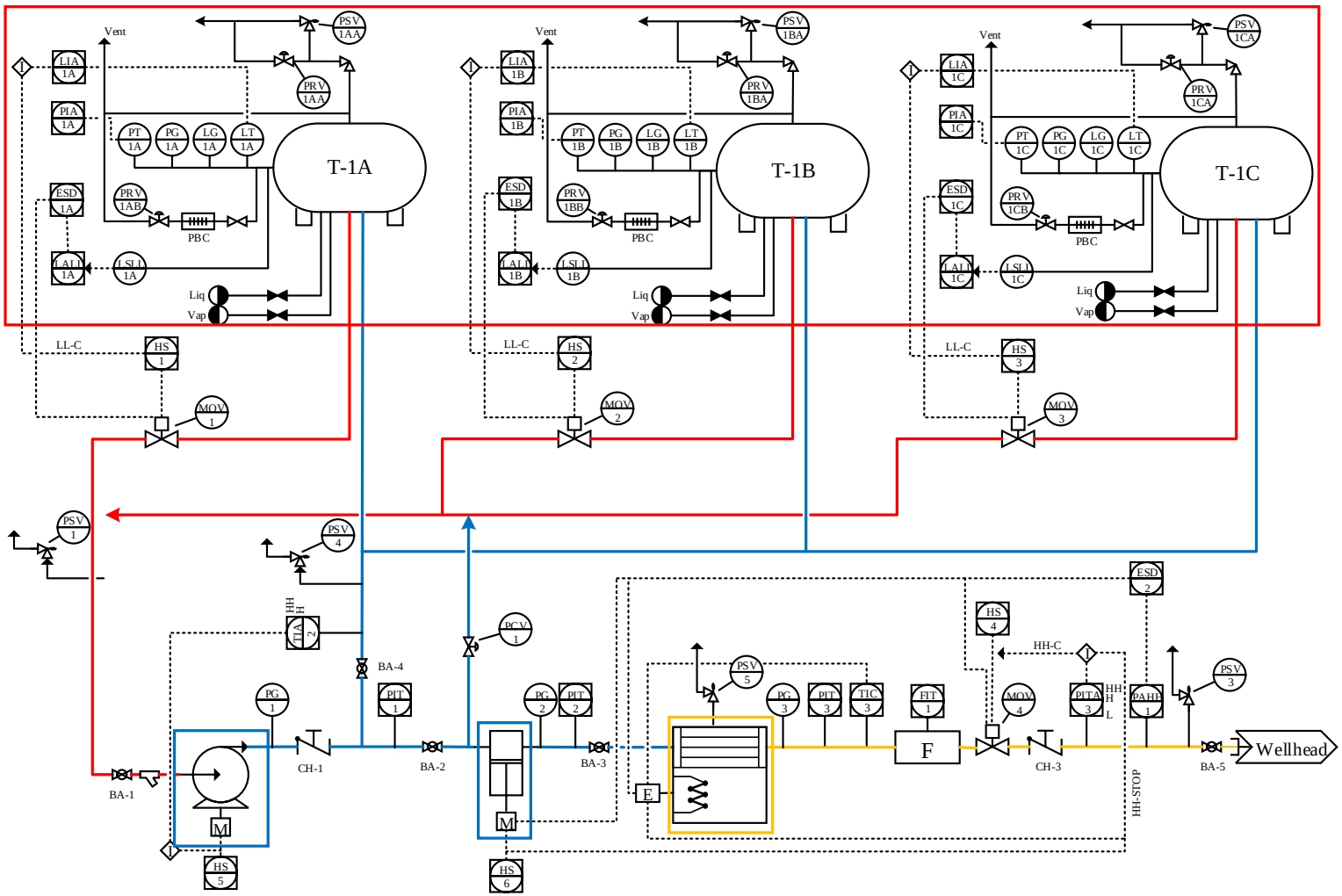

Figure 4-5. Node selection of the injection process (red line: node 1, blue line: node 2, and yellow line: node 3).

4.3.1. Result and Discussion

The major results of HAZOP analysis of each node are explained in this section. The worksheets of HAZOP analysis attached in Appendix contain guidewords, deviation, causes, consequences, safeguard, action required, and risk rank.

4.3.1.1. Node 1

4.3.1.1.1 MOV: Closed

Guideword	Deviation	Causes	Consequences
No	No Flow	MOV 1~3 is fail-closed	• Pump gas suction • Temperature increase in pipeline

[Cause]

If MOV is fail-closed, the pipeline after the MOV does not have the normal CO_2 flow. Once the pump P-1 sucks all the remaining liquid CO_2, vapor phase is formed to fill the space in pipeline.

[Consequences]

The pump P-1 sucks the vapor if it is under operation mode, which causes pump failure. In addition, temperature increases if there is no cold liquid CO_2 flow in pipeline due to the heat flow from the outside, causing pipeline rupture by increased vapor volume.

[Action required]

Interlock system is introduced to trip the pump in case that MOVs are all-closed. To detect the MOV all-close situation, valve position indicate control (ZIC) and position switch control (ZSC) are added. To observe the rapid temperature increase in pipeline, TI, TE, and TG is installed, and flow switch and alarm (FSL) for low flow is also added prior to the pump P-1.

4.3.1.1.2 MOV: Less Open

Guideword	Deviation	Causes	Consequences
Less	Less Flow	MOV 1~3 is less open	• Pump P-1 and P-2 failure due to gas suction

[Cause]

If MOVs are not fully open, liquid CO_2 may be vaporized to fill the space in pipeline.

[Consequences]

The pump sucks the vapor and causes the pump failure.

[Action required]

Operator training is carried out to make sure the valves stay fully open. Valve position failure alarm is set to inform the valves are not fully open.

4.3.1.2. Node 2

4.3.1.2.1 Failure in PRV on Recirculation Line

Guideword	Deviation	Causes	Consequences
More	Higher Pressure	Failure in PRV 1	• Pressure increase in pipeline between P-1 and P-2

[Cause]

PRV 1 fails to depressurize the CO_2 stream before sending the stream to the pump suction line.

[Consequences]

The discharge pressure of the pump P-1 is increase as following the characteristic curves with the higher suction pressure.

[Action required]

Pressure high alarm, PCV, and PSV are installed in the pump P-1 discharge line and circulation line.

4.3.1.3. Node 3

4.3.1.3.1 CO_2 Leakage Inside of Heater

Guideword	Deviation	Causes	Consequences
No	No Flow	CO_2 leakage inside heater	• Damage to heater

[Cause]

Liquid CO_2 leaks to the water bath of the heater HX-1 when tube side have leakage, causing no or less flow in pipeline after the heater.

[Consequences]

Cold liquid CO_2 may be vaporized by the warm water and the water bath leaks or is ruptured by the high pressure of leaked CO_2.

[Action required]

PSV is installed to both the tube and bath sides, and flow low-low alarm is added to FIQ-1 to recognize the situation of liquid CO_2 vaporization.

4.3.1.3.2 Overheating

Guideword	Deviation	Causes	Consequences
More	Higher Pressure	HX-1 overheating	• CO_2 Vaporization • Leakage

[Cause]

The temperature of CO_2 stream exceeds the design temperature due to feedback control failure. The phase change to vapor or supercritical cause the pressure increase in the tube side of the heater HX-1.

[Consequences]

The leakage or rupture of the tube and the bath side may occur.

[Action required]

Temperature low and high alarm is added to TIC-3.

4.3.1.3.3 Additional Revision of P&ID

The interlock system of PITA 3 is removed to avoid malfunction of interlock system of PITA 3 and ESD 2 of PAHH, which stop the pumps P-1 and P-2 and the heater HX-1 and close MOV-4 in situation of pressure high-high.

The separate header line for cold CO_2 vapor to vented to safe location is recommended to prevent any safety issues such as operator frostbite and suffocation and equipment damage. Figure 4-6 is a revised simplified P&ID after HAZOP study.

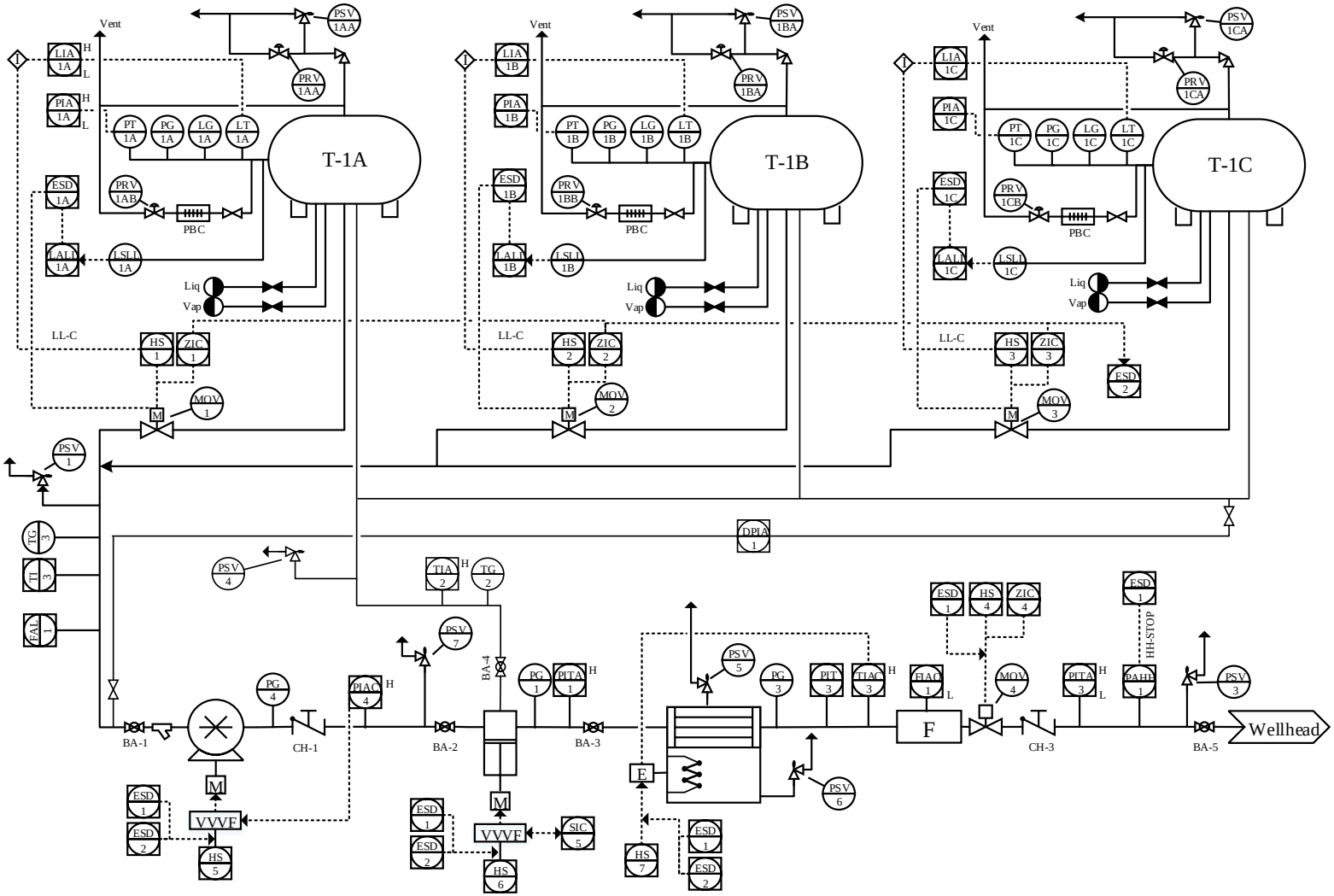

Figure 4-6. Revised P&ID after HAZOP study of the injection process (simplified)

CHAPTER 5. Concluding Remarks

5.1. Conclusions

Carbon capture and storage (CCS) is considered a realistic near-term technology to decelerate the global temperature rise. Unfortunately, the energy and economic burden to the commercial power plants is one of the biggest obstacles to implementation of CCS, and the lack of experience in demonstration of commercial scale, which is up to 500 MW or more, is pointed out as another issue to overcome. Carbon dioxide contained in flue gas from the boiler of the power plants is captured, compressed, dehydrated, and liquefied for the long-term isolation. Numerous process alternatives and configurations for standalone process of capture and liquefaction to reduce the energy requirement, but they are not considered as an integrated process, ignoring the non-linear relationship between the operating conditions of each process and the energy penalty, the power de-rate. In addition, the dehydration process is rarely studied compared to capture and liquefaction process.

The thesis is to propose economical and efficient commercial scale CCS process from post-combustion capture using monoethanolamine (MEA), dehydration using triethylene glycol (TEG), liquefaction process using cold CO_2 itself, and finally to offshore injection process.

Firstly, the energy penalty generated by introducing CCS process into the power plant (which is called *power de-rate* in this thesis) is reduced by manipulating influential variables of capture and liquefaction process. A simulation of a 550 MWe supercritical power plant with a post-combustion amine based capture process and liquefaction process is carried out based on the data for a 0.1 MW CO_2 capture pilot plant in Boryeong, South Korea. The stripper pressure and liquid to gas ratio (L/G) are chosen as the manipulated variables by variable evaluation. The result shows that the stripper operating pressure is the most influential parameter that affects not only the capture process but the liquefaction process. In addition, the regeneration energy is sensitive to L/G and an optimal value is observed according to stripper pressure. As the stripper pressure increased, the regenerated energy in the capture process and the compression energy in the liquefaction process decreased. Extraction of a minimum amount of steam for reboiler from the steam cycle reduces power output loss in turbine train. However, an increased temperature in the reboiler requires higher quality steam, which decreases the expansion ratio of the backup turbine and thus recovers less power. Consequently, the total power de-rate is minimized when operating at a lower stripper pressure and an optimum L/G ratio of 1.25 bar and 4.05 L/m3, respectively, with steam extracted from the first LP turbine and using option (b) backup turbine for the steam extraction unit. The suggested operating conditions are different from the optimum

conditions for the unit processes (capture and liquefaction processes). The power de-rate is reduced to 17.7 % from 27.0 % for the base case.

Secondly, the techno-economic assessment of CO_2 dehydration process is investigated through superstructure-based optimization. The superstructure of CO_2 dehydration process is built using Aspen Plus, and economically optimized through genetic algorithm (GA) with a combined Aspen Plus-MATLAB interface. Dehydration specification is set to 50 ppmv in order to avoid any operational problem such as corrosion and hydrate formation. To develop rigorous process model, NRTL-RK thermodynamic model is used with the regressed binary parameter of TEG-water. The optimal dehydration process includes contactor, still column, lean/rich TEG heat exchanger, a cooler, a pump, a JT valve, and cold rich solvent split option. The optimal equipment configurations and operating conditions are also identified. Total annualized cost of the optimum process is 5.7 M$/year corresponding to 1.80 $/ton$CO_2$. The annualized capital investment cost occupies much larger portion compared to the annualized operation cost. The refrigerant and middle pressure steam are the two biggest utility costs in the annualized operation cost. The sensitivity analysis based on Monte Carlo simulation of five representative sub-optimal process alternatives is also performed to identify the tendency of the total annualized cost (TAC) according to utility cost volatility. The refrigerant and steam costs are most influential on the TAC of the optimal process.

Finally, the small-scale topside CO_2 injection process for offshore platform is designed and improved by the hazard and operability (HAZOP) study. L-CO_2 is temporarily stored in ISO tank containers in 20 barg and -20°C, pressurized by two pumps in series, and increased in temperature by the heat exchanger. Piping and instrument diagram (P&ID) is developed and revised by the result of HAZOP study. The major recommendation from the HAZOP study is about the pressure-related safety issues to detect and manage the abnormal state and automatically shut the process down partially or entirely.

Reference

Abu-Zahra, M.R.M., Schneiders, L.H.J., Niederer, J.P.M., Feron, P.H.M., Versteeg, G.F., 2007. CO2 capture from power plants: Part I. A parametric study of the technical performance based on monoethanolamine. International Journal of Greenhouse Gas Control 1, 37-46.

Ahn, H., Luberti, M., Liu, Z., Brandani, S., 2013. Process configuration studies of the amine capture process for coal-fired power plants. International Journal of Greenhouse Gas Control 16, 29-40.

Alabdulkarem, A., Hwang, Y., Radermacher, R., 2012. Energy consumption reduction in CO2 capturing and sequestration of an LNG plant through process integration and waste heat utilization. International Journal of Greenhouse Gas Control 10, 215-228.

Aroonwilas, A., Veawab, A., 2007. Integration of CO 2 capture unit using single-and blended-amines into supercritical coal-fired power plants: implications for emission and energy management. International Journal of Greenhouse Gas Control 1, 143-150.

Aspelund, A., Jordal, K., 2007. Gas conditioning—The interface between CO2 capture and transport. International Journal of Greenhouse Gas Control 1, 343-354.

Aspelund, A., Mølnvik, M., De Koeijer, G., 2006. Ship transport of CO2: technical solutions and analysis of costs, energy utilization, exergy efficiency and CO2 emissions. Chemical Engineering Research and Design 84, 847-855.

Biliyok, C., Lawal, A., Wang, M., Seibert, F., 2012. Dynamic modelling, validation and analysis of post-combustion chemical absorption CO 2 capture plant. International Journal of Greenhouse Gas Control 9, 428-445.

Chang, H., Shih, C.M., 2005. Simulation and Optimization for Power Plant Flue Gas CO2 Absorption-Stripping Systems. Separation science and technology 40, 877-909.

Chapoy, A., Burgass, R., Tohidi, B., Alsiyabi, I., 2014. Hydrate and phase behavior modeling in CO2-rich pipelines. Journal of Chemical & Engineering Data 60, 447-453.

Choi, Y.-S., Nesic, S., Young, D., 2010. Effect of impurities on the corrosion behavior of CO2 transmission pipeline steel in supercritical CO2− water environments. Environmental science & technology 44, 9233-9238.

Ciferno, J., 2008. Pulverized coal oxycombustion power plants. Final Report, revised August.

Cifre, P.G., Brechtel, K., Hoch, S., García, H., Asprion, N., Hasse, H., Scheffknecht, G., 2009. Integration of a chemical process model in a power plant modelling tool for the simulation of an amine based CO2 scrubber. Fuel 88, 2481-2488.

Cole, I.S., Corrigan, P., Sim, S., Birbilis, N., 2011. Corrosion of pipelines used for CO 2 transport in CCS: Is it a real problem? International Journal of Greenhouse Gas Control 5, 749-756.

Conn, A.R., Scheinberg, K., Vicente, L.N., 2009. Introduction to derivative-free optimization. SIAM.

Cousins, A., Wardhaugh, L.T., Feron, P.H.M., 2011. A survey of process flow sheet modifications for energy efficient CO2 capture from flue gases using chemical absorption. International Journal of Greenhouse Gas Control 5, 605-619.

Dave, N., Do, T., Palfreyman, D., Feron, P.H.M., 2011. Impact of liquid absorption process development on the costs of post-combustion capture in Australian coal-fired power stations. Chemical Engineering Research and Design 89, 1625-1638.

Davis, J., Rochelle, G., 2009. Thermal degradation of monoethanolamine at stripper conditions. Energy Procedia 1, 327-333.

Elliott, T., Chen, K., Swankamp, R., 1998. Standard handbook of power plant engineering McGraw-Hill. London.

Eslick, J.C., Miller, D.C., 2011. A multi-objective analysis for the retrofit of a pulverized coal power plant with a CO2 capture and compression process. Computers & Chemical Engineering 35, 1488-1500.

Fernandez, E.S., Bergsma, E.J., de Miguel Mercader, F., Goetheer, E.L., Vlugt, T.J., 2012. Optimisation of lean vapour compression (LVC) as an option for post-combustion CO 2 capture: Net present value maximisation. International Journal of Greenhouse Gas Control 11, S114-S121.

Figueroa, J.D., Fout, T., Plasynski, S., McIlvried, H., Srivastava, R.D., 2008. Advances in CO 2 capture technology—the US Department of Energy's Carbon Sequestration Program. International journal of greenhouse gas control 2, 9-20.

Gao, H., Zhou, L., Liang, Z., Idem, R.O., Fu, K., Sema, T., Tontiwachwuthikul, P., 2014. Comparative studies of heat duty and total equivalent work of a new heat pump distillation with split flow process, conventional split flow process, and conventional baseline process for CO2 capture using monoethanolamine. International Journal of Greenhouse Gas Control 24, 87-97.

Geske, J., Berghout, N., van den Broek, M., 2015. Cost-effective balance between CO2 vessel and pipeline transport: Part II – Design of multimodal CO2 transport: The case of the West Mediterranean region. International Journal of Greenhouse Gas Control 33, 122-134.

Grossmann, I.E., 1985. Mixed-integer programming approach for the synthesis of integrated process flowsheets. Computers & Chemical Engineering 9, 463-482.

Grossmann, I.E., 1989. MINLP optimization strategies and algorithms for process synthesis.

Grossmann, I.E., 1990. Mixed-integer nonlinear programming techniques for the synthesis of engineering systems. Research in Engineering Design 1, 205-228.

GSAP, 2004. GPSA Engineering Data Book. GSAP.

Hanak, D.P., Biliyok, C., Yeung, H., Białecki, R., 2014. Heat integration and exergy analysis for a supercritical high-ash coal-fired power plant integrated with a post-combustion carbon capture process. Fuel 134, 126-139.

Harkin, T., Hoadley, A., Hooper, B., 2010. Reducing the energy penalty of CO2 capture and compression using pinch analysis. Journal of Cleaner Production 18, 857-866.

Hasan, M.M.F., Baliban, R.C., Elia, J.A., Floudas, C.A., 2012. Modeling, Simulation, and Optimization of Postcombustion CO2 Capture for Variable Feed Concentration and Flow Rate. 1. Chemical Absorption and Membrane Processes. Industrial & Engineering Chemistry Research 51, 15642-15664.

Heggum, G., Weydahl, T., Roald, W., Mølnvik, M., Austegard, A., 2005. CO2 conditioning and transportation. Carbon dioxide capture for storage in deep geologic formations 2, 925-936.

Hikita, H., Asai, S., Ishikawa, H., Honda, M., 1977. The kinetics of reactions of carbon dioxide with monoethanolamine, diethanolamine and triethanolamine by a rapid mixing method. The Chemical Engineering Journal 13, 7-12.

House, K.Z., Harvey, C.F., Aziz, M.J., Schrag, D.P., 2009. The energy penalty of post-combustion CO 2 capture & storage and its implications for retrofitting the US installed base. Energy & Environmental Science 2, 193-205.

IEAGHG, 2014a. CO_2 Pipeline Infrastructure.

IEAGHG, 2014b. Evaluation and analysis of the performence of dehydration units for CO2 capture.

IPCC, 2011. IPCC special report on renewable energy sources and climate change mitigation.

Jarne, C., Blanco, S., Artal, M., Rauzy, E., Otí, S., Velasco, I., 2004. Dew points of binary carbon dioxide+ water and ternary carbon dioxide+ water+ methanol mixtures: Measurement and modelling. Fluid phase equilibria 216, 85-93.

Jassim, M.S., Rochelle, G.T., 2006. Innovative absorber/stripper configurations for CO2 capture by aqueous monoethanolamine. Industrial & Engineering Chemistry Research 45, 2465-2472.

Jensen, M.D., Schlasner, S.M., Sorensen, J.A., Hamling, J.A., 2014. Operational Flexibility of CO2 Transport and Storage. Energy Procedia 63, 2715-2722.

Jeong, Y.S., Jung, J., Lee, U., Yang, C., Han, C., 2015. Techno-economic analysis of mechanical vapor recompression for process integration of post-combustion CO 2 capture with downstream compression. Chemical Engineering Research and Design 104, 247-255.

Jung, J.-Y., Huh, C., Kang, S.-G., Seo, Y., Chang, D., 2013a. CO2 transport strategy and its cost estimation for the offshore CCS in Korea. Applied Energy 111, 1054-1060.

Jung, J., Jeong, Y.S., Lee, U., Lim, Y., Han, C., 2015. New Configuration of the CO2 Capture Process Using Aqueous Monoethanolamine for Coal-Fired Power Plants. Industrial & Engineering Chemistry Research 54, 3865-3878.

Jung, J., Jeong, Y.S., Lim, Y., Lee, C.S., Han, C., 2013b. Advanced CO 2 Capture Process Using MEA Scrubbing: Configuration of a Split Flow and Phase Separation Heat Exchanger. Energy Procedia 37, 1778-1784.

Kang, K., Huh, C., Kang, S.-G., Baek, J.-H., Noh, H.J., 2014. Estimation of CO2 pipeline transport cost in south korea based on the scenarios. Energy Procedia 63, 2475-2480.

Karimi, M., Hillestad, M., Svendsen, H.F., 2011. Capital costs and energy considerations of different alternative stripper configurations for post combustion CO 2 capture. Chemical Engineering Research and Design 89, 1229-1236.

Karimi, M., Hillestad, M., Svendsen, H.F., 2012a. Investigation of the dynamic behavior of different stripper configurations for post-combustion CO 2 capture. International journal of greenhouse gas control 7, 230-239.

Karimi, M., Hillestad, M., Svendsen, H.F., 2012b. Positive and Negative Effects on Energy Consumption by Inter–heating of Stripper in Co 2 Capture Plant. Energy Procedia 23, 15-22.

Kemper, J., Sutherland, L., Watt, J., Santos, S., 2014. Evaluation and Analysis of the Performance of Dehydration Units for CO 2 Capture. Energy Procedia 63, 7568-7584.

Khalilpour, R., Abbas, A., 2011. HEN optimization for efficient retrofitting of coal-fired power plants with post-combustion carbon capture. International Journal of Greenhouse Gas Control 5, 189-199.

Knoope, M.M.J., Ramírez, A., Faaij, A.P.C., 2015. Investing in CO2 transport infrastructure under uncertainty: A comparison between ships and pipelines. International Journal of Greenhouse Gas Control 41, 174-193.

Krogh, E., Nilsen, R., Henningsen, R., 2012. Liquefied CO2 injection modelling. Energy Procedia 23, 527-555.

Lawal, A., Wang, M., Stephenson, P., Yeung, H., 2009. Dynamic modelling of CO2 absorption for post combustion capture in coal-fired power plants. Fuel 88, 2455-2462.

Le Moullec, Y., Kanniche, M., 2011. Screening of flowsheet modifications for an efficient monoethanolamine (MEA) based post-combustion CO 2 capture. International journal of greenhouse gas control 5, 727-740.

Lee, S.G., Choi, G.B., Lee, J.M., 2015. Optimal design and operating conditions of the CO2 liquefaction process, considering variations in cooling water temperature. Industrial & Engineering Chemistry Research 54, 12855-12866.

Lee, U., Mitsos, A., Han, C., 2016. Optimal retrofit of a CO2 capture pilot plant using superstructure and rate-based models. International Journal of Greenhouse Gas Control 50, 57-69.

Lee, U., Yang, S., Jeong, Y.S., Lim, Y., Lee, C.S., Han, C., 2012. Carbon Dioxide Liquefaction Process for Ship Transportation. Industrial & Engineering Chemistry Research 51, 15122-15131.

Liang, H., Xu, Z., Si, F., 2011. Economic analysis of amine based carbon dioxide capture system with bi-pressure stripper in supercritical coal-fired power plant. International Journal of Greenhouse Gas Control 5, 702-709.

Liebenthal, U., Linnenberg, S., Oexmann, J., Kather, A., 2011. Derivation of correlations to evaluate the impact of retrofitted post-combustion CO2 capture processes on steam power plant performance. International Journal of Greenhouse Gas Control 5, 1232-1239.

Liew, P.Y., Klemeša, J.J., Doukelis, A., Zhang, N., Seferlis, P., 2014. Identification of Process Integration Options for CO2 Capture in Greek Lignite--Fired Power Plant. Chemical Engineering Transactions 39.

Lin, C.-C., Chen, Y.-W., 2011. Performance of a cross-flow rotating packed bed in removing carbon dioxide from gaseous streams by chemical absorption. International Journal of Greenhouse Gas Control 5, 668-675.

Llamas, B., Hernández, Á., Mazadiego, L.F., Pous, J., 2016. Economic modeling of the CO2 transportation phase and its application to the Duero Basin, Spain. Greenhouse Gases: Science and Technology 6, 648-661.

Lucquiaud, M., Chalmers, H., Gibbins, J., 2009. Capture-ready supercritical coal-fired power plants and flexible post-combustion CO2 capture. Energy Procedia 1, 1411-1418.

Lucquiaud, M., Gibbins, J., 2011. Effective retrofitting of post-combustion CO2 capture to coal-fired power plants and insensitivity of CO2 abatement costs to base plant efficiency. International Journal of Greenhouse Gas Control 5, 427-438.

Machado, P.B., Monteiro, J.G., Medeiros, J.L., Epsom, H.D., Araujo, O.Q., 2012. Supersonic separation in onshore natural gas dew point plant. Journal of Natural Gas Science and Engineering 6, 43-49.

Maldal, T., Tappel, I., 2004. CO 2 underground storage for Snøhvit gas field development. Energy 29, 1403-1411.

Mcclung, A.M., Jeff; Lerche, Andrew, 2013. Pipeline Transport of Supercritical Carbon Dioxide. 2012 GMRC Gas Machinery Conference. Austin, Texas.

Metz, B., Davidson, O., De Coninck, H., Loos, M., Meyer, L., 2005. IPCC special report on carbon dioxide capture and storage. Cambridge University Press, New York, NY (United States); Intergovernmental Panel on Climate Change, Geneva (Switzerland). Working Group III.

Miyazaki, T., Osawa, H., Matsuura, M., Ohta, M., Ozaki, M., 2013. Offshore operational availability of onboard direct injection of CO2 into sub-seabed geological formations. Energy Procedia 37, 3168-3175.

Moser, P., Schmidt, S., Sieder, G., Garcia, H., Stoffregen, T., 2011. Performance of MEA in a long-term test at the post-combustion capture pilot plant in Niederaussem. International Journal of Greenhouse Gas Control 5, 620-627.

Mostafazadeh, A.K., Rahimpour, M.R., Shariati, A., 2009. Vapor−Liquid Equilibria of Water + Triethylene Glycol (TEG) and Water + TEG + Toluene at 85 kPa. Journal of Chemical & Engineering Data 54, 876-881.

Na, J., Kshetrimayum, K.S., Lee, U., Han, C., 2017a. Multi-objective optimization of microchannel reactor for Fischer-Tropsch synthesis using computational fluid dynamics and genetic algorithm. Chemical Engineering Journal 313, 1521-1534.

Na, J., Lim, Y., Han, C., 2017b. A modified DIRECT algorithm for hidden constraints in an LNG process optimization. Energy 126, 488-500.

Nakazawa, N., Kikuchi, K., Ishii, K.-i., Yamaguchi, T., Ohta, M., Ozaki, M., 2013. Ship-based CO 2 Injection into Subseabed Geological Formations using a Flexible Riser Pipe Pickup System. Energy Procedia 37, 3176-3183.

NETL, D., 2011. NETL Advanced Carbon Dioxide Capture R&D Program: Technology Update May 2011.

Netusil, M., Ditl, P., 2011. Comparison of three methods for natural gas dehydration. Journal of Natural Gas Chemistry 20, 471-476.

Netusil, M., Ditl, P., 2012. Natural Gas Dehydration, Natural Gas - Extraction to End Use.

Noothout, P., Wiersma, F., Hurtado, O., Macdonald, D., Kemper, J., van Alphen, K., 2014. CO2 Pipeline infrastructure–lessons learnt. Energy Procedia 63, 2481-2492.

Oexmann, J., Kather, A., 2010. Minimising the regeneration heat duty of post-combustion CO2 capture by wet chemical absorption: The misguided focus on low heat of absorption solvents. International Journal of Greenhouse Gas Control 4, 36-43.

Omata, A., 2011. Preliminary feasibility study on CO2 carrier for ship-based CCS. Final Report of Chiyoda Corporation, supported by Global CCS Institute, 4-29.

Onda, K., Takeuchi, H., Okumoto, Y., 1968. MASS TRANSFER COEFFICIENTS BETWEEN GAS AND LIQUID PHASES IN PACKED COLUMNS. Journal of Chemical Engineering of Japan 1, 56-62.

Ozaki, M., Ohsumi, T., Kajiyama, R., 2013. Ship-based offshore CCS featuring CO 2 shuttle ships equipped with injection facilities. Energy Procedia 37, 3184-3190.

Padurean, A., Cormos, C.-C., Cormos, A.-M., Agachi, P.-S., 2011. Multicriterial analysis of post-combustion carbon dioxide capture using alkanolamines. International Journal of Greenhouse Gas Control 5, 676-685.

Patiño-Echeverri, D., Hoppock, D.C., 2012. Reducing the Energy Penalty Costs of Postcombustion CCS Systems with Amine-Storage. Environmental Science & Technology 46, 1243-1252.

Paymooni, K., Rahimpour, M.R., Raeissi, S., Abbasi, M., Baktash, M.S., 2011. Enhancement in triethylene glycol (TEG) purity via hydrocarbon solvent injection to a TEG+ water system in a batch distillation column. Energy & Fuels 25, 5126-5137.

Plaza, J.M., Van Wagener, D., Rochelle, G.T., 2010. Modeling CO 2 capture with aqueous monoethanolamine. International Journal of Greenhouse Gas Control 4, 161-166.

Reddy, S., Scherffius, J., Freguia, S., Roberts, C., 2003. Fluor's Econamine FG Plus SM Technology, Proceedings of the second annual conference on carbon sequestration. Citeseer, pp. 5-8.

Redlich, O., Kwong, J.N.S., 1949. On the Thermodynamics of Solutions. V. An Equation of State. Fugacities of Gaseous Solutions. Chemical Reviews 44, 233-244.

Renon, H., Prausnitz, J.M., 1968. Local compositions in thermodynamic excess functions for liquid mixtures. AIChE Journal 14, 135-144.

Rincon, M.D., Jimenez-Junca, C., Duarte, C.R., 2016. A novel absorption process for small-scale natural gas dew point control and dehydration. Journal of Natural Gas Science and Engineering 29, 264-274.

Rochelle, G.T., 2012. Thermal degradation of amines for CO2 capture. Current Opinion in Chemical Engineering 1, 183-190.

Roussanaly, S., Jakobsen, J.P., Hognes, E.H., Brunsvold, A.L., 2013. Benchmarking of CO2 transport technologies: Part I—Onshore pipeline and shipping between two onshore areas. International Journal of Greenhouse Gas Control 19, 584-594.

RP, A., 2000. 520, Sizing, Selection and Installation of Pressure-Relieving Devices in Refineries, Part I, Sizing and Selection, 7th. American Petroleum Institute, Washington, DC.

Rubin, E.S., Yeh, S., Antes, M., Berkenpas, M., Davison, J., 2007. Use of experience curves to estimate the future cost of power plants with CO 2 capture. International journal of greenhouse gas control 1, 188-197.

Sanpasertparnich, T., Idem, R., Bolea, I., deMontigny, D., Tontiwachwuthikul, P., 2010. Integration of post-combustion capture and

storage into a pulverized coal-fired power plant. International Journal of Greenhouse Gas Control 4, 499-510.

Scheffknecht, G., Al-Makhadmeh, L., Schnell, U., Maier, J., 2011. Oxy-fuel coal combustion—A review of the current state-of-the-art. International Journal of Greenhouse Gas Control 5, S16-S35.

Scholes, C.A., Stevens, G.W., Kentish, S.E., 2012. Membrane gas separation applications in natural gas processing. Fuel 96, 15-28.

Singh, D., Croiset, E., Douglas, P.L., Douglas, M.A., 2003. Techno-economic study of CO2 capture from an existing coal-fired power plant: MEA scrubbing vs. O2/CO2 recycle combustion. Energy Conversion and Management 44, 3073-3091.

Skaugen, G., Roussanaly, S., Jakobsen, J., Brunsvold, A., 2016. Techno-economic evaluation of the effects of impurities on conditioning and transport of CO 2 by pipeline. International Journal of Greenhouse Gas Control 54, 627-639.

Soave, G., 1972. Equilibrium constants from a modified Redlich-Kwong equation of state. Chemical Engineering Science 27, 1197-1203.

Soave, G., Feliu, J.A., 2002. Saving energy in distillation towers by feed splitting. Applied Thermal Engineering 22, 889-896.

Steeneveldt, R., Berger, B., Torp, T.A., 2006. CO2 Capture and Storage. Chemical Engineering Research and Design 84, 739-763.

Teh, C., Barifcani, A., Pack, D., Tade, M.O., 2015. The importance of ground temperature to a liquid carbon dioxide pipeline. International Journal of Greenhouse Gas Control 39, 463-469.

Trespalacios, F., Grossmann, I.E., 2014. Review of Mixed-Integer Nonlinear and Generalized Disjunctive Programming Methods. Chemie Ingenieur Technik 86, 991-1012.

Van Peteghem, T., Delarue, E., 2014. Opportunities for applying solvent storage to power plants with post-combustion carbon capture. International Journal of Greenhouse Gas Control 21, 203-213.

Van Wagener, D.H., Rochelle, G.T., 2011. Stripper configurations for CO 2 capture by aqueous monoethanolamine. Chemical Engineering Research and Design 89, 1639-1646.

Versteeg, P., Rubin, E.S., 2011. A technical and economic assessment of ammonia-based post-combustion CO 2 capture at coal-fired power plants. International Journal of Greenhouse Gas Control 5, 1596-1605.

Wall, T., Stanger, R., Santos, S., 2011. Demonstrations of coal-fired oxy-fuel technology for carbon capture and storage and issues with commercial deployment. International journal of greenhouse gas control 5, S5-S15.

Wetenhall, B., Aghajani, H., Chalmers, H., Benson, S., Ferrari, M., Li, J., Race, J., Singh, P., Davison, J., 2014. Impact of CO2 impurity on CO2 compression, liquefaction and transportation. Energy Procedia 63, 2764-2778.

Whittaker, S., Perkins, E., 2013. Technical aspects of CO2 enhanced oil recovery and associated carbon storage. Global CCS institute.

Witkowski, A., Rusin, A., Majkut, M., Stolecka, K., 2014. The analysis of pipeline transportation process for CO2 captured from reference coal-fired 900 MW power plant to sequestration region. Chemical and Process Engineering 35, 497-514.

Yoo, B.-Y., Choi, D.-K., Kim, H.-J., Moon, Y.-S., Na, H.-S., Lee, S.-G., 2013. Development of CO2 terminal and CO2 carrier for future commercialized CCS market. International Journal of Greenhouse Gas Control 12, 323-332.

You, H., Seo, Y., Huh, C., Chang, D., 2014. Performance analysis of cold energy recovery from CO2 injection in ship-based carbon capture and storage (CCS). Energies 7, 7266-7281.

Zachary, J., 2008. Options for reducing a coal-fired plant's carbon footprint, Part II. Power 152.

Zahid, U., An, J., Lee, U., Choi, S.P., Han, C., 2014. Techno-economic assessment of CO2 liquefaction for ship transportation. Greenhouse Gases: Science and Technology 4, 734-749.

Zhang, D., Wang, Z., Sun, J., Zhang, L., Li, Z., 2012. Economic evaluation of CO 2 pipeline transport in China. Energy Conversion and Management 55, 127-135.

Zhang, K., Liu, Z., Wang, Y., Li, Y., Li, Q., Zhang, J., Liu, H., 2014. Flash evaporation and thermal vapor compression aided energy saving CO2 capture systems in coal-fired power plant. Energy 66, 556-568.

Appendix

A. HAZOP Worksheet

Index

Process: Topside process for CO_2 injection
Chemicals: Carbon Dioxide
Scope: From three ISO containers to the wellhead

Node: (1) T-1 to before P-1
Intention: To store safely L-CO_2 before injected to the reservoir, and to send L-CO_2 to P-1
Parameter: Flow

GW	DV	Causes	Consequences	Safeguards	Likelihood	Severity	Risk Rank	Recommendations

No	No Flow	ISO container is empty	1.1 Pump P-1 failure due to gas suction	MOV 1~3 T-1A~C switchover BA 1 LG, LT 1A~C LIA 1A~C low, low low LALL 1A~C ESD 1	2	B(4)	IV	
			1.2 Process shutdown, Target press. is not satisfied	PG, PT 1 PIA 3				
			1.3 Vaporization after HX-1					
			2.1 Increase of internal temperature of the pipeline and the tanks	PSV 1 PSV, PRV 1AA~CB				
			2.2 Increase of internal pressure of the pipeline and the tanks					
			2.3 Pipe rupture					
			2.4 Injure operators due to pipe rupture					
		MOV 1~3 is closed	1.1 Pump P-1 failure due to gas suction	MOV 1~3 ZIH, ZIL T-1A~C switchover, interlock	3	C(3)	IV	- pump stop interlock (MOV 1~3 all closed)

				BA 1				
			1.2 Process shutdown, Target press. is not satisfied	PG, PT 1 PIA 3 low				
			2.1 Increase of internal temperature of the pipeline	PSV 1				- TT, TG (P-1 suction line)
			2.2 Increase of internal pressure					
			2.3 Pipeline rupture					
			2.4 Injure operators due to pipeline rupture					
		Formation of CO_2 hydrate	1.1 Pump P-1 failure due to hydrate suction	Y type strainer (STR 1) PT 1	3	C(3)	IV	- Check source CO2 water content < 50 ppm - Check drying status after hydrostatic test - Hydrate formation (Operator training) - FS (Pump suction line.) - Drain valve (before MOV-1~3)
			1.2 Process shutdown, Target press. is not satisfied	PG, PT 1 PIA 3 low PAHH 1				
			2.1 Increase of internal temperature and pressure	PSV 1				
			2.3 Pipeline rupture					
			2.4 Injure operators due to pipeline rupture					
		LALL 1A~C malfunction	1.1 Pump P-1 failure due to gas suction	MOV 1~3 ZIH, ZIL T-1A~C switchover	2	B(4)	IV	

				BA 1 LSLL 1A~C				
			~~1.2 Process shutdown, Target press. is not satisfied~~	PG, PT 1 PIA 3 low				
			2.1 Increase of internal temperature of the pipeline	PSV 1				
			2.2 Increase of internal pressure					
			2.3 Pipeline rupture					
			2.4 Injure operators due to pipeline rupture					
Less	Less Flow	MOV 1~3 is less open	2.2.2 Pump P-1 failure due to gas suction	MOV 1~3 ZIH, ZIL	2	B(4)	IV	- Operator training - Mov 1~3 position fail alarm
		Formation of CO_2 hydrate	1.1 Pump P-1 failure due to hydrate suction		3	C(3)	IV	- Check source CO2 water content < 50 ppm - Check drying status after hydrostatic test - Hydrate formation (Operator training) - FS (Pump suction line)
			1.2 Breakage of pump blade					
			3.1 Less flow in P-1					
			3.2.1 Target press. is not satisfied	PG, PT PIA 3				

				PAHH				- Drain valve (before MOV-1~3)
			3.2.2 Pump P-1, P-2 failure due to gas suction	MOV 1~3 T-1A~C switchover, interlock BA 1 Bypass line				
As Well As	Water Content	Not enough dehydration & drying	1.1 Hydrate formation		3	C(3)	IV	
			1.2.1 Pipeline is (completely / partially) blockage					- Check source CO_2 water content < 50 ppm
			1.2.2 Pump failure					
			1.3.1 Pipeline rupture due to higher press.	PSV 1				
			1.3.2 No / less flow in downstream					- PG
			1.4.1 Injure operators					- Hydrate formation (Operator training)
			1.4.2 Ice / hydrate formation around the leakage points					- FS (Pump suction line)
			1.4.3 Back flow from wellhead	CH 3				
			1.4.4 Target pres. & temp. are not satisfied	TIC 1				- Drain valve (before MOV-1~3)
			2.1 Pipeline corrosion due to carbonic acid					

			2.2 Pipeline rupture 2.3.1 Injure operators 2.3.2 Ice / hydrate formation around the leakage points					

Node: (1) T-1 to before P-1
Intention: To store safely L-CO_2 before injected to the reservoir, and to send L-CO_2 to P-1
Parameter: Pressure

GW	DV	Causes	Consequences	Safeguards	Likelihood	Severity	Risk Rank	Recommendations
More	Higher Pressure	Vaporization (when not in operation) due to temp. increase in pipeline and tanks	1.1.1 Pipe rupture		4	D(2)	IV	
			2.1 Tank explosion					
		After PBC PRV 1AC~CC malfunction	1.1 Tank explosion		2	B(4)	IV	- By vendor (Tank) V/V numbering
		Tank pres. Relif PRV 1AA~CB malfunction	1.1 Tank explosion		2	B(4)	IV	

		PBC fails(Coil trouble) to compensate the pressure drop	1.1 Lower pump suction pressure	PIA 1A~C low	2	B(4)	IV	- Additional actions based on frequency of occurrence (low low or Interlock added) - Manuals for using recirculation line and/or other containers when pressure low low situation
			1.2 Target press. is not satisfied	PG, PT 1				
		Tank and Pipeline rupture	1.2 Ice formation around the rupture		2	B(4)	IV	- CO_2 detector
			1.3 Injure operators (Suffocation, frostbite)					
			1.4 Shortage of CO_2 to inject					
		PSV, PRV failure			2	B(4)	IV	

Node: (1) T-1 to before P-1
Intention: To store safely L-CO_2 before injected to the reservoir, and to send L-CO_2 to P-1
Parameter: Phase

GW	DV	Causes	Consequences	Safeguards	Likelihood	Severity	Risk Rank	Recommendations

As Well As	Generation of other phase	1.1 Decrease in temperature (hydrate formation)	1.1 Hydrate formation		3	C(3)	IV	- Check source CO_2 water content < 50 - Check drying status after hydrostatic test - Hydrate foramtion (Operator training) - FS (Pump suction line.) - Drain valve (before MOV-1~3)
			1.2.1 Pipeline is (completely / partially)	PSV 1				
			1.2.2 Pump failure					
			1.3.1 Pipeline rupture due to higher press.					
			1.3.2 No / less flow in downstream					
			1.4.1 Injure operators					
			1.4.2 Ice / hydrate formation around the					
			1.4.3 Back flow from wellhead	CH 3 TIC 1				
			1.4.4 Target press. & temp. are not satisfied					
			2.1 Pipeline corrosion due to carbonic acid					
			2.2 Pipeline rupture					
			2.3.1 Injure operators					
			2.3.2 Ice / hydrate formation around the					

		1.2 Increase in temp. (vaporization)	1.1.1 Pipeline rupture	PSV 1 Pipeline C insulation	3	C(3)	IV	
			2.1 Tank explosion	PSV , PRV 1AA~CB PIA 1A~C high				

Node: (1) T-1 to before P-1
Intention: To store safely L-CO_2 before injected to the reservoir, and to send L-CO_2 to P-1
Parameter: Level

GW	DV	Causes	Consequences	Safeguards	Likelihood	Severity	Risk Rank	Recommendations
No	No Level	Tank rupture	1.2 Ice-formation around the rupture		2	B(4)	IV	- CO_2 detector
			1.3 Injure operators (Suffocation, frostbite)					
			1.4 Shortage of CO_2 to inject					
		All CO_2 is transported	2.1 Pump P-1, P-2 failure due to gas suction	MOV 1~3 T-1A~C switchover BA 1 LG, LT 1A~C	2	B(4)	IV	
				LIA 1A~C low, low low LALL 1A~C ESD 1				
				PG, PT 1				

			2.2 Process shutdown, Target pres is not satisfied	PIA 3 low				
			2.3 Vaporization after HX-1					
			3.1 Increase of internal termpresure of the pipeline and the tanks					
			3.2 Increase of internal pressure of the pipeline and the tanks	PSV 1 PSV, PRV 1AA~CB				
			3.3 Pipeline rupture					
			3.4 Injure operators due to pipeline rupture					
Less	Lower Level	Tank rupture	1.2 Ice formation around the rupture		2	B(4)	IV	- CO_2 detector
			1.3 Injure operators (Suffocation, frostbite)					
			1.4 Shortage of CO_2 to inject					
		PBC vaporization	1.1.1 Pipeline rupture	PSV 1 Pipeline C insulation	2	B(4)	IV	
			2.1 Tank explosion	PSV , PRV 1AA~CB PIA 1A~C high				

		PRV vent CO_2 too much	1.2 Ice formation around the PRV	PRV stand-by	2	B(4)	IV	
			1.4 Shortage of CO_2 to inject	PG, PIA 1A~C				

Node: (2) P-1 to before HX-1
Intention: To increase the pressure of L-CO_2, to measure the flowrate, to send L-CO_2 to HX-1, and to operate cool-down in startup and recirculation in steady-state operations
Parameter: Flow

GW	DV	Causes	Consequences	Safeguards	Likelihood	Severity	Risk Rank	Recommendations
No	No Flow	Ball valve(BA 2) is closed by operator's mistakes	1.1 Increase of internal pressure of the pipeline due to P-1	PSV 2	2	D(2)	IV	- Locked open, Limit switch installation
			1.2 Pipeline rupture	PG, PT 1				
			1.3 Injure operators due to pipeline rupture					
			2.1 Increase of internal temperature and pressure	PSV 2				
			2.2 Pipeline rupture					
			2.3.1 Injure operators due to pipeline rupture					
			2.3.2 Damage to pipeline/equipment					

		Pipeline rupture	1.1 Ice formation around the leakage point		3	C(3)	IV	- CO_2 detector
			1.2 Damage to pipeline/equipment around the leakage point					
			1.3 Injure operators					
			2.1 Less flow than normal condition in HX-1	TIC 1				
			2.2 Target temp. is not satisfied					
			3.1 Less flow in P-1, P-2					
			3.2 Target press. is not satisfied	PG, PT 1				
		Pump fail stop	1.1 Stop CO_2 injection	Send fault signal to monitoring system (XL 005)	2	B(4)	IV	
			2.1 Pressure increase in pipeline after HX-1 due to temperature increase	PSV (in HX-1)				
More	More Flow	Increase of P-1 stroke	1.1 Target temp. is not satisfied	TIC 1	2	B(4)	IV	
			2.1 Target press. is not satisfied after pump	PG 1, PT 1, 3 PIA 3 high, high high PAHH 1 PSV of P-1				

Less	Less Flow	Pipeline rupture	1.1 Ice / hydrate formation around the leakage point & equipment rupture		3	C(3)	IV	- CO_2 detector
			1.2 Injure operators (frostbite)					
		Decrease of P-1 stroke	1.1 Target press. is not satisfied after pump	PG 1, PT 1, 3 PIA 3 low	2	B(4)	IV	
		BA 004 is opened by operator's mistakes	1.1 Increase of tank pressure by rapid vaporization	PSV, PRV 1AA~CB PIA 1A~C high PG, PT 1A~C	2	D(2)	IV	- Locked open, Limit switch installation - CO_2 detector
			1.2 Tank explosion					
			2.1 Recycle pipeline (to the tanks) rupture	PSV 004				
			2.2.1 Ice / hydrate formation around the leakage point & equipment rupture					
			2.2.2 Injure operators (frostbite)					
As Well As	Water	Not enough dehydration & drying	1.1 Hydrate formation		3	C(3)	IV	- Check source CO_2 water content < 50 ppm - Check drying status after hydrostatic test - Hydrate
			1.2 Pipe is (completely / partially) blockage					
			1.3.1 Pipeline rupture due to higher press. by P-1	PSV of P-1				
			1.3.2 No flow in downstream					

			1.3.3 Less flow than normal condition in downstream equipment					formation (Operator training) - FS (Pump suction line.) - Drain valve (before MOV-1~3)
			1.4.1 Injuire operators					
			1.4.2 Ice formation around the leakage points					
			1.4.3 Back flow from wellhead	CH 3				
			1.4.4 Target press. & temp. are not satisfied	TIC 1 PG 1, PT 1, 3 PIA 3 low				
			2.1 Pipe corrosion due to carbonic acid					
			2.2 Pipe rupture					
			2.3.1 Injure operators					
			2.3.2 Ice formation around the leakage points					

Node: (2) P-1 to before HX-1
Intention: To increase the pressure of L-CO_2, to measure the flowrate, to send L-CO_2 to HX-1, and to operate cool-down in startup and recirculation in steady-state operations
Parameter: Pressure

GW	DV	Causes	Consequences	Safeguards	Likelihood	Severity	Risk Rank	Recommendations
More	Higher Pressure	Vaporization of L-CO_2	1.1 Pressure increase by vaporization	Pipeline cold insulation	4	D(2)	IV	
			1.2 Pipeline rupture	PSV of P-1				

			1.3.1 Injure operators	PG, PT 1				
			1.3.2 Damage to other process equipment					
		Increase of P-1 stroke	1.1 Target press. is not satisfied after pump	PG 1, PT 1, 3 PIA 3 high, high high PAHH 1 PSV of P-1	2	B(4)	IV	
		Ball valve(BA 2) is closed by operator's mistakes	1.1 Increase of internal pressure of the pipeline due to P-1	PSV 2 PG, PT 1	2	D(2)	IV	- Locked open, Limit switch installation
			1.2 Pipeline rupture					
			1.3 Injure operators due to pipeline rupture					
			2.1 Increase of internal temperature and pressure	PSV 2 PCV 1, RO 1				
			2.2 Pipeline rupture					
			2.3.1 Injure operators due to pipeline rupture					
			2.3.2 Damage to pipeline/equipment					
			3.1 No flow in downstream	CH 1~3				
			3.2 Back flow from wellhead					

Less	Lower Pressure	Decrease P-1 stroke	1.1 Target press. is not satisfied after pump 1.2.1 Vaporization after HX-1 1.2.2 Target temp. is not satisfied	PG 1, PT 1, 3 PIA 3 low TIC1	2	B(4)	IV	

Node: (2) P-1 to before HX-1
Intention: To increase the pressure of L-CO_2, to measure the flowrate, to send L-CO_2 to HX-1, and to operate cool-down in startup and recirculation in steady-state operations
Parameter: Phase

GW	DV	Causes	Consequences	Safeguards	Likelihood	Severity	Risk Rank	Recommendations
As Well As	Generation of other phase	1.1 Decrease in temperature (hydrate formation)	1.1 Hydrate formation		3	C(3)	IV	- Check source CO_2 water content < 50 ppm - Check drying status after hydrostatic test - Hydrate formation (Operator training) - FS (Pump
			1.2.1 Pipeline is (completely / partially)					
			1.2.2 Pump failure					
			1.3.1 Pipeline rupture due to higher press.	PSV of P-1				
			1.3.2 No / less flow in downstream					
			1.4.1 Injure operators					
			1.4.2 Ice / hydrate formation around the					
			1.4.3 Back flow from wellhead	CH 3				
			1.4.4 Target press. & temp. are not satisfied	TIC 1				

			2.1 Pipeline corrosion due to carbonic acid					suction line.) - Drain valve (before MOV-1~3)
			2.2 Pipeline rupture					
			2.3.1 Injure operators					
			2.3.2 Ice / hydrate formation around the					
		1.2 Increase in temp. (vaporization)	1.1.1 Pipeline rupture	PSV of P-1 Pipeline cold insulation				

Node: (3) from HX-1 to wellhead
Intention: To increase the temperature of L-CO_2 and to send to wellhead
Parameter: Flow

GW	DV	Causes	Consequences	Safeguards	Likelihood	Severity	Risk Rank	Recommendations
No	No Flow	CO_2 Leakage inside of heater	1.1 Damage to heater	ESD PG PIA 3 PAHH FT 1	2	B(4)	IV	- Installation of PSV in Vendor package - FIQ 1 low low alarm
			1.2 Backflow from wellhead	CH 3 PAHH 1 BA 3, MOV 004				
		Pipeline rupture	1.1 Ice formation around the leakage point		3	C(3)	IV	- CO_2 detector
			1.2 Damage to pipeline/equipment around the leakage point					
			1.3 Injure operators					

			2.1 Flow meter (FT-1) error					
Less	Less Flow	CO_2 Leakage inside of heater	1.1 Damage to heater	ESD PG PIA3 PAHH FT 1	2	B(4)	IV	
			1.2.1 Target temp. is not satisfied	TIC 1 TG 1				
			1.2.2 Target press. is not satisfied	ESD 2 PG 2 PIA 3 low, high, high high PAHH 1				
		Blockage of Strainer before HX-1	1.1 Target press. is not satisfied	ESD 2 PG 3 PIA 3 low, high, high high PAHH 1	2	C(3)	IV	- Check the vendor package

Node: (3) from HX-1 to wellhead
Intention: To increase the temperature of L-CO_2 and to send to wellhead
Parameter: Temperature

GW	DV	Causes	Consequences	Safeguards	Likelihood	Severity	Risk Rank	Recommendations
More	Higher Temperature	Heater fails to satisfy target T	1.1 Target temp. is not satisfied	TIC 1	2	B(4)	IV	
			1.2 Pressure increase by vaporization	ESD 2 PIA 3 high, high high PSV 3				
			1.2.1 Pipeline rupture					

			1.2.2 Injure operator due to rupture					
			2.1 Supercritical phase of CO_2					
Less	Lower Temperature	Heater fails to satisfy target T	1.1 Target T after HX-1 is not satisfied	TIC 1	2	B(4)	IV	

Node: (3) from HX-1 to wellhead
Intention: To increase the temperature of L-CO_2 and to send to wellhead
Parameter: Pressure

GW	DV	Causes	Consequences	Safeguards	Likelihood	Severity	Risk Rank	Recommendations
Less	Lower Pressure	Pipeline leakage	1.1 Ice / hydrate formation around the leakage		3	C(3)	IV	
			1.2 Damage to pipeline/equipment around the leakage point					
			1.2.2 Injure operators					
		Leakage inside heater	1.1 Damage to heater	PG 2, TG 1, 002	2	B(4)	IV	- PG inside HX-1
			1.2.1 Target temp. is not satisfied	TIC 1				
			1.2.2 Decrease in pressure	PIA 3 low				
More	Higher Pressure	Temp. increase	1.1 Pressure increase	Pipeline H insulation PSV 3	3	C(3)	IV	
			1.2 Pipeline rupture					

			1.3 Injure operators due to rupture					
		HX-1 overheating	1.1 Pressure increase by vaporization	PSV 005	2	B(4)	IV	- TIC → TIAC - Operator training - Check pipeline size and measurement functioning in supercritical phase
			1.2 Leakage inside heater					
			1.3 Damage to heater					
			1.4.1 Target temp. is not satisfied	TIC 1 TG 1				
			1.4.2 Decrease in pressure	PIA 3 low				
			2.1 Backflow from downstream	CH 3				

Node: (3) from HX-1 to wellhead
Intention: To increase the temperature of L-CO_2 and to send to wellhead
Parameter: Phase

GW	DV	Causes	Consequences	Safeguards	Likelihood	Severity	Risk Rank	Recommendations
As Well As	Generation of other phase	Increase in temperature: vaporization / Supercritical phase	1.1 Pressure increase	Pipe H insulation PSV 3	3	C(3)	IV	- TIC → TIAC - Operator training - Check pipeline size and measurement functioning in
			1.2 Pipeline rupture					
			1.2.1 Ice formation around the leakage point					
			1.2.2 Damage to pipe/equipment around the leakage point					

			1.2.3 Injure operators					supercritical phase

Nomenclature

Symbols

$\Delta\alpha$	Difference between rich loading and lean loading
D	Power de-rate
η	Efficiency
h	Equality constraints
J	Partial derivation of objective function
L	Lean solvent flow rate
$\dot{m}$	Steam flow rate
P_1	Pressure of inlet stream
P_2	Pressure of outlet stream
P_{str}	Operating pressure of stripper
R	Universal gas constant
γ	Ratio of heat capacities or Penalty parameter
r_i	Compression ratio at ith compression stage
T_1	Temperature of inlet stream
V	Molar volume
$\dot{W}$	Power generated by turbine work
x_i	Variable
x	Binary and integer variables
y	Continuous variables
μ	Utility average cost
σ	Cost variance

Abbreviations

AIC	Annualized capital investment cost
AOC	Annualized operation cost
BA	Ball valve
BT	Backup turbine
C	Compression or Cold
CCS	Carbon dioxide capture and storage
CH	Check valve

CL	Circulation line
CSSF	Cold solvent slit flow
CW	Cooling water
DPT	Pressure differential transmitter
DPIA	Pressure differential indicating alarm
E	Energy or Energy consumption
ECO	Economizer
EIC	Equipment installation cost
EOS	Equation of state
EPC	Equipment purchase cost
ESD	Emergency shutdown
FAL	Low flow alarm
FE	Flash evaporator
FIAQ	Flow indicating alarm totalizer
FIQ	Flow indicating totalizer
FSL	Low flow switch
FT	Flow transmitter
FWH	Feedwater heater
GA	Genetic algorithm
GHG	Greenhouse gas
H	Hot
HEN	Heat exchanger network
HFE	Heated flash evaporator
HP	High pressure
HS	Hand switch
HX	Heat exchanger, heater, or cooler
IGCC	Integrated gasification combine cycle
JT	Joule-Thompson valve
IMTP	INTALOX® metal tower packing
IP	Intermediate pressure
LALL	Level alarm low low
LB	Lower bound
L/G	Liquid to gas ratio
LG	Level gauge
LP	Low pressure
L/R	Lean/rich
LSLL	Level switch low low

LT	Level transmitter
LVC	Lean vapor compression
MEA	Monoethanolamine
MINLP	Mixed integer non-linear programming
MOV	Motor operated valve
MTA	Minimum temperature approach
NC	The number of component
NDG	The number of data group
NP	The number of point
NRTL	Non-random two-liquid
P	Pressure or Pump
PAH	Pressure alarm high
PAHH	Pressure alarm high high
PG	Pressure gauge
P&ID	Piping and instrument diagram
PI	Pressure indicator
PIC	Pressure indicating controller
PRV	Pressure relief valve
PSHH	Pressure switch high high
PSV	Pressure safety valve
PT	Pressure transmitter
Regen	Regeneration
RH	Reheater
RK	Redlich-Kwong
RL	Recirculation line
SH	Superheater
T	Temperature
TAC	Total annualized cost
TE	Temperature transmitter
TEG	Triethylene glycol
TG	Temperature gauge
TI	Temperature indicator
TIAC	Temperature indicating alarm controller
TT	Temperature transmitter
TTD	Terminal temperature difference
TVC	Thermal vapor compressor
SG	Stripping gas

SIC	Speed indicating controller
SRK	Soave-Redlich-Kwong
UB	Upper bound
USC	Ultrasupercritical
ZAF	Valve position alarm failure
ZIO	Opened valve position indicator
ZIC	Closed valve position indicator
ZSC	Closed position switch
ZSO	Open position switch

Subscripts

aux	Auxiliary
bt	Backup turbine
c	Condenser
comp	Compression
cond	Condensate
ex	Extracted steam
fg	Flue gas
fw	Feedwater
p	Pump
lean	Lean MEA solvent
R	Ratio
rich	Rich MEA solvent
str	Stripper
sat	Saturated
top	At column top

Abstract in Korean (국문초록)

이 논문은 상업 규모의 석탄화력 발전소에의 이산화탄소 포집 및 저장 기술 도입을 위해 경제적이고 효율적인 이산화탄소 처리 공정의 최적 설계를 제안한다. 논문에서 제시하는 발전소-이산화탄소 처리 공정은 이산화탄소 포집 공정, 이산화탄소 압축-탈수-액화 공정, 이산화탄소를 영구 격리하기 위한 해상 주입 공정을 포함한다.

우선 이산화탄소 처리 공정을 포함한 개장 발전소에서 효율 감소 문제를 해결하기 위하여 공정 설계 및 운전 조건을 제안하였다. 모노에탄올아민을 이용한 연소 후 이산화탄소 포집 공정은 기술적 신뢰도가 높고 기존 화력 발전 시설과의 연계가 용이하여 대표적인 이산화탄소 포집 기술로 꼽히지만 포집 공정에서의 흡수제 재생과 포집 후 이산화탄소 저장을 위한 처리 공정에서 에너지 소비가 많아 발전소 효율을 감소시킨다. 이러한 이유로 흡수제 재생 및 액화에 필요한 에너지 절감을 위하여 단일 공정에서 다양한 공정 개선안 연구가 진행되어 왔으나 통합 공정에서 변수 간 복잡한 비선형적 관계를 고려하지 못하는 단점이 있다. 따라서 이산화탄소

처리 공정을 모두 포함한 개장 발전소의 수학적 모델링을 상용 공정모사기를 통해 구성하였다. 7 개의 연속 변수와 2 개의 이진 변수에 대해 에너지 사용에 대한 평가를 통해 총 4 개의 변수 및 주요 운전 조건을 선정하였다. 발전소 출력 감소를 최소화하는 최적화 문제를 구성하고 주요 운전 변수에 최적점을 제안하여 기존 발전소의 효율 저하를 최대 30%에서 17.7%까지 개선하였다.

두 번째로 이산화탄소 압축-탈수 공정의 최적 설계를 제안하고 경제적 강인성을 보여주었다. 이산화탄소 탈수 공정은 수송 및 주입 단계에서의 공정 안전에 큰 영향을 주는 주요 불순물인 수분을 제거하는 매우 중요한 단위 공정 임에도 불구하고 공정 연구가 수행되지 않아 경제적으로 과소평가 되었다. 초구조 최적화 기법을 이용하여 이산화탄소 압축-탈수 공정의 기술-경제적 평가를 실시하여 최적 압축-탈수 공정 설계를 제안하였다. 트라이에틸렌 글라이콜과 수분 간 VLE 실험 데이터를 사용하여 예측 매개 변수를 포함한 열역학 모델을 검증하였다. 가능한 공정 구조, 운전 조건, 기기 사이징 및 비용을 수학적 모델링과 최적화를 통해 동시에 선택할 수 있는 초구조를 상용 공정 모사기에 구성하였다. 제약 등식을 포함한 혼합 정수 비선형 문제를 유전 알고리즘을 통해

최적해를 도출하고 최적 설계를 보여주었다. 또한 제안한 최적 설계와 정 변수를 조합하여 만든 4 가지 공정 대안에 대해 유틸리티 비용 변화에 따른 민감도 분석을 몬테-카를로 방법을 통해 실시하여 최적 설계에 대한 경제적 강인성을 입증하였다.

마지막으로 액화한 건조 이산화탄소의 해상 주입 공정을 상세히 설계하고 공정의 위험 및 운전성 (HAZOP) 분석을 실시하여 공정배관계장도(P&ID)를 제시하였다. 주입 공정은 임시 저장을 위한 3 대의 ISO 탱크 컨테이너, 두 대의 직렬 펌프, 열교환기 및 주입구 헤드로 구성되어있다. 해당 공정을 3 개의 노드로 분리하고 각 노드에서 해당되는 변수와 가이드워드를 조합한 편차에 대해 원인과 결과, 그리고 제안사항을 분석하고 공정배관계장도에 반영하여 더욱 안전한 설계를 제안하였다.

이 연구에서 제안하는 공정 설계는 이산화탄소 처리 공정을 포함한 개장 발전소의 발전량 효율을 개선하고 이산화탄소 압축-탈수 공정과 실제 주입 설비 설치에 필요한 설계를 제안하여 상업 규모의 석탄화력 발전소의 이산화탄소 포집 및 저장 전 기술을 도입하고 실증하는데 기여할 것으로 판단된다.

주요어: 이산화탄소 포집 및 저장 기술; 연소 후 이산화탄소 포집 공정; 초구조 최적화; 이산화탄소 탈수 공정; 이산화탄소 주입 공정; 공정 위험 요소 및 운전성 분석

학 번: 2015-30215